A PHOTOMETRIC STUDY OF RS CANUM VENATICORUM INCLUDING CRITICAL ANALYSES OF THE DISTORTION WAVE AND PERIOD VARIATIONS

By

ELWYN WHIT LUDINGTON

A DISSERTATION PRESENTED TO THE GRADUATE COUNCIL OF
THE UNIVERSITY OF FLORIDA
IN PARTIAL FULFILLMENT OF THE REQUIREMENTS FOR THE
DEGREE OF DOCTOR OF PHILOSOPHY

UNIVERSITY OF FLORIDA

1978

Dedicated to the memory of my grandfather,

Elijah Whitfield Fisher

ACKNOWLEDGEMENTS

I wish to express my appreciation to the many people who have helped me accomplish the task of writing this dissertation.

First, I acknowledge my mother's years of love and encouragement. While maintaining a secure home environment, she required of me a high degree of independence which I feel has been invaluable in my pursuit of higher education. Second, I thank Mr. and Mrs. Robert E. Ludington, my uncle and aunt, for promoting my interest in amateur astronomy. Third, the guidance of Dr. Frederick Decker during my undergraduate years must be acknowledged. His advice was the beginning of my pursuit of astronomy as a career. Fourth, I thank Nancy A. Ludington for her encouragement during my initial years of graduate study. I wish to express my undying gratitude to Dr. John E. Merrill and Barbara M. Oliver for the words of wisdom which they gave me during the most trying times of my graduate student career. There are many others who deserve my thanks for their personal involvement in my life: Charles Jackman, Karen Rockwell, Charles H. Morgan, Jr., David Killian, and Mary Horn, to name a few.

Professionally, I would like to thank Dr. John P. Oliver for suggesting the topic of this dissertation, and for his expert guidance during the course of the research. The members of my supervisory committee are also thanked for their assistance. Of equal importance to the successful completion of this work were the many graduate students with whom I have had the pleasure of working. In particular, I would like to thank David Fierkowski, Gregory Fitzgibbons, Patricia Guida, Charles

Jackman, David Killian, Norman Markworth, and Elizabeth Mullen for our many discussions which greatly stimulated my endeavors.

Steven Gladin and John Young are thanked for their kind and very helpful assistance with computer programming

Finally, I would like to thank Karen P. Rockwell for her assistance with the reduction of the chart recordings and her help with this manuscript.

TABLE OF CONTENTS

ACKNOWLEDGEMENTS . . . [illegible]
TABLE OF CONTENTS . . . v
LIST OF TABLES . . . vii
LIST OF FIGURES . . . viii
ABSTRACT . . . x

Chapter

I. INTRODUCTION . . . 1
    Topic of Current Research . . . 1
    Historical View . . . 2
    Scope of Dissertation . . . 44
II. INSTRUMENTATION . . . 45
    The Basic Equipment . . . 45
    Amplifier Calibration . . . 48
III. PROCEDURE AND DATA REDUCTION . . . 51
    Observational Procedure . . . 51
    PHRED . . . 54
    DEXTOR . . . 65
    Data Reduction . . . 67
IV. DATA ANALYSIS PROCEDURE . . . 74
    Introduction . . . 74
    Outline of WAVE Procedure . . . 74
    The WINK Program . . . 78
    The ROMC Program . . . 81
    The FOURFIT Program . . . 81
    The LCPLOT Program . . . 82
    Detailed WAVE Procedure . . . 82
V. ANALYSIS AND SOLUTION . . . 87
    Introduction . . . 87
    The Data Analyzed . . . 87

The Analysis 97
The Final Solution 99
The Distortion Wave 102
Period Changes 104

VI DISCUSSION 139

Introduction 139
The Distortion Wave 139
Orbital Period Variations 147
Conclusion 149

APPENDIX 153

LIST OF REFERENCES 167

BIOGRAPHICAL SKETCH 173

LIST OF TABLES

1. JOY'S ABSOLUTE DIMENSIONS 5
2. POPPER'S RESULTS FOR RS CVN 13
3. LIST OF RS CVN BINARIES 24
4. LUDINGTON-OLIVER FORMAT 56
5. DIFFERENTIAL MAGNITUDES AND COLORS OF CHECK STAR 71
6. WINK PARAMETERS 78
7. ASSUMED PARAMETER VALUES 80
8. SOURCE OF DATA 88
9. SUMMARY OF RS CVN SOLUTION 92
10. FINAL VALUES OF WINK PARAMETERS 100
11. FINAL VALUES OF EPOCH-DEPENDENT PARAMETERS 101
12. NORMAL POINTS FOR 1921 DATA 117
13. NORMAL POINTS FOR 1963 DATA 119
14. NORMAL POINTS FOR 1964 DATA 121
15. NORMAL POINTS FOR 1965 DATA 123
16. NORMAL POINTS FOR 1966 DATA 125
17. NORMAL POINTS FOR 1975v DATA 127
18. NORMAL POINTS FOR 1976v DATA 129
19. NORMAL POINTS FOR 1975b DATA 131
20. NORMAL POINTS FOR 1976b DATA 133
21. NORMAL POINTS FOR 1975u DATA 135
22. NORMAL POINTS FOR 1976u DATA 137
23. TIMES OF MINIMA AND CHARACTERISTICS OF THE DISTORTION WAVE 141

LIST OF FIGURES

1. 1975 Visual Light Curve of RS Canum Venaticorum 29
2 Schematic Diagram of Instrumentation 47
3 Fine-Gain Stability 49
4 Coarse-Gain Stability 49
5. JCL Cards for PHRED 59
6 Differential Magnitudes of Check Star 70
7 Outline of Basic WAVE Procedure 75
8 Sample Plot from LCPLOT Program 77
9. The WAVE Procedure 83
10 Input Stream which uses the WAVE Procedure 85
11. 1921 Light Curve of KO Star in RS CVn 106
12. 1963 Light Curve of KO Star in RS CVn 107
13. 1964 Light Curve of KO Star in RS CVn 108
14 1965 Light Curve of KO Star in RS CVn 109
15 1966 Light Curve of KO Star in RS CVn 110
16. 1975v Light Curve of KO Star in RS CVn 111
17. 1976v Light Curve of KO Star in RS CVn 112
18. 1975b Light Curve of KO Star in RS CVn 113
19. 1976b Light Curve of KO Star in RS CVn 114
20 1975u Light Curve of KO Star in RS CVn 115
21. 1976u Light Curve of KO Star in RS CVn 116
22 Distortion Wave Amplitude 142

23. Phase of Distortion Wave Minimum 143
24. Shape of Spotted Region 146
25. Photoelectric O-C Diagram 148

Abstract of Dissertation Presented to the Graduate
Council of the University of Florida in Partial Fulfillment of the
Requirements for the Degree of Doctor of Philosophy

A PHOTOMETRIC STUDY OF RS CANUM VENATICORUM INCLUDING CRITICAL ANALYSES OF THE DISTORTION WAVE AND PERIOD VARIATIONS

By

Elwyn Whit Ludington

December 1978

Chairman: John P. Oliver
Major Department: Astronomy

Photoelectric data in the UBV system were obtained by the author in 1975 and 1976 at Rosemary Hill Observatory. These data of RS Canum Venaticorum were analyzed together with the published Catania data. The analysis included the use of a modified version of D. B. Wood's (A.J., 76, 701) computer program WINK. A truncated Fourier series representation of the distortion wave was subtracted from the observed light curve so improved elements could be determined from the difference by use of the WINK program. This process was not at all like the usual rectification procedure; it was an iterative procedure which greatly improved the confidence in the determination of the elements of RS CVn. With the single exception of the effective temperature of the K0 III star, the eclipsing elements are consistent for all epochs and colors studied. Using these elements, it was possible for the distortion wave to be isolated; therefore, it will now be possible for theories of its origin and structure to be tested more critically. The results are consistent

with a spotted surface for the K0 star. However, the sunspot analogy does not accurately describe the nature of the spots.

CHAPTER I
INTRODUCTION

Topic of Current Research

The eclipsing binary star RS Canum Venaticorum (RS CVn) is the prototype of a very interesting, but poorly understood, group of stars. It has been chosen for further study because it has the most complete observational record of this group, and because it is sufficiently bright to allow observations with the available equipment. The RS CVn binaries (also known in the literature as RS CVn systems, RS CVn-type binaries, RS CVn stars, etc.) have been recently reviewed by Hall (1976). He concludes that the group is best defined by systems in which (1) the hotter star is of spectral type F or G and luminosity type V or IV, (2) strong Ca II emission is present in the H and K lines, and (3) the orbital period of the binary system is between approximately a day and 2 weeks. There are other charecteristics which are common to many of the systems listed by Hall, but which were deemed unnecessary for the purpose of classification. Some of these characteristics would be mass ratios near unity, cooler components near spectral class K0 III, and photometric distortions superimposed on the normal eclipse phenomena (if it exists). It is the complications caused by the last of these characteristics to which this dissertation is addressed.

A new set of observations of RS CVn will be presented which will extend the basic astronomical knowledge of the system and confirm the earlier observations. A new technique of solution is developed which circumvents the previous problems encountered when deriving elements from a light curve with unexplained light variations. A natural result of this technique is to isolate the unexplained light variation (referred to as a 'distortion wave' in this work) so that it may be studied independently. It is also hoped that the times of minima can be improved with this technique so that a better representation of the period variations can be obtained.

In the remainder of this chapter the literature on RS CVn and RS CVn binaries will be reviewed and the scope of the dissertation will be outlined. In the chapters to follow the new photoelectric data will be presented, starting with the instrumentation and procedure used. Following this will be a discussion of the distortion wave and period variations. The dissertation will conclude with a summary of the results, interpretation as to their meaning, and suggestions for future research.

Historical Review

The review of the literature shall start with a chronological history of the research on RS CVn. When this review reaches the early 1970's, it will be more convenient to speak in terms of the RS CVn systems, rather than RS CVn itself.

RS Canum Venaticorum from 1914 to 1972

RS CVn was first reported as a variable star by L. Ceraski in 1914. She reported that the star was observed to be fainter, on photographic plates read by M.S. Blazko, on 7 April 1896 (by $1^{m}5$), 15 May 1907 (by $1^{m}0$), and 3 May 1911 (by $1^{m}0$). Numerous observers studied this system during the following 16 years. The results of these observations culminated in the solution of the light curve presented by Sitterly (1930). Sitterly summarized the considerable observational material obtained between 1914 and 1928 by Townley (1915), Hoffmeister (1915, 1919), Maggini (1916), Gadomski (1926), Schneller (1928) and others. He presented the times of minima that these various observers had collected up to 1928 and discussed the period changes. He noted that the period steadily increased during the interval 1900 to 1928. This can easily be verified from the times of minima as plotted on the O-C diagram (Observed time of minima minus the Calculated time of minima from a linear ephemeris). He had accumulated 710 visual estimates using the 23-inch Princeton refractor and 351 photographic estimates from Harvard plates. The visual estimates were obtained during the years 1920 to 1922 (mostly in 1921), while the photographic estimates covered a much longer time (from 1892 to 1922). The visual light curve showed asymmetry outside eclipse and in primary eclipse. The photographic light curve, on the other hand, showed no asymmetry outside eclipse, nor did it show a secondary eclipse. In retrospect, this can be understood in terms of a moving distortion wave averaging out the asymmetry over the much longer interval of time during which the photographic estimates were made. This process would, of course result in a much larger standard error for points of the photographic light curve, but this would be expected in any case because of the lower precision of this technique. Except for the asymmetry outside eclipse, Sitterly's visual light curve solution was in good agreement with the photographic light curve. The solution was complicated by a small secondary eclipse, only $0^{m}03$ deep, which compares with a depth of $0^{m}2$ by modern photoelectric photometry. Sitterly determined a depth of

$1^m.27$ for primary eclipse, which is in reasonable agreement with a modern value of $1^m.1$. He attempted a solution in which the following sides of both stars were more luminous than the advancing sides. This was necessary in order to explain the outside eclipse asymmetry, which amounted to a peak to peak difference of $0^m.13$ between the portion of the light curve preceding and following primary eclipse. This gave much better residuals than the other solutions but it was discarded because it seemed so physically inexplicable, particularly since it required the fainter star to have a difference in brightness from one side to the other of 56%! The solution which was finally adopted as the best representation of the true values was obtained by solving the visual light curve without any rectification. The resulting elements were:

Uniform disks assumed,

$k = 0.30$, $i = 79.9$ degrees,

$r_1 = 0.289$ $r_2 = 0.0867$,

$L_b = L_2 = 0.690$, $L_f = L_1 = 0.310$,

where the subscript b (or 2) refers to the brighter star, and the subscript f (or 1) refers to the fainter star. The estimated probable error for a visual observation was $\pm 0^m.0364$, while the estimated probable error for a photographic observation was $\pm 0^m.05$. It is therefore wise that he chose to base the solution on the visual light curve. The comparison star used was BD+36° 2345, and the differential magnitudes were originally given as comparison minus variable.

In the same year, Joy (1930) published spectroscopic data on RS CVn. He used the results of Sitterly's photometric solution along with his own spectroscopically determined radial velocities to arrive at absolute dimensions. A summary of Joy's results is given in Table 1 (the subscripts have the same meaning as noted above).

TABLE 1
JOY'S ABSOLUTE DIMENSIONS

$K_1 = 91.6$ km/s	$m_1 \sin^3 i = 1.79\ M_\odot$
$K_2 = 99.0$ km/s	$m_2 \sin^3 i = 1.66\ M_\odot$
$\gamma = -8.9$ km/s	$m_2/m_1 = 0.93$
$a_1 \sin i = 6.04 \times 10^6$ km	$r_b = 1.6\ R_\odot$
$a_2 \sin i = 6.53 \times 10^6$ km	$r_f = 5.3\ R_\odot$
$m_b = 1.85\ M_\odot$	$m_f = 1.71\ M_\odot$

Joy concluded from the spectroscopic absolute magnitude and from the spectral class that both stars are dwarfs. However, the size and brightness of the fainter star were in direct conflict with this. Joy ended his article by saying, " . . . the secondary star is certainly peculiar and cannot readily be classified among other stars for which we know the physical characteristics' (p. 45). Joy agreed with Sitterly's interpretation that the fainter secondary star is 'a sort of 'subgiant.'"

C. Payne-Gaposchkin (1939) made a study of the period changes and light curve asymmetries of RS CVn as a part of a paper on variable stars. She collected approximately 4000 photographic estimates of the brightness from Harvard plates exposed between the years 1892 and 1936. From the data, 17 times of minima were computed and plotted. In addition, a light curve was made by combining individual points into normals. In primary eclipse each normal was made up of 10 individual points, while outside eclipse each normal was comprised of 100 individual points. The normal points were computed after each individual point was corrected for the change in period, as she had estimated it. The resulting light curve agreed with Sitterly's in its general characteristics. However, it did not agree with the asymmetry that Sitterly had observed from his visual light curve. Recall that Sitterly had presented a visual and photographic light curve for RS CVn, but his photographic light curve failed to show a secondary minimum or any asymmetry outside eclipse. Payne-Gaposchkin, on the other hand, found a shallow secondary eclipse in her photographic light curve (of depth $0\overset{m}{.}06$), and a difference in the height between the two maxima of only a few hundredths of a magnitude. She noted, however, that when the light curve is made from points taken about the same time as those of Sitterly, a somewhat larger difference was found. In an effort to summarize the differences in magnitude between the two maxima, she presented a table of these differences at four epochs of minima. She noted that if the difference is assumed to be a periodic phenomena, then the period would be approximately 8000 days (22 years) or 1670 orbital periods, i.e., the approximate period of the orbital period changes. She estimated that an absolute orbital radius of 2×10^9 km would be necessary to explain the period changes as a light-time effect. Further, she determined that if this were due to a third body, then the required mass of 4 $M_\odot$ would seem larger than could possibly go undetected photometrically. This represented the first convincing evidence that the period changes were of an unusual nature, and the first time that the differences in heights of maxima were ascribed to be of a possibly periodic nature. The most significant aspect of this paper was that the differences in the height of the two maxima were ascribed to the redder (and fainter) of the two stars. This was based on her realization that the size of the asymmetry was greater in the visual light curve than in the blue photographic light curve.

W. A. Hiltner (1947) noted that a define group of stars existed which showed Ca II emission. In this short note he collected the scattered data on the 13 systems known to him at that time (RZ Eri, SS Cam, AR Mon, RU Cnc, RS Cnc, RW UMa, RS CVn, SS Boo, WW Dra, Z Her, AW Her, RT Lac and AR Lac). Hiltner found from his study of RS CVn the same characteristics reported by other observers whose data he had collected together. The emission was noted to be usually from the fainter of the two stars in the eclipsing system and the emission was apparently '... not situated uniformly around the parent-star' (p. 481). In fact he stated that the emission approached invisibility only at the secondary eclipse when the fainter star is partially covered by the brighter, but smaller star. This led him to agree with Struve (1946) and others that the Ca II emission in these stars originates from a tidally extended region above the photosphere of the fainter star. The emitting region was isolated at the extremes of this tidal bulge along the line joining the two stars. Struve's and Hiltner's papers could be considered the first recognition that there was a group of stars (today referred to as RS CVn binaries) which warranted consideration as a group.

Gratton (1950) studied 19 systems which showed H and K lines of Ca II emission in the last section of a paper published just a few years after Hiltner's. This list included the 13 stars in Hiltner's paper plus six others which were not eclipsing binaries, but were of a binary nature. These six stars were primarily more luminous and of longer periods than those in Hiltner's list. Gratton attempted to give additional evidence that the tidal bulge proposed by Struve and Hiltner was the proper mechanism for the explanation of the H and K emission.

Briefly, Gratton's analysis followed these lines. By assuming that all stars with a tidal distortion above some lower limit would show emission lines, it was then expected that the giant stars which show emission would have longer orbital periods. This condition led to the relation

$$\frac{R}{a_1 + a_2} > k_1,$$

where it was assumed that the variation in mass could be neglected, R was the radius of the star, a_1 and a_2 were the relative orbital radii, and k_1 was a constant. Since the stars being studied were of approximately the same spectral type (and therefore had the same surface brightness), the radius was proportional to the square root of the luminosity. In addition, the sum of the relative orbital radii was proportional to the period (P) to the two-thirds power. Therefore the period and the absolute magnitude (M) for the binaries showing H and K emission lines were above a line $0.3\ M + \log P = \text{constant}$.

Gratton plotted the absolute magnitude versus log P for 13 of the 19 stars in the list. The binaries SS Cam, Z Her, 56 Peg, AW Her, AR Lac, and RU Cnc were excluded because of the lack of data. Gratton stated, "It is seen that there is a definite correlation between M and P, we may tentatively take the limiting line $0.3\ M + \log P = 2.5$" (p. 40). Stars above the line $0.3\ M + \log P = 1.0$ are practically in physical contact, for these stars the distortion would be too great and might cause instability.

It seems to the present writer that the assumptions which led to this conclusion are reasonable, with the possible exception of the correlation between the emission and the degree of tidal distortion. More recently, Young and Koniges (1977) have investigated this relationship; this will be discussed later.

Keller and Limber (1951) used an unfiltered 1P21 photomultiplier tube to obtain a light curve of RS CVn during the spring of 1949. They used BD+35° 2421, BD+35° 2422, and BD+35° 2415 as comparison stars, with the differential luminosity expressed relative to BD+35° 2422. Inside eclipse, individual points were tabulated, but outside eclipse only the normal points were given. From an expanded plot of these data around the primary minimum Keller and Limber noticed a systematic difference in luminosity. They found that this variation in the depth of primary was most probably due to intrinsic variability of the fainter star. They also noted the same asymmetry outside eclipse observed by Sitterly and Payne-Gaposchkin. It is important to note that the observations of Keller and Limber were taken over only a three-month interval, so that the normals they produced outside eclipse were not affected as much by variations in the asymmetry as was the case for the observations of Sitterly (mostly one year of data) or Payne-Gaposchkin (nearly 47 years of data). The asymmetry observed by Keller and Limber was of the same general character as that of the previous observers; it had a higher maximum after primary eclipse than prior to primary eclipse. The difference in the two maxima was $0^{m}04$. The rectified light curve was solved using a limb darkening coefficient of 0.8 with the aid of the Merrill (1950) tables. The elements so determined were:

$L_b = 0.726,$ $L_f = 0.274,$

$k = 0.365,$ $r_f = 0.265,$

$i = 82^{\circ}.5 \pm 0^{\circ}.5.$

From the luminosity and radius of each component they computed the ratio of surface intensities. This ratio, approximately 20, could not be reconciled with the value of 5.5 they computed on the basis of the energy distribution of the stars (corrected for the effects of the Balmer discontinuity, atmospheric transmission, and the response of the instrumentation). This, of course, was the same problem Joy had commented upon.

Keller and Limber very crudely estimated the polytropic index of the fainter star to be 2.55. They used an O-C diagram made from all the available times of minima, and an orbital eccentricity determined from a single estimate of the time of secondary minimum based on their own data.

While it is obvious that their observations are the best of any available at that time, it is equally obvious (as can be seen from the light curve in their paper) that the time of secondary minimum is greatly complicated by the asymmetry of the light curve. It was therefore wise of them to state, "It is not possible to obtain the phase of the secondary with much precision" (p. 647).

Bidelman (1954) published a list of stars which were known to show emission lines and whose spectral types were later than B. The list for stars showing Ca II emission, which are also spectroscopic binaries, continues to be referenced today. RS CVn as well as all of the other stars in Hiltner's paper were among the 72 stars in Bidelman's table.

Popper (1961) observed RS CVn in an effort to improve the quality of the spectroscopic orbit and to add photoelectric observations on a standard system to the body of existing data. He obtained 12 spectrograms between the years 1954 and 1959 which showed the same general features previously observed by Joy (1930) and Hiltner (1947). The only major difference between his spectrograms and those of the previous observers was the sharpness of the absorption lines due to the brighter component of spectral class F4. Joy had designated the spectral type as F4n, which would mean that the lines were "nebulous." Popper noted the bright H and K emission lines of Ca II from the cooler (fainter) component, as well as the variable emission intensity of the H_α line. The solution of Popper's radial velocity curve was compared with Joy's. Both observers assumed a circular orbit. Popper's results gave slightly smaller masses for both stars. In addition, he believed that the difference in the systemic radial velocity of 6 km/s was probably a real (but unexplained) phenomenon. The photometry was done during the summer of 1956, in January 1958, and in January 1959. No attempt was made to cover the entire light curve. The comparison star was HD 114778 (BD+35° 2420), i.e., the same star used later by Chisari and Lacona (1965), Catalano and Rodono (1967) and the present writer. The photometry of this star from the three seasons resulted in the following magnitudes

$V = 8^{m}42$, $B-V = +0^{m}46$, and $U-B = -0^{m}04$

This star was $0^{m}03$ fainter in 1960 than it was during the 1958-59 observing seasons. Popper was not sure whether this difference was due to a real variation, to the difference in the zenith angles involved, or to the difference in the set of standard stars used.

As expected, primary eclipse was observed to be deeper for shorter wavelengths, and secondary minimum was observed to be deeper in the yellow than it was in the blue. Surprisingly, the depth of primary eclipse was $0\overset{m}{.}3$ different in 1956 than it was in 1958-59. This must be attributed to the fainter star, since this eclipse is a total one. No such variation was found in the system's brightness outside eclipse, so the intrinsic variation of the fainter star was not uniform over its surface. A similar, but a much smaller, difference existed between the other observed primary minima. The observed difference in depth of primary could be explained by a change in the radius of the fainter star. Unfortunately, there were insufficient data to determine if this was the case. Another possible explanation would have been a change in the color of the fainter star. The data available to Popper indicated a change in color of the proper sense but of insufficient size to account for the observed difference. Also, since the variations outside eclipse had the same color as the fainter star it was very reasonable to expect this star to be the source of the variation. These two effects (variation in the depth of eclipse and the variations outside eclipse) could have been due to a combination of pulsation and "spottedness" of the fainter star, according to Popper. He pointed out that the depth of secondary eclipse as observed by Keller and Limber (1951) was greater than expected from their values of k and the depth of primary minimum. This led him to believe that there was a large uncertainty in the value of k. Popper also found a discrepancy in the ratio of surface brightness as calculated from the spectral types and that obtained from the light curve. He noted, however, that the discrepancy was probably not as large as that found by Keller and Limber. For reference, the results of Popper are summarized in Table 2.

TABLE 2
POPPER'S RESULTS FOR RS CVN

$a \sin i = 16.7\ R_\odot$

$M_b \sin^3 i = 1.32\ M_\odot$

$M_f \sin^3 i = 1.38\ M_\odot$

$i = 82^\circ - 90^\circ$

$a = 16.7 - 16.85\ R_\odot$

$r_b = 0.09 - 0.12$

$r_f = 0.20 - 0.27$

$(B-V)_b = 0.39 - 0.44$

$(B-V)_f = 0.91$

$T_b(\mathrm{eff}) = 5500^\circ - 6800^\circ K$

$T_f(\mathrm{eff}) = 4700^\circ K$

$(B.C.)_b = 0^m.0$

$(B.C.)_f = -0^m.3$

$M_b = 1.32 - 1.35\ M_\odot$

$M_f = 1.38 - 1.42\ M_\odot$

$R_b = 1.5 - 2.0\ R_\odot$

$R_f = 3.3 - 4.6\ R_\odot$

$L_b = 3.7 - 7.8\ L_\odot$

$L_f = 5.0 - 9.1\ L_\odot$

$(M_{bol})_b = 2.5 - 3.4$

$(M_{bol})_f = 2.4 - 3.0$

$(M_v)_b = 2.5 - 3.4$

$(M_v)_f = 2.7 - 3.3$

Plavec, Smetanova, and Pekny (1961) showed by their calculations that the periodic term in the period variation could not possibly be due to a third body (unless this third body greatly violated the mass-luminosity relation). They found that in the extreme case, the mass of the third body would have to be of the same order as that of the stars in the system. A similar conclusion was reached earlier by Payne-Gaposchkin (1939). Their calculations were based on the much more reliable data of Keller and Limber (1951) and Popper (1961). Popper's data were used by them to make a new estimate of the effects of apsidal motion, and here again the results indicated that this hypothesis could not be responsible for the periodic term of the period variations.

Chisari and Lacona (19[illegible]) observed RS CVn from the S. Agata Li Battiati station using a 30 cm (12 inch) Cassegrain telescope in 1963 and 1964. Their effective wavelength was stated to be 6150 A°, which is slightly bluer than that for the standard V filter. The bandwidth was not given, but the EMI 6256A photomultiplier tube was filtered with a yellow Galileo G 1-26 filter. They used the same star as Popper for a comparison (HD114778 = BD+35° 2420). However, they did not correct the observations for the effects of atmospheric extinction, because they considered the closeness of the comparison to the variable sufficiently small to make correction unnecessary. After rectification of the light curve they solved the 1964 observations to obtain the following elements:

initial epoch (Julian Date) = 2438467.1282,
Period = $4^{d}.797680$,
$x = 0.8$, $i = 84°$,
$k = 0.45$, $L_1 = 0.269$,
$r_1 = 0.244$, $L_2 = 0.731$,
$r_2 = 0.112$, $a = 0.0$ (assumed)

They found the period to be decreasing in the same sense as Keller and Limber (1951) had found, but not by the amount predicted by observations obtained prior to 1936. They concluded that the system was semi-detached and that the material one would expect in such a system was leaving the larger star. Thus a cloud would be formed which would cause the anomalous light variations in the light curve. This does not agree with subsequent research.

Plavec (1967) studied the properties of Algol-like close binaries with double-line spectra. RS CVn was among the stars studied and was found to be detached by a significant amount. Several other stars were noticed to have similar properties which were different from genuine Algol binaries. RS CVn, WW Dra, Z Her, AR Lac, and SZ Psc were considered by Plavec to form a well-defined sub-group. It is significant that except for SZ Psc all of these stars were in Hiltner's list of 13 systems showing Ca II emission.

Catalano and Rodono (1967) presented additional photoelectric observations of RS CVn taken with the same equipment Chisari and Lacona had used in 1963 and 1964. However, it may be of importance to note that the observations were not all taken at the same site. The data for 1965 were apparently obtained from the same place as those of Chisari and Lacona, but the equipment was then moved to Serra La Nave. The subsequent data taken in 1966 were from this site using the same telescope and equipment. All of the observations used the same comparison star as Popper, Chisari and Lacona, and the present writer, namely BD+35° 2420. They also observed a check star (BD+35° 2422), which showed, contrary to Popper's earlier suspicions, that the comparison star BD+35° 2420 is of constant light. They made no attempt at a solution, in the classical sense, to the new observations, but instead they pointed out an important fact about the distortion wave in RS CVn.

The distortion wave was found to shift with respect to the eclipses in the direction of decreasing phase, and completed one cycle in 2400 orbital periods. To explain this phenomenon a model was developed in which a ring of material circled the hotter star. This was similar to the proposal of Chisari and Lacona, but the model developed by Catalano and Rodono was much more detailed. In this model a non-uniform ring of material was located around the smaller star of the system. They assumed that the material would make Keplerian orbits around this star and were therefore able to compute the distance between the star and the ring. The period of the quasi-sinusoidal distortion wave represented one orbit of a particle in the ring. The results required that the material be outside the limiting Roche lobe for the star. In this case the ring would be unstable, but they proposed that the material lost from the system be replaced by material from the larger star. If the primary star is inclined to the orbital plane, its axis would be expected to precess with a period which they computed to be about the same as that of the retrograde period of the distortion wave. The quasi-sinusoidal shape would then be due to the non-uniform distribution of material in the ring, but there was no exlanation for the persistence of this particular distribution over the time scale of the observations (1963 to 1966). The 1965 light curve showed no appreciable variations beyond those already known, but the data for 1966 indicated that the depth of primary eclipse was not the same for all nights during which this portion of the light curve was observed. The phenomenon was earlier reported by Keller and Limber and by Popper. Whether this was real or a result of the new observatory site, in the case of Catalano and Rodono's data, is not known.

Nelson and Duckworth (1968) reported, in an abstract, on the observations they had obtained of RS CVn from 1965 to 1967. Their observations were not given, but they reported that the light curves show variations in the depth of primary and secondary eclipses of up to a quarter of a magnitude in the violet, and similar but smaller variations in the other colors. They also reported that the data showed changing shapes for the eclipses and the portions of the light curve outside eclipse, over the three years they observed the system.

Catalano and Rodono (1969) summarized several aspects of their observations of RS CVn in a more widely accessible forum than their previous publication. First, they found additional evidence for the distortion wave's retrograde shift. From the observations of Keller and Limber, Popper, Chisari and Lacona, their own published data for 1965 and 1966, and new unpublished data for 1967 and 1968, they were able to more accurately determine the period of the retrograde shift. Unfortunately, for their previous model, the results were incompatible with the theoretical precession rate of 2400 orbital periods. They found that the distortion wave retrograde shift period was of the order of 800 orbital periods or less. The new data for 1967 and 1968 were obtained on the standard UBV system, which allowed them to determine the color of the system outside eclipse. From the graph of the color index and outside eclipse variation, it was obvious that the color index increased with decreasing intensity of the distortion wave. Since the color of the distortion wave became bluer as it became fainter, they suggested that the investigations of Mergentaler (1950) could be a possible explanation. They reported that Mergentaler proposed that systems which show such a color change can be explained by a gas of negative hydrogen ions of different optical thicknesses. Catalano and Rodono noted that this would require that the gas be in an equilibrium configuration in order to maintain the shape of the distortion wave as they had observed it. Variations in the depth of primary minimum had been observed in the past, but their more consistent and more extensive observations were able to confirm this phenomenon and to show that it was correlated with the position of the distortion wave. Since the primary eclipse was total, only the secondary (larger, cooler star) of the system was visible at that time, thus this star was probably responsible for the distortion wave phenomenon. It is not clear to the present writer if Catalano and Rodono were referring to the secular (800 orbital period) shift of the distortion wave across the primary eclipse as the source of variations in its depth or to some sort of flaring activity on the larger star. In the former case it would be difficult to explain changes in depth of primary eclipse which have been observed on much shorter time scales. Nevertheless, their conclusion was in complete agreement with the earlier conclusions of Payne-Gaposchkin (1939), Keller and Limber (1961), and Pepper (1961) regarding the source of the light variations (in eclipse and/or out of eclipse).

The period variations had been well known previously, but there had been significant evidence that the variations were due to apsidal motion (Keller and Limber 1961, and Plavec and Smetanova 1955). However, more recent studies of Plavec, Smetanova and Pekny (1961) have cast considerable doubt on the appropriateness of apsidal motion to explain the period variations. Catalano and Rodono showed that the existence of a moving distortion wave made the measurement of photometric eccentricity highly questionable. In fact they stated, the displacement of secondary minimum resulting from our observations is incompatibly smaller than the orbital period variations" (p. 440).

Finally, the Catania astronomers concluded the article with some notes on the spectroscopic peculiarities in RS CVn. They had observed the same emission lines of H_α, and Ca II as Hiltner (1947), Joy (1930), and Pepper (1961). Unlike Hiltner they were unable to notice the disappearance of the H and K lines at secondary eclipse.

In a theoretical presentation, Hall (1972) discussed an alternative model for RS CVn. This model attempted to explain the following characteristics of the system:

1. The existence of the distortion wave
2. The migration of the wave to decreasing phase
3. The anomalous depth of secondary eclipse
4. The non-uniform migration rate of the distortion wave
5. The variable depth of primary minimum as a function of time
6. The displacement of secondary minimum from a position mid-way between adjacent primary minima
7. The variable amplitude of the distortion wave
8. The changes in orbital period

The model that was proposed by Hall, by analogy with the sun, was that of spots on the cooler component of the system. It was well known that the sun has dark spots on its surface from time to time. Starting from this, Hall felt that it was reasonable to expect that other stars would have similar spots. In the case of RS CVn, he anticipated that the spot or spots would cover between 30% and 60% of the facing stellar disk of the K0 star. This spotted region was, for whatever reason, confined to one hemisphere and to the equatorial region between about ± 30°. Hall reasoned that the star would be rotating differentially, again by analogy with the sun. The equatorial region would rotate faster than the polar regions, as is the case in the sun (which also has a convective envelope). The stars of the system were expected to be in synchronous rotation, but the latitude at which the rotation was synchronized with the orbit was expected to be of the order of ± 30°. Again relying on the analogy with the sun, he assumed that the spot activity would be periodic, with a cycle of 1800 orbital periods. Further, he assumed that the spots on the cooler component of RS CVn would form at higher latitudes at the beginning of each spot cycle, and proceed to form at lower and lower latitudes as the cycle progressed.

With this model the existence of the distortion wave is easily explained. Differential rotation of the star explains why the distortion wave moves to decreasing phase. Since the surface of the cooler star is not of uniform brightness, the depth of primary eclipse will vary depending on the location of the spotted hemisphere at the time of this eclipse. Furthermore, the location of the spotted region can cause the location of the minimum during the secondary eclipse to be shifted to either side of phase 0.5. Since the model assumes that the spot activity is periodic in a fashion similar to the sunspot cycle, and that the star rotates differentially, then the migration rate of the distortion wave will vary depending on the latitude of the spotted region and the amplitude of the distortion wave will vary in a similar fashion.

Hall presented very convincing evidence to support this model. The spotted region would only have to be 1000°K cooler than the surrounding photosphere in order to account for the typical amplitude of the distortion wave. This was of the proper value to also explain the anomalous depth of secondary eclipse, if it was assumed that the spotted region was eclipsed at secondary minimum. Hall noted that this implies that as the spotted region migrates, due to differential rotation, around the star, the depth of secondary eclipse should vary accordingly. This has not been confirmed.

Catalano and Rodono (1968) had shown the correlation between the position of the distortion wave and the depth of primary minimum. Hall's model provided an explanation for this. The deepest primary minima occurred during times when differential rotation brought the spotted region to the hemisphere facing the earth. The displacement of secondary eclipse from the mid-point of the light curve had been explained by Catalano and Rodono (1968) as a consequence of the migration of the distortion wave. Hall's model clarified this in terms of the location of the spotted region during the secondary eclipse. If the spotted region was located so that it faced the earth at quadrature, then the loss of light during secondary eclipse would be asymmetric. From a plot of the available estimates of the amplitude of the distortion wave as a function of epoch, Hall was able to represent the variation with the periodic function

$$\Delta V(\text{max-min}) = -0^{m}12 - 0^{m}07 \sin((E+450)/1800)$$

He used the linear ephemeris of Schneller (1928) to calculate the value of E. Note that this function can be used to predict the value of the amplitude of the distortion wave at any time. Hall also presented another graph which allowed the prediction of the distortion wave migration rate. In Fig. 2 of his paper he plotted the orbital phase of the minimum of the distortion wave as a function of epoch (E). From this graph one was able to see that the discontinuities in the migration rate occur at the minimum of the spot cycle. This was the result expected from the analogy with the sun and differential rotation. Arnold and Hall (1973) later made corrections to the model without changing the substance of the results.

In the remainder of the paper Hall attempted to explain the period variations as the result of mass ejections from the spotted active region. The required mass loss rate was rather high (of the order 10^{-6}

solar masses per year). The conclusion he reached on the evolutionary status of RS CVn was not decisive, but he considered the star to be most likely in a pre-main-sequence state of evolution.

RS CVn Binaries

The early stages in the development of the definition of this group of binary stars have been discussed in the preceeding paragraphs. Certainly, the research results of Struve (1946) and Hiltner (1947) were the first clues to the existence of a group of stars which are different from the classical binary and significantly different from other peculiar systems. The research effort over the subsequent 30 years (Gratton 1950, Plavec 1967, Popper 1967, 1970, Oliver 1971, 1973, 1974; and Hall 1976) slowly developed a clearer picture of the physical and observational characteristics of these stars which separates them from any other group which has been classified.

Popper (1967, 1970) listed approximately 20 systems which he believed to be of special interest because of their spectroscopic characteristics, light variations, and unique placement in the H-R diagram. Oliver (1974) was the first to undertake a comprehensive study of these stars as a group. This research led Oliver (1971, 1973, 1974) to list the criteria for inclusion in the group and to propose a list of stars which would therefore be members. To date, the best review of the RS CVn binaries is the recent paper by Hall (1976). In the paragraphs to follow, the current understanding of the RS CVn phenomenon will be discussed. Since the most characteristic observational property of the group is strong H and K emission, the discussion will begin with the spectroscopic characteristics. Variations in the observed light of the systems are an observational property of many of the systems in the group. The discussion of these variations will be followed by a short report on ultraviolet and infrared excess. Period variations have also been noticed in many of the RS CVn binaries, the short and long-term variations will be reviewed. The recent discovery of radio and soft X-ray emission from several of the RS CVn binaries has been very exciting. The report here will attempt to summarize these observations and the resulting implications. Finally, this section will conclude with a review of the proposed evolutionary status of these stars. However, before beginning, it will be useful to state the properties of RS CVn binaries which Hall (1976) proposed as the defining characteristics. They are as follows

1. Orbital period between 1 day and 2 weeks
2. Strong H and K emission seen outside eclipse
3. The hotter star is F or G, IV or V

The list of members in this group which has been developed over the last few years is given in Table 3. This list is derived from Hall's (1976) review paper and new discoveries.

Spectroscopic characteristics

The existence of strong H and K emission in the RS CVn binaries has been well documented by Struve (1946), Hiltner (1947), Eggen (1955), Popper (1967, 1970), Oliver (1974) and Weiler (1978a). The emission is strong in the sense that it is usually significantly above the continuum. In no case is this H and K emission to be confused with the normal emission core reversal in late-type single stars which gives rise to the Wilson-Bappu effect.

Struve (1946) studied the variation in the strength of the H and K lines as a function of phase angle in several stars. It was his conclusion that the maximum strength was at the quadrature points (0^{P}25 and

TABLE 3

LIST OF RS CVN BINARIES

Name	V_{max} (a)	Orbital Period(b)	Spectral Type hot + cool(b)	Masses (a,c) hot + cool
UX Ari	6.5	6.438	G5V + K0IV	0.63 + 0.71
CQ Aur	9.0	10.621	G0	
SS Boo	10.3	7.606	dG5 + dG8	1.00 + 1.00
SS Cam	10.0	4.824	dF5 + gG1	— ...
RU Cnc	10.1	10.173	dF9 + dG9	
RS CVn	8.4	4.798	F4V-IV + K0IV	1.35 + 1.40
AD Cap	9.8	6.118(d)	G5	0.5 + 1.1
UX Com	10.0	3.642	G5-9	0.95 + 1.12
RT CrB	10.2	5.117	G0	1.27 + 1.34
WW Dra	8.8	4.630	sgG2 + sgK0	1.4 + 1.4
Z Her	7.3	3.993	F4V-IV + K0IV	1.22 + 1.10
AW Her	9.7	8.801	G2IV + sgK2	1.38 + 1.36
MM Her	9.5	7.960	G8IV	1.20 + 1.24
PW Her	9.9	2.881	G0	1.4 + 1.5
GK Hya	9.4	3.587	G4	1.2 + 1.3
RT Lac	9.0	5.074	sgG9 + sgK1	0.6 + 1.5
AR Lac	6.9	1.983	G2IV + K0IV	1.30 + 1.30
RV Lib	9.0	10.722	G5 + K5	2.2 + 0.4
VV Mon	9.4	6.051	G0	...
LX Per	8.1	8.038	G0V + K0IV	1.23 + 1.32
SZ Psc	7.3	3.966	F8V + K1V-IV	1.33 + 1.65
TY Pyx	6.9	3.199	G5 + G5	1.20 + 1.22
RW UMa	10.2	7.328	dF9 + K1IV	1.50 + 1.45
RS UMi	10.1	6.2(e)	F8(e)	
HR 1099	5.9	2.8(e)	G5(e)	0.18 + 0.23
HR 5110	5.0	2.613	F2IV + KIV	0.02 + 0.005
HD 5303	—	1.840(f)	G2V + F0(f)	— —
HD 224085	7.6(g)	6.724(g)	K2-3IV-V(g)	
W92	11.7(h)	0.745(h)	K0IVp(h)	...

Notes for Table 3

a Unless otherwise noted values from Popper and Ulrich (1977).
b Unless otherwise noted values from Hall (1976)
c $M \sin^3 i$
d Popper and Ulrich (1977) list as 3.0 days
e Popper and Ulrich (1977).
f Hearnshaw and Oliver (1977).
g Rucinski (1977)
h Walker (1978).

$0\overset{p}{.}75$) Oliver (1974) summarized the existing data by saying that the emission was usually at a minimum during the secondary eclipse, but not in all cases, nor at all times. Hiltner (1947) had found a disappearance of the H and K emission lines at secondary eclipse in RS CVn. This led him to believe that the emission originated from localized sources at the extremities of a tidal bulge along the line joining the two stars. Struve (1946) had earlier offered a similar explanation for the origin of the emission in similar cases. Catalano and Rodono (1968) were unable to confirm the disappearance of the Ca II emission lines at secondary minimum, thus raising some doubt as to the validity of Hiltner's tidal bulge hypothesis. More recent studies by Weiler (1975a, 1978a) find that the emission is associated with the larger star, but the emission is not localized. Furthermore, Weiler does not find the strengthening at the quadriture points or the tendency for the emission to weaken at secondary minimum.

The existence of Ca II emission is indicative of chromospheric activity (Young and Koniges 1977, Weiler 1975a, Naftilan and Drake 1977, and Weiler 1978a). This emission must originate from the larger (cooler) component because the emission lines have velocities which agree well with the absorption lines for this component (Popper 1961, Oliver 1974). In addition, the width of the emission lines is of the proper amount to be explained by the synchronous rotation of the larger star (Popper 1970).

The emission lines of Ca II are not the only emission lines which have been reported. Weiler (1978a) studied 6 RS CVn systems and found H_α to be in emission in all 6. Naftilan (1975) found H_α to be in emission (weakly) in RS CVn itself. The H_α emission in AR Lac has been associated with the cooler star by Naftilan and Drake (1977). The H_α emission in the six systems studied by Weiler (1975a, 1978a) was variable to a significant degree in four of them. Similar emission in the H_α line has been reported by Bopp (1976) for the systems HR 1099 and UX Ari. However, it was noted that these were the only two stars from a survey of about 30 stars which showed persistent H_α emission. Three other stars showed sporadic H_α emission at the resolution used. Weiler (1978b) points out that at higher resolution it is possible that all RS CVn binaries may show some filling in of the H_α line by emission.

The H_α and H and K emission in several RS CVn binaries has shown correlation with the phase position of the distortion wave and the phase of greatest emission (Bopp 1976, Herbst 1973; and Weiler 1975b, 1978a). In addition Weiler finds the distortion wave more pronounced the greater the correlation. This is strongly suggestive of a physical relationship between the causes of the two phenomena. Weiler (1978a) suggests that the emission is due to an active photosphere which in turn drives an active chromosphere in the region of the photospheric activity. Young and Koniges (1977) attribute this to tidal coupling which increases the density scale height and thereby changes the acoustic-wave power spectrum. These investigators feel that the results support Hall's (1972) model for a spotted surface on the cooler component in RS CVn, and possibly other stars with similar characteristics.

Oliver (1974) found a variation in the absorption line strengths but the correlation with light curve variations was weak.

The abundance of metals in binary systems was studied by Miner (1966). In the systems he studied, an underabundance of metals was found in eclipsing binaries. The underabundance does not appear to be as great in the 3 RS CVn systems which were included in the project as for the other eclipsing systems. The sub-giant components of 12 Algol-like binaries were observed by Hall (1967) and found to have an underabundance of heavy elements. Naftilan (1975) found the cooler stars in RS CVn and RW UMa to be underabundant in iron and chromium, which he noted is in contradiction to a pre-main-sequence state of evolution. The cooler component of AR Lac was also found to be deficient in metals by Naftilan and Drake (1977). Andersen and Popper (1975) concluded that from the observed radius and temperature of the stars in TY Pyx there is an indication of an abundance (or opacity) anomaly in both stars. This would seem to indicate that RS CVn binaries are not very young. Naftilan and Drake (1977) have concluded from their research that the anomalously low metal abundance is not due to free-free emission filling-in the metal lines in AR Lac, nor is it due to a circumstellar shell. Recent soft X-ray emission from UX Ari has led Walter, Charles, and Bowyer (1978) to conclude that the heavy element depletion in this system is real, because they do not observe an Fe emission line at 0.85 KeV as was seen in the X-ray spectrum of Capella.

Lithium (Li) has not been detected in several RS CVn binaries, this supports the view that these stars are not very young (Naftilan and Drake 1977, Young and Koniges 1977, and Conti 1967). On the other hand, Wncinski (1977) has found a weak Li line in HD 224085. This system was recently added by Hall (1978) to the list of RS CVn type binaries.

As has been mentioned previously, a correlation between chromospheric Ca II emission and tidal coupling has been found by Gratton (1950), Young and Koniges (1977), and Glebocki and Stawikowski (1977). The investigators do not agree, however, as to the cause of the emission.

Young and Koniges believe that this is evidence that when a star's outer atmosphere is affected by gravitational attraction of a close companion the result is a change in the density scale height. This shifts the acoustic-wave power spectrum to lower frequencies, which results in a large increase in the dissipation of energy into the chromosphere. Gratton believed that the tidal distortion would produce localized regions of emission in accordance with Hiltner's model. However, the latter interpretation was excluded by Struve (1949) when he was unable to find the expected degree of linear polarization from such a localized region. Weiler (1978a) was also unable to find the variation in the H and K emission lines as a function of phase that would be expected from the tidally distorted bulge. He concluded that the emission may well be somewhat localized, but not at the extremities of a tidal bulge formed along the line joining the two stars. Glebocki and Stawikowski believe that their study of H and K emission supports the tidal bulge hypothesis, while Weiler feels that his research clearly points to an active chromosphere. Time may resolve the dispute.

Photometric anomalies

The light curves of many (if not all) of the RS CVn binaries show various anomalies. The most common and striking light curve anomaly is a quasi-sinusoidal wave that distorts the normal eclipse phenomenon as can be seen in Figure 1. This wave-like distortion has been referred to as the 'distortion wave' by Oliver (1974), this term will be used throughout this dissertation. There are, however, other phenomena which are abnormal in the light curves of these binaries. Several of the systems show season-to-season changes in the system brightness, while a few have exhibited increases in brightness over very short time scales. The

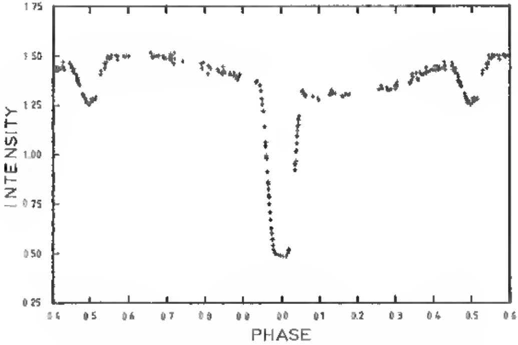

Fig. 1 -The 1975 visual light curve of RS Canum Venaticorum.

short time scale variations have been referred to as flare-like activity by some observers. These irregular changes in the light of the system cannot be explained by changing parameters of the distortion wave, and are therefore discussed as separate (but perhaps related) phenomena. Besides the variations in the light of the system, the light curves of these binaries have two additional anomalies which warrant mention. First, the depth of the primary eclipse in several systems has shown variations, which are not associated with changes in system brightness. Second, the secondary eclipse for many systems has shown variations in its position and depth.

The distortion wave in RS CVn was first noted by Sitterly (1930) as a difference in the heights of the maxima. This observation was noted by several researchers before the true picture was developed by the Italian astronomers at Catania. Following the advice of Popper (1961) the Catania astronomers (Chisari, Lacona, Catalano, and Rodono) started a long-term program of photoelectric observations of RS CVn. This work produced the remarkable discovery that the difference in the heights of the maxima was changing, and the changes could be explained by a migrating quasi-sinusoidal wave superimposed on the light curve. Chisari and Lacona (1965) and Catalano and Rodono (1967, 1968) showed very convincing evidence for the existence of this wave, and for the slow migration to decreasing phase angle from season-to-season. They referred to the slow shift of the distortion wave to decreasing phase as a "retrograde migration." Oliver (1974) has shown that this property is very common in the RS CVn binaries which he studied. It is commonly held that the existence of the distortion wave and the retrograde migration are properties that all RS CVn binaries share. The evidence is not complete for all the systems considered to be of the RS CVn binary type, but many systems have shown this phenomenon (Bopp, Espenak, Hall, Landis, Lovell, and Rencreft 1977, Oliver 1974, Hall 1972, 1977, Popper 1974, Chambliss 1976, Milone 1968; Nelson and Duckworth 1968; Hall, Henry, Burke, and Mullins 1977; Hall, Montle, and Atkins 1975, Blanco and Catalano 1970, Landis, Lovell, Hall, Henry, and Renner 1978, Hearnshaw and Oliver 1977, and Rucinski 1977). Many of the above investigators reported migration rate changes, and variations in the amplitude of the distortion wave from season-to-season. Perhaps significantly, Eaton (1977) has found the distortion wave to be moving to increasing phase in the system SZ Psc. The retrograde migration in SS Boo has apparently reversed itself according to Hall (1978). The color dependence of the distortion wave amplitude is very interesting. For most of the systems (reported in the aforementioned publications) the amplitude is greater in the V band than in the B band. However, there are notable exceptions to this: WW Dra (Oliver 1974), RT Lac (Milone 1968), UV Psc (Sadik 1978), and SZ Psc (Eaton 1977).

In addition to variations in the amplitude of the distortion wave within a system, the size of the amplitude varies a great deal from system to system. The largest amplitude appears to be about $0^{m}2$ for RS CVn (in the V band), and the smallest appears to be about $0^{m}02$ for several other systems. Recently, information as to the actual shape of the distortion wave has become available. Rucinski (1977) noted an interesting change in the shape of the light variations for HD 224085, and the present writer (Ludington 1978) has noted changes in the detailed shape of the distortion wave in RS CVn. Hall, Montle, and Atkins (1975) noticed a change in the shape and/or amplitude of UX Ari from their UBV and JHKL photometry in 1972. The significance of these variations is not clear, but they would seem to point to dynamic structures on the stellar surfaces

Popper (1967) and Oliver (1974) have noted that the RS CVn systems show small irregular variations in the system brightness. Wood (1946) was perhaps the first to observe these irregular variations in the system AR Lac. More recently, Bopp et al. (1977) have found evidence for irregular variations of $\pm 0^{m}02$ in the output of HR 1099. Larger variations have been discovered in the brightness of UX Ari by Hall (1977) and Landis et al. (1978). The latter group also detected a flare-like event of JD 2443054.76 which lasted for approximately one hour, and increased the system brightness by $0^{m}15$.

The irregular variations discussed in the last paragraph refer to the total system brightness. Light variations have been reported during the primary eclipse by Wood (1946) and Keller and Limber (1951) for AR Lac and RS CVn, respectively. Similar changes during primary eclipse have been noted by Popper (1961) for RS CVn, Milone (1977) for RT Lac, Nelson and Duckworth (1968) for RS CVn, and Oliver (1974) for SS Boo, WY Cnc, RS CVn, Z Her, AR Lac, RT Lac, and SZ Psc. It should be noted that several of these systems have total (occultation) primary eclipses. Therefore, if the variation is seen during this total phase, it is expected that the variation is due to intrinsic variability of the larger (cooler) star only. In the case of AR Lac, this is not the case. The total portion of primary eclipse was seen to have small or no variation (Kron 1947). Kron found that the variation occurred during the ingress and egress branches of the eclipse.

Since the primary eclipse in RS CVn is total, then the secondary eclipse will be annular. Thus, since the larger star is still visible, it is not surprising that this eclipse also shows anomalous behavior

Keller and Limber (1951) found that from the depth of the eclipse the ratio of intensities was much less than would be expected for stars of the spectral types which make up RS CVn. Popper (1961) found the same inconsistency with the system but also found the discrepancy to be less severe. In addition, Keller and Limber reported a small eccentricity from the displacement of secondary eclipse. Neither the spectroscopic orbit of Joy (1930), nor the orbit of Popper (1961) showed anything but a circular orbit. The distortion wave discovered by the Catania observers supplies the explanation for both the changing depth of primary minimum and for the displacement of the secondary eclipse from the 0^P5 position. The variation in brightness at the total phase of primary eclipse and the displacement of secondary eclipse are correlated with the migration of the distortion wave. Hall's (1972) model took the distortion wave explanation one step farther. If the spotted region that Hall predicts does indeed exist, then the anomalous depth of secondary eclipse is explained by the variation of the surface brightness of the larger star. Hall's spot model also explains the displacement of secondary eclipse in more concrete terms.

Optical and radio polarization

The polarization of the electromagnetic radiation from RS CVn binaries was first searched for by Struve (1948). In this study he attempted to locate the linear polarization which would result from the tidal bulge proposed by Hiltner (1947) as the origin of the Ca II emission. The H and K lines of AR Lac showed no evidence of linear polarization. Struve placed an upper limit of 10% on the polarization from this star. In a survey of unevolved and evolved main-sequence binary systems Pfeiffer and Koch (1977a) found that the unevolved systems showed no significant linear polarization. The evolved binaries showed intrinsic linear polarization if the log S was greater than or approximately equal to 1.0. Here the 'S' represents the separation of the stellar photospheres in units of solar radii. They further stated that the incidence of polarization in this group does not depend on mass ratio, total system mass, fractional component size, rotational velocity, the stage of evolution (Case A or Case B), or the detached or semi-detached state of the system. It was their belief that this was evidence for the necessity of sufficient "free" volume to allow more material and/or greater asymmetry to produce the linear polarization.

Three RS CVn binaries have been reported to have some degree of polarization. RS CVn was reported to display variable linear polarization by Pfeiffer and Koch (1973). The variation was cyclic with orbital period and showed random short-term variation. This was suggestive to them of electron and/or Rayleigh scattering in an active circumstellar envelope. Only an upper limit could be set by Pfeiffer and Koch (1977b) for the linear polarization in the visual band for HR 1099 (less than 0.02%). At radio wavelengths no significant linear polarization has been detected for HR 1099 or UX Ari, but a significant degree of circular polarization has been detected (Owen et al. 1976, and Spangler 1977). The degree of circular polarization was found by them to be a function of wavelength, and was only detected during outburst activity. This was suggestive of microwave bursts like those observed from the sun.

Pfeiffer (1978) recently reported on some very detailed polarization studies of RS CVn. He concludes that the polarization is due to scattering in a large cloud which engulfs the system. He also comments that RS CVn itself is the only RS CVn binary in which he has been able to detect linearly polarized light, as of the time of his presentation.

Ultraviolet and Infrared excess

Oliver (1974) has done the most comprehensive study of ultraviolet (UV) excess in the RS CVn binaries. It was his conclusion that an ultraviolet excess was a common occurrence in the U-B color index of the cooler component. Since few of the stars have UBV data available, it is conceivable that virtually all the systems have a cooler component with a UV excess. Recently, Rhombs and Fix (1977) presented data which confirmed very clearly the UV excess in RS CVn, AR Lac, and UX Ari. They also were able to show that the cooler component was responsible in each case. Hall (1972) suggested that the excess could possibly be analogous to the excess in T Tauri stars. Rhombs and Fix, on the other hand, concluded that free-free emission from a hot circumstellar gas was the best explanation.

Infrared (IR) excess, like the ultraviolet excess, appears to be a common characteristic of nearly all RS CVn binaries. The problem of the infrared excess has been discussed by several authors (Atkins and Hall 1972, Hall, Montle, and Atkins 1975; Hall 1976, and Milone 1976a, 1976b). There is general agreement that at least the majority of RS CVn binaries display some degree of infrared excess, but the source of the excess is controversial. Milone (1976b) found an IR excess in 10 of 14 systems showing light curve asymmetries, which were chosen at random for study. Of this group, 5 systems are classed by Hall (1976) as RS CVn binaries. Three of these were definitely found by Milone to have an infrared excess. He cautioned, however, that the other two stars (SS Boo and WW Dra) may well show the excess because the spectral type and light ratios were taken from the literature and could cause a mis-evaluation of the excess. Atkins and Hall (1972) found an infrared excess in 5 or 6 systems for which they had sufficient data to make an adequate evaluation. Milone (1976a,b) considers the IR excess to be due to a circumstellar gas around the more massive component of the system. Atkins and Hall (1972) did not consider a circumstellar cloud a possible explanation for the JHKL photometry they had obtained. This question remains unsettled, but in light of the polarization data of Pfeiffer (1978) it would seem that a circumstellar cloud may be the correct explanation at least in the single case of RS CVn itself.

Period variations

The period variations in many of the systems listed by Hall (1976) are very pronounced. He noted that a linear ephemeris in some cases can lead to errors of about a quarter of an orbital cycle in only 10 years or so. Hall suspects that virtually all of the systems have these large period variations, because about a third are known to, and the rest have insufficient data.

Since the RS CVn binaries are detached systems, the period changes are not due to the same mechanism as in the semi-detached Algol-type binaries. In the previous section on the history of RS CVn it became apparent that the period changes are also not due to apsidal motion or light-time effects of orbital motion. Therefore, it is very clear that the mechanism responsible is rather unusual.

Flare-type mass ejection from one hemisphere has been proposed as an explanation for the short-term period changes (Hall 1972, Arnold and Hall 1973, Hall 1975b, and Hall 1976). In this model the brighter hemisphere is ejecting matter by a high-velocity impulse-type mechanism. This results in a correlation between the observable short-term period changes and the observable phase of the distortion wave minimum. The mass loss rate required to account for the period variations is rather large $10^{-6} M_{\odot}$/year. In the latest version of this model, Hall (1976) suggests that the effective moment arm is some Alfven radius so that the required mass loss rate is reduced.

Several aspects of this model have been criticized. Catalano and Rodono (1974) objected to ejection of material from the brighter hemisphere on the grounds that one would expect flare-type mass ejection from the active spotted hemisphere. They also pointed out that the measurement of the time of minimum was affected by the deformation of primary eclipse by the distortion wave. This effect would have the same sense as the correlation of distortion wave minimum with period change. Hall (1975b) was able to show that, while it was true that the effect had the same sense, the magnitude of the O-C variations by deformation of primary eclipse were 25 times too small.

In the case of AR Lac it has been possible to use a modification, for this specific system, of the model to explain the long-term period changes (Hall, Richardson and Chambliss 1976). The long-term period variations in the other systems have not been adequately explained. Further research, both observational and theoretical, is greatly to be desired in this area.

The possibility of an enhanced stellar wind in RS CVn binaries has been proposed by Oliver (1974), Ulrich and Popper (1974) and Popper and Ulrich (1977). This is a conceivable source of period changes and deserves further investigation as pointed out by Hall (1976).

Emission at radio wavelengths

The detection of an RS CVn binary at radio wavelengths by Gibson and Hjellming (1974) was believed by them at first to indicate mechanisms similar to those for known Algol-like flares. The spectral index of the flare was definitely non-thermal as was the case for the Algol-like flares. Later work by Gibson, Hjellming, and Owen (1975) showed that the flares were non-thermal in UX Ari but that an evolving synchrotron source was a more likely mechanism than the infall of matter.

Gibson et al. (1975) compared the flare from UX Ari with those of UV Ceti stars, and found that there was little similarity. The spectral index for a UX Ari flare was about +0.2, while typical values for UV Ceti stars range from -3 to -5. Even at the end of the flare observed on 11, 12 August 1974 the spectral index of UX Ari only reached -0.6. Therefore, the type of flare is different from those in UV Ceti stars.

This was supported by the decay time-scales in the 2 types of flares. Gibson et al. (1975) found that a UX Ari flare decayed on a time-scale of days. This was about 100 to 200 times the decay rate of a flare in a typical UV Ceti star.

Circularly polarized emission has been detected at radio wavelengths by Spangler (1977), and Owen, Jones, and Gibson (1976) from 2 RS CVn binaries (UX Ari and HR 1099). The level of polarization was about 5% (for UX Ari) to 20% (for HR 1099) at 1400 MHz, about 9% (for HR 1099) at 8085 MHz, and less than 2% (for HR 1099) at 2695 MHz. The detection of circular polarization in these stars contrasts sharply with the lack of circularly polarized emission from Algol.

No linear polarization has been detected at radio wavelengths from any RS CVn binary at the time of this writing. Owen et al. (1976), however have put an upper limit of 2-3% at 2695-8085 MHz for the linearly polarized emission from HR 1099.

No correlation has been found between optical and radio variability as reported by Chambliss (1976) and Spangler (1977). This is not a surprising result if the flare-like activity is similar to the typical solar microwave flare. In these solar flares the energy output in the radio region is much greater than in the optical region.

Radio binaries tend to be of late spectral type (G and K), and they tend to be above the main-sequence according to Owen and Spangler (1977). This may be part of the explanation for the high frequency of radio emitters among RS CVn binaries. On the other hand, and perhaps more likely, the statistics may be biased by the selection of RS CVn binaries as candidates for radio emission surveys. More data are required to establish this point more clearly either way.

Owen and Spangler (1977) were unable to detect any change in the observed flux from AR Lac at 4585 MHz during any eclipse. This is a good indication, as they pointed out, that the source is not a compact region between the two stars. They computed that the radius and brightness temperature of a source located in this region would be limited by $r > 3 \times 10^{11}$ cm, and $T_b > 4 \times 10^{9}$ °K.

Gyrosynchrotron radiation has been suggested as the source of the radiation (Gibson et al. 1975, Owen et al. 1976, Spangler 1977, and Owen and Spangler 1977). These authors have found that this mechanism explains the radio flare observations better than other alternatives they have considered. It accounts for the observed non-thermal spectral index, the circularly polarized emission during flare events, and the absence of linear polarization (if reasonable assumptions are made about the physical properties of the emitting region).

A magnetic field of about 30 Gauss and an electron density of about 2.4×10^{10} cm^{-3} would be indicated by Spangler's (1977) calculations. Spangler et al. (1977) felt that this model compliments Mullan's (1974, 1976) theory, and therefore would also seem to support the starspot hypothesis of Hall (1972, 1976).

Soft X-ray emission

A most exciting discovery has been the recent detection of soft X-ray emission (0.2 to 2.8 KeV) from many RS CVn binaries. As of June 1978, Liller (1978) reported that 11 of the RS CVn binaries had been identified as X-ray sources. This compares with two or three identifications reported by Charles (1978) in April 1979. This discovery, along with the previously known radio emission, gave additional credence to the solar analogy of highly active regions in the atmosphere of the sub-giant component as proposed by Hall (1972, 1976).

Cash, Bowyer, Charles, Lampton, Garmire, and Riegler (1978) were able to fit a solar abundance plasma at about 10^7 °K to the soft X-ray spectrum of Capella. This star was included as a related system to the RS CVn binaries in Hall's (1976) discussion. It is not a "classical" RS CVn binary, so the importance of the above paper is clear only when subsequent soft X-ray data are reviewed. The soft X-ray spectrum of the "classical" RS CVn binary UX Ari was fit with a plasma of 10^7 °K, but it could not be fit with a plasma of solar abundance (Walter, Charles, and Bowyer 1978a). This gives additional evidence for an underabundance of heavy metals in RS CVn systems. This result was confirmed in two other "classical" systems, RS CVn itself and HR 1099, by Walter, Charles, and Bowyer (1978b). The spectra of these two stars could not be fit as nicely as was the case for UX Ari, but the authors found that the results were consistent with a 10^7 °K thermal spectra in both cases.

Walter et al. (1978a) felt that the soft X-ray spectra of RS CVn binaries was consistent with an active spotted region. In this model they saw the active region as associated with flare-like activity, which in turn would continuously supply sufficient energy to power a 10^7 °K corona. At this temperature they computed the velocity of the ions to be sufficient to rapidly deplete the matter. However, they noted that a magnetic field of only 50 Gauss would be enough to bottle up the hot plasma.

In addition to the above, Walter et al. (1978a) noted three interesting facts about the new information obtained from the X-ray detectors. First, they noted that if UX Ari is anything like a typical RS CVn binary, then from the space density of $\sim 10^{-5}$ pc^{-3} the RS CVn binaries contribute a full 10% of the soft X-ray background at low galactic latitudes. Second, they computed the mass loss rate from their emission measure. The value they obtained (10^{-10} $M_\odot$/year) is in reasonable agreement with that proposed by Ulrich and Popper (1974). Third, they reported that White, Sanford, and Weiler (1978) have detected a flare in the X-ray spectrum of HR 1099 which was coincident with a radio flare.

The evolutionary status

The evolutionary status of the RS CVn binaries has been an especially difficult problem. The mass of the components is generally of the order 0.5 to 1.5 $M_\odot$. This is for both stars and therefore, with few exceptions, the mass ratio is very close to unity. The picture that has developed over the last 10 or 15 years regarding binary star evolution has, in general, shown that mass ratios near unity should be the exception. RS CVn binaries are much too numerous to be an exceptional case. Thus a problem appears, either the binary evolutionary scheme is wrong or the RS CVn systems do not exist. Obviously, this is much too "black-and-white" a statement. More to the point, it would be expected that the theory needs some adjustment in order for the large number of systems with unity mass ratio to be explained. It is important to realize that the binary evolutionary theory referred to above explains the evolution after the existence of the binary pair on the main sequence. The evolution prior to this point is not well understood, and could very easily be the key to the unity mass-ratio puzzle.

The similarity of the characteristics of the cooler component of RS CVn to those of T Tauri stars led Hall (1972) to conclude that RS CVn was in pre-main-sequence evolution. This was in contradiction to the earlier investigation by Field (1969), who found that RS CVn as well as AR Lac were not in pre-main-sequence contraction. The age of the RS CVn binaries as determined by Montle (1973) supported the pre-main-sequence evolutionary picture.

Eventually, a clearer case arose for the post-main-sequence evolutionary status for the RS CVn binaries. This process started with Oliver's (1974) evaluation of the evolutionary status and his suggestion of a slow mass transfer by means of a strong stellar wind. Ulrich and Pepper (1974) proposed that by allowing for such a stellar wind it would be possible for the evolutionary status of these stars to be explained on the basis of normal single star models.

The pre-main-sequence status for binaries of the RS CVn type was almost conclusively eliminated as a possibility by Hall (1975b), and Biermann and Hall (1976). Hall (1975b) found that the visual companion of the eclipsing RS CVn binary WW Dra was a normal F8 V star. The most important thing about is was the estimate of its mass. It was less massive than either star in the WW Dra system. This clearly would indicate that the stars in WW Dra could not be in pre-main-sequence contraction. Hall also showed that there was sufficient evidence of binary motion for the possibility of an optical pair to be insignificant.

Biermann and Hall (1976) gave very convincing arguments to exclude the pre-main-sequence evolutionary status. They concluded by a process of elimination that the RS CVn binaries were the result of the fission of a single star as it leaves the main-sequence.

At the time of this writing, the consensus is that the evolutionary picture as presented by Popper and Ulrich (1977) is the closest to reality. They presented the following circumstantial evidence of post-main-sequence evolution of RS CVn binaries:

1. They are not associated with regions of known star formation.
2. For the mass and radius range the post-main-sequence life-time is 100 times longer than the pre-main-sequence life-time.
3. The larger radius is associated with the more massive component.
4. WW Dra and HR 1099 have dwarf companions of lower luminosity.

In addition, they recalculated the age of the RS CVn binaries using Mentle's (1973) value for the velocity dispersion and Wielen's (1974) calibration. The results indicated that the RS CVn binaries are about $3x10^9$ years old (i.e. about the same age as similar main-sequence stars). In fact, they felt that the age is very slightly greater than a main-sequence star, and that the RS CVn binary phenomenon develops when stars of this general nature reach the Hertzsprung gap. In some cases they proposed that it would be necessary to modify simple single star evolutionary processes by a slow stellar wind ($\approx 6 \times 10^{-11} M_{\odot}$/year) in order to account for the system's current position on the H-R diagram.

Scope of Dissertation

The intent of this dissertation can be summarized by two goals:

1. To obtain two new light curves of RS CVn in (at the minimum) two colors, separated in time by approximately one year, however, the data for each must be obtained within a three month term in order to minimize the effect of a migrating distortion wave,
2. To determine the elements of the eclipsing system for RS CVn by a new technique which eliminates the problems introduced by the photometric distortion wave.

In meeting these two goals, several others will, by necessity, result:

3. The constancy of the comparison star BD+35° 2420 will be confirmed.
4. The distortion wave will be isolated so that it may be studied in a future research effort.
5. The radial pulsation model for the photometric distortion wave will be refuted.

CHAPTER II
INSTRUMENTATION

The Basic Equipment

The instrumentation used in collecting the data presented in this dissertation may appear to some in the avant-garde of instrumental development as antiquated. This sentiment is partially due to the enormous technological development during the past decade. In addition, this attitude reflects a prevailing view that innovation is superior. Snobbery and high technological advance aside, the important point is that the data presented here of RS CVn are of the highest quality.

The 46 cm telescope used in this investigation is located at Rosemary Hill Observatory, 8.5 km from Bronson, Florida. The optics, telescope tube, equatorial fork mount, and pier were built by R. E. Brandt. The electrical drive, slow motion controls, secondary mirror mount, finder scope, counter weight, and setting circles were installed by the staff at the University of Florida (primarily, John P. Oliver, E. Whit Ludington, and Ell Graves). The optical system is an f/10.5 Ritchey-Chrétien design. The mirrors of the system are aluminized and Beral overcoated.

The photometer has been described by Chen and Rekenthaler (1966). Four diaphragms are available; they are small circular openings of 0.500, 0.2500, 0.079 and 0.038-inch diameters on a rotatable disk. The smallest opening was used in all of the photometry presented here, this corresponds to a diameter of 42.5 arc seconds on the sky.

There are three filters which the user may select. The light passes through only one filter at a time, and the observer must manually move the slide on which the filters are mounted to the desired filter before a reading is taken. The ultraviolet filter (u) is made from Corning 9863, the blue filter (b) is made from Corning 5030 and Schott GG13 in combination, and the yellow (or visual) filter (v) is made from Corning 3389. These filters, in union with the same instrumentation used in this photometry of RS CVn, have been found by Markworth (1977) to match closely the standard UBV system. The photomultiplier tube used in this work was an EMI 9781, operated at 900 volts.

A DC electrometer amplifier designed by Oliver (1976) was used to amplify the current from the photomultiplier tube. This amplifier, called PA-10, has many different gains which may be selected by rotary switches. This allows an amplification from 0 to 10^5. The amplifier was used with a time constant of ½ second.

All of the data were recorded on a Heath chart recorder with a fiber-tip pen operated by a servo-type motor. The observer may select from a wide range of speeds on this chart recorder. In all the recordings of RS CVn, speeds of either 1 inch/min or 0.5 inch/min were used.

The data from 5, 6 March 1976 onward were also recorded manually from a digital integrator. This instrument, referred to as DA-10, was designed and built by John P. Oliver. It integrates the signal by counting the pulses from a voltage-to-frequency converter in the PA-10 amplifier. The observer has the option of many integration times from 1 second to 100 seconds. The integrations are started manually, but are stopped and displayed by the internal electronics.

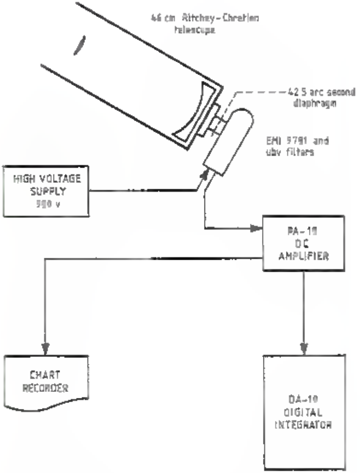
46 cm Ritchey-Chretien telescope
42.5 arc second diaphragm
EMI 9781 and ubv filters
HIGH VOLTAGE SUPPLY 900 v
PA-10 DC AMPLIFIER
CHART RECORDER
DA-10 DIGITAL INTEGRATOR

Fig. 2.--Schematic diagram of the instrumentation used to obtain the photometric data of RS CVn at Rosemary Hill Observatory during the years 1975 and 1976

A schematic diagram of the instrumentation appears in Fig. 2.

From MJD 42469 to MJD 42492, inclusive, the attachment of the photometer to the telescope required the use of a glass-prism diagonal. The glass in the prism is opaque to the ultraviolet region of the spectrum, for this reason only the v and b filters were used. Since no u data were obtained during this time, it was impossible to compute the u-b color. This explains the absence of values for these dates in the tabulation in the appendix.

Amplifier Calibration

It is desirable that the amplifier be linear and stable for high quality photometry. The linearity of the PA-10 has been demonstrated by Oliver (1976). The stability can be demonstrated by the nightly calibrations obtained during the course of this research.

Usually at the beginning and end of each night of observing, a calibration sequence was obtained. A calibration sequence consisted of a set of deflections with the input to the amplifier disconnected and the internal calibration source as the input current. The calibration consisted of four steps:

1. Establish the value of true zero.
2. Measure the relative gain of adjacent settings on the rotary switch that selects the smaller gain increments (called the fine-gain switch).
3. Measure the gain of each setting on the rotary switch that selects the larger gain increments (called the coarse-gain switch) relative to the 'CAL' setting.
4. Check the zero value.

The results of the above measurements were then used in the data reduction (see Chapter III).

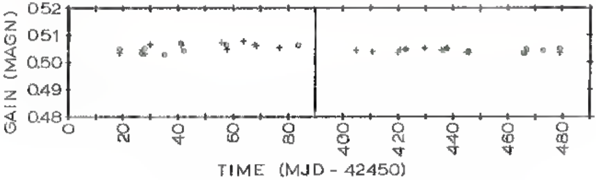

Fig. 3.-Fine-gain stability. The start and the end of a night calibration is indicated by o and +

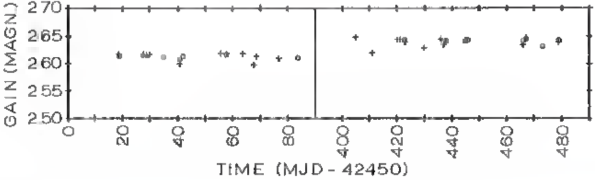

Fig. 4.-Coarse-gain stability. The start and the end of a night calibration is indicated by o and +

In Figures 3 and 4, the relative gains for settings of the fine-gain and coarse-gain switches are presented, respectively. From inspection of these figures, it is clearly evident that the short-term stability and the long-term stability of the amplifier are very good. In Fig. 4 a difference in the level of the coarse-gain is evident from 1975 to 1976. This is of no significance in differential photometry such as that presented here on RS Canum Venaticorum.

CHAPTER III
PROCEDURE AND DATA REDUCTION

Observational Procedure

The accuracy that can be achieved with modern photoelectric photometers is limited by the earth's atmosphere more than by any other factor. The earth's atmosphere is not completely transparent; it does not even have the same transparency at all wavelengths of light. The problem of measuring the intensity of stars is further complicated by the random and unpredictable fluctuations in the transparency of the atmosphere as a function of time, and the somewhat predictable change as a function of airmass.

There are means of reducing the effects of a real atmosphere on the measurement of a star's light. The most important is to measure the light differentially. By this it is meant that a star of constant brightness, called the comparison star, is chosen as a reference. The brightness of the program star, called the variable star, is measured under the same atmospheric conditions as the brightness of the comparison star. If the atmospheric conditions are exactly the same when the brightnesses of the two stars are measured, and the comparison star is indeed of exactly constant brightness, then any variation in the ratio of the variable star brightness to the comparison star brightness is due solely to the variable star.

Of course, it is not possible in practice to guarantee that the atmospheric conditions are exactly the same during the measurement of both stars The best way to insure that these conditions are as nearly identical as possible is to choose a comparison star which is very near in the sky to the variable star, and then to measure their brightnesses in as short a time span as possible. The nearness in the sky of the comparison star to the variable star and the nearness in time of measurement of their respective brightnesses are the two most important factors in high accuracy differential photoelectric photometry. Other criteria which will help improve the accuracy of the differential measurement are the following

1. The comparison star should be nearly the same color as the variable star
2. The comparison star should be of nearly the same brightness as the variable star
3. The amount of atmosphere through which the measurements are taken should be kept to a minimum.
4. The amount of scattered light from the background sky (which cannot be avoided) should be measured and minimized.

For the observations presented here, these conditions have been quantitatively met by the following procedures

1. The comparison star is only 71 arc minutes from the variable star in the sky
2. The typical sequence used to obtain the intensity measurement and the time required are given schematically on the following page.

1975	time required (sec)	1976	time required (sec)
	45		45
C	3 x 30	C	3 x 30
	30		30
SC	3 x 30	SC	3 x 30
	30		45
C	3 x 30	V	3 x 30
	45		30
V	3 x 30	VS	3 x 30
	30		
VS	3 x 30		
	30		
V	3 x 30		
total time	750 (≈12¼ min)		510 (≈8½ min)

Where C represents the measurement of the comparison star's brightness in three colors (v,b,u), CS is the three-color measurement of the sky near the comparison star, V is the three-color measurement of the variable star, and VS is the three-color measurement of the sky near the variable star. The integration time for each color measurement was always 30 seconds, the time to set the telescope on the comparison star or the variable star was usually about 45 seconds, and the time to move the telescope to a region of the sky near a star (or back again) devoid of visible stars was typically 30 seconds.

3. The colors of the comparison and variable stars are

   Variable (RS VCn) B-V = 0.55 and U-B = 0.05 (Oliver 1974)
   BD+35° 2420 B-V = 0.47 and U-B = 0.03 (Oliver 1974)

4. In no case was a differential measurement made through more than two air masses.

5. Typically the sky brightness was measured at least every half hour, or after the measurement of each star, if the sky brightness was changing rapidly. To minimize the sky contribution to the signal, the smallest diaphram available on the photometer was always used (42.5 arc seconds in diameter).

6. To determine if the comparison star was indeed of constant light, a check star was observed occasionally.

The above discussion assumes that the instrumentation is linear and stable to within the requirements of differential accuracy. If this is the case and the above criteria are met, then all that remains is the calculation of the ratio of the variable star brightness to the comparison star brightness. In making these calculations it will be possible to correct, in part, for the atmospheric extinction which has been minimized, but not eliminated by the proper choice of a comparison star.

It was pointed out in Chapter II that the majority of the data exists in two forms— chart records and tabulations manually recorded from the DA-10 digital integrator. The chart records made prior to 5, 6 March 1976 were read and recorded in a tabulation form exactly like that used on and after 5, 6 March 1976. The keypunch shop of the Northeast Regional Data Center was engaged to punch these data on standard computer cards, in a format called the "Ludington-Oliver" format (see Table 4). A computer program called PHRED (PHotoelectric REDuctions) was written to accept this format for the raw data and to do the reduction to the instrumental system (except for the inclusion of the effects of atmospheric extinction). The application of the effects of a real atmosphere to the partially reduced output of PHRED is handled by a computer program called DEXTOR.

PHRED

Introduction

PHRED is a computer program that is written in the PLI programming language. It is a very versatile program for reducing photoelectric observations to the instrumental system. It has far vaster capabilities and fewer limitations than any other available reduction program. It is limited by the size of the computer used rather than by the observations. It can, for example, handle the observations of over 600 different objects in 200 different filters taken during one night of observing. PHRED can be instructed to produce a plot for any object-filter combination the user may desire. This can be very helpful in evaluating the quality of the observations. In addition, the user can instruct PHRED to calculate the principal extinction coefficients, the outside-the-atmosphere magnitude and the standard errors of each. Furthermore, the program is not restricted to variable star data. It can also do the reduction of standard stars to the instrumental system. PHRED does all normal reduction, except atmospheric extinction and the reduction to the standard system. For example, it corrects for a zero offset in the data-gathering system. It converts to heliocentric Modified Julian Date. It applies gains, unless the user is using a pulse counting system, in which case the gains will be ignored. All in all, the user has a great deal of control over the operation of the program, and very few assumptions have been made about the way the data must be taken, or the organization they must be in for reduction by this program. Of equal importance to the user of PHRED is the detailed log of the reduction and the warning messages to help the user gain the desired results.

Program Control

The user instructs the program to do certain things by use of Control Cards. These are records that start with an asterisk (*). The asterisk is followed by one letter of the alphabet. This letter determines the option that is to be used or the type of parameter cards that will follow it. Any characters after the first letter will not be recognized by the program.

The first step in using PHRED is to have the data prepared on cards in the Ludington-Oliver format. The outline of this format is given in Table 4. Any item on which a deflection can be taken is defined by the user with an object code. This includes sky deflections,

TABLE 4

LUDINGTON - OLIVER FORMAT

ITEM	COLUMN	FORMAT	EXAMPLE-COMMENTS
Object Code	01-02	A(2)	C0,SC,S1,S2, etc
Object Name	03-12	A(10)	BD-16 1734, RS CVN, etc
Modified JD(a)	13-17	F(5)	42451, 00000, any 5 digits
Filter Code 1	18	A(1)	V, Y, R, etc (c)
UT 1	19-24	F(6)	043012, hhmmss
Gain 1	25-27	A(1), A(2)	D04, 'D' is coarse gain, '04' is fine gain
Defl 1	28-32	F(5)	00120, 00120, 98766, etc
Filter Code 2	33	A(1)	B, I, X, etc
UT 2	34-39	F(6)	105959
Gain 2	40-42	A(1), A(2)	E04
Defl 2	43-47	F(5)	00001
Filter Code 3	48	A(1)	U, S, B, etc
UT 3	49-54	F(6)	001059
Gain 3	55-57	A(1), A(2)	A02
Defl 3	58-62	F(5)	00000
Observer	63-65	A(3)	EWL, JPO, REN, FDW, etc
Telescope	66-68	A(3)	046, 300, dia in centimeters
Photometer(b)	69-71	A(1),A(1),A(1)	Codes for amplifier, filter set, photomultiplier tube
Observatory	72-74	A(3)	RHO, FAS, MCD, etc

Notes for Table 4.

(a) The Modified Julian Date of each deflection is calculated by the following equation

$$MJD(obs) = MJD(col\ 13\text{-}17) + DEC(UT)/24$$

(b) The photometer code is divided into three subcodes. The first is for the amplifier, the second is for the filter set used, and the third is for the photomultiplier tube used.

(c) Each record has room for only three deflections. If there are more than three deflections for each object code, these are then put on the following cards with the proper filter code for each. All other columns should be copied from the first card.

dark current, zero offset, variable star, standard star, etc There are two characters on the card for the object code There are no restrictions on which of the 256 characters of the EBCDIC character set may be used The filter code is used in a like manner There is room on a card for three filters to be coded If more are required, the data are continued on the next card by copying the object code The gain is an instrumental setting that causes the input from the photomultiplier tube to be amplified by a specific amount This must be accounted for in order to arrive at the true value before amplification The code that is used on the Ludington-Oliver format is comprised of two parts. The first part is for a setting of a coarse-gain switch, while the second is for a setting of a fine-gain switch. PHRED does not make any distinction between the two. It reads the three characters as a single code, therefore, the user must supply (in the control card section) the value for this combination of coarse and fine-gain control settings The deflection that is recorded will of course include the amplification indicated by the gain code The deflection is restricted to five digits. This should be sufficient for the most majority of the photoelectric photometry. The deflection fields must not include embedded blanks. A deflection is possible even when the signal current from the photoelectric device is exactly zero This is called the zero offset and must be removed from other deflections if the proper results are to be achieved. Therefore, PHRED will recognize an object code 'Z0' as the zero reading It will ignore the gain setting used and take the average of all such readings for that night and substract that value from all deflections before the gains are applied. The user must be aware of the proper use of the time for each observation. The Modified

Julian Date (which was defined by the IAU in 1973) is recorded on each card, this is actually the interger part of the Modified Julian Date The Universal Time (UT) is also recorded for each deflection Six columns are used for each UT The first two digits are for the hours, the second two digits are for the minutes, and the last two digits are for the seconds.

PHRED has been designed to perform several tasks for the user PHRED can process one night or multiple nights of observations in a single submission The first night of observations begins with a set of control cards, these might include the *LIBRARY, *FILTERS, *CODES, *SORT, *VARIABLE, *PLOTS, *BEGIN, and *TITLE control cards. The last two, however, have a special importance. The *BEGIN must be the first card in the control section and the *TITLE must be the last control card before the data The other control cards may be in any order. There are three additional control cards which are of special importance These are the *DATA, *ADD, and *END control cards *DATA must follow the title cards and proceed the data *END must follow the data *ADD is used if the user wishes to add additional data, but does not wish them to be considered as the original data For example, the observer may have neglected to take a comparison star deflection at the very beginning of the night. While this will not prevent the normal operation of PHRED, it will require extrapolation. To avoid this, the user can add an artificial deflection with the *ADD control card After the original set of data has been ended with an *END card, the user inserts the *ADD card followed by as many cards of additional data (in the Ludington-Oliver format) as he desires. The additional data are also ended with an *END card. The next night of observations will then follow, beginning with the *BEGIN CARD. It is not necessary to repeat all control cards for the second night if they were already used in the first night's control card section. That is, the second night will be processed with the same instructions as for the first night, unless the user changes them. For example, it is unlikely that the gains will have exactly the same values from night to night. Therefore, the *GAIN control card will probably be necessary in the second night's control section. On the other hand, the stars that were observed and the filters that were used will probably be the same, therefore, the user does not need the *LIBRARY, *CODES and *FILTER control cards in the control card section for the second night. Four of the control cards work in a "flip/flop" fashion, i.e., they are "off" until they appear for the first time, then they are "on" until they appear again, and then they are "off", etc. These are *MAGNITUDES, *INTERPOLATE ALL SKY, *SORT, and *VARIABLE.

In Figure 5 is a listing of the JCL cards for using PHRED. Notice that this assumes the existence of a load module for PHRED.

```
//JOBLIB  DD DSN=BDD350D1.S13.ATYLIB,DISP=SHR
//STEP1   EXEC PGM=PHRED
//SYSPRINT  DD SYSOUT=A,DCB=BLKSIZE=120
//RAWD      DD SYSOUT=A,DCB=BLKSIZE=120
//GRAPH     DD SYSOUT=A,DCB=BLKSIZE=120
//LOG       DD SYSOUT=A,DCB=BLKSIZE=120
//NSKY      DD SYSOUT=A,DCB=BLKSIZE=120
//DECK      DD SYSOUT=A,DCB=BLKSIZE=100
//DISK  DD UNIT=SYSDA,DSN=&&DISK,SPACE=(TRK,(3,3),,CONTIG),
//        DCB=(RECFM=F,BLKSIZE=80,DSORG=DA),DISP=(NEW,DELETE,DELETE)
//CARDS  DD  *,DCB=(RECFM=F,BLKSIZE=80,LRECL=80)
```

Fig. 5 - JCL cards for PHRED

Control Cards

Listed here are the control cards and their meanings.

*ADD -- Adds additional Data Cards to those already read and writes them into the Raw Data file (RAWD). The additional data should be ended with *END. The Ludington-Oliver format is used for additional data

*BEGIN -- The card should appear at the beginning of each new night of data. Each time this card is encountered, the previous night is known by PHRED to be complete and is then processed.

*BOTTOM -- This card should be the last card in the input deck. It will insure the processing of the last night of data.

*CODES FOR OBJECTS -- The following parameter cards define the object codes. A blank code terminates object code input. The codes are two characters long, left justified in a four-column field. For example,

V   SV C   SC K   SK

is the default if no codes are defined. Any code used in the data but not defined will cause a warning message to be printed in the LOG file, and the data will be ignored. Any code that is defined, but for which there are no data will not, of itself, cause an error. Note that stellar codes should be odd (1st, 3rd, 5th, etc.), sky codes should be even (2nd, 4th, 6th, etc.). The order of the codes is important if the *VARIABLE option is used.

*DATA -- This card signals the beginning of the data card observations. The data should be ended with *END. The data will be written into the Raw Data file (RAWD). The *DATA card must follow the last title card (see *TITLE).

*END -- This card is used to end a group of data cards. Either the original data or any and all additions to it are ended with *END.

*FILTER CODES -- The following parameter cards define the filter codes. A blank code terminates the set. The codes are one character in length, left justified in two-column fields. For example,

V B U

is the default if no codes are defined.

*GAINS -- The following parameter cards define the gain codes and their values. A blank code and value terminates the set. The codes are three characters in length, while the value can be as much as 12 columns long. The code and its value are separated by one space (an equal sign or any other single character may be used). Therefore, together they comprise 16 columns. For example,

```
D04=0.5049    E02=2.5D1234567 A06=-0.4999
```

is a valid gain code parameter card.
The default for this control card is to apply a gain of zero magnitudes to all the data points. A message will be written into the LOG to indicate this.

*HARDCOPY -- This card is included if a punched deck (or other machine readable copy) is desired of the reduced data. The parameter card can be used to control the contents of this output file. The parameter card format is a six-character field in columns one through six. There are, at the present, only three possibilities for the user to choose from.

ALL
NONE
V/C

"ALL" will cause the total of the NSKY printed file to be put into the DECK output file. "NONE" will cause nothing to be put into the DECK output file, while "V/C" will cause only the variable minus comparison data to be put into the DECK output file.

*INTERPOLATE ALL SKY -- Usually an observer will take deflections on a star and on the nearby sky. This will allow him to subtract the sky from the star deflection and be left with just the deflection due to the star. If this card is inserted, the program will use any even code interpolation of sky deflections. This means that if there are sky observations only with the comparison and none for the variable, the user must include this card. Without this card, the program subtracts the interpolated value of an even code from the value from the next smaller odd code. With this card, all even code values are combined and copied in place of the original even code values.

*JD OVERRIDE -- The following parameter card defines a five-digit number that will override the integer Modified Julian Date on the data cards. It must not have a decimal point or sign. For example,

42451

is a valid parameter card. The default is to use the integer Modified Julian Date on the data cards. Note that the integer Modified Julian Date coded on each card is used to compute the time for each of the deflections on the card. Therefore, the use of this control card option will cause all the cards to have the same Julian Date, even if the original data cards for a single night contained more than one Julian Date. The default is reestablished at the beginning of a new night of data.

*K-EXTINCTION COEFF -- If the user wishes to have extinction coefficients calculated, he may specify on the following parameter card(s) which star (or sky) and filter(s) he wishes used. There are no limits to this combination of object code and filter code. The format for the parameter card is a four-column field with the object code in the first two columns and the filter code in the third column (the last column is blank). For example,

V␢V SVV C␢V SCV

will produce extinction coefficients for the variable star, for the sky readings next to the variable, for the comparison, and for the comparison sky, all for the visual filter (assuming the object and filter codes defined in the examples for *CODES FOR OBJECTS and FILTERS) The default is to not calculate any coefficients.

*LIBRARY STARS -- The following parameter cards contain the "vital statistics" on the stars being reduced. The format for these cards appears below.

ITEM	VALUE	EXAMPLE	COLUMNS	FORMAT
Object code	comp star	C6	01-02	A(2)
name	BD-15°1734	BD-15 1734	03-12	A(10)
RA	$7^h15^m12^s$	7.2533333333	14-28	F(15,10)
Dec	-15°32'28"	-15.5411111111	29-43	F(15,10)

Note that when punched on the cards, the right ascensions and declinations must be converted to hours and decimal hours and degrees and decimal degrees. The last card must be a blank card to terminate the set. If no library parameter cards are used, then the *K-EXTINCTION COEFF control card option should not be used.

*MAGNITUDE -- If this card is used, the output will be in magnitudes instead of intensity units. The default is output in intensity units.

*N FULL SCALE -- The following parameter card will give the fullscale value expected for the data. This value will then be used to normalize all the deflections. This means that before anything else, the values punched on the data cards will be divided by this number. The number is read in from the first six columns of the parameter card using an F(6) format. For example,

```
100000
 10000
  1000
```

are all valid full-scale values. The default value is 10000.

*OBSERVATORY -- The following parameter card is used to read in the longitude, latitude, and (optionally) the station code for the observatory at which the data were taken. For example,

+82 5866666666 +29 377777777 RHO

is the default and/or the parameter card for Rosemary Hill Observatory. It is read by (F(15,10),F(15,10),X(5),A(3)) PL1 format. Longitude is a number between -180.0 and +180.0.

*PLOTS -- The following parameter cards are used exactly like the one for *K-EXTINCTION COEFF. They specify which object-filter combinations the user wants plotted. The codes and formats are the same as for the *K-EXTINCTION COEFF parameter cards. The plots are in magnitudes as a function of local time. No plot is the default.

*SORT -- This card, when used, will cause the sorting of every object-filter combination into time order. Sorted data are necessary for proper functioning of FHRED.

*TITLE -- This card signals the beginning of the title cards. The first of these cards will be used as a heading on all pages pertaining to this night of data. The rest (and there is no limit) will be printed on the heading of the RAWD print file. There must be a *TITLE card and at least one card following it. the *DATA card must then follow the last title card.

*VARIABLE -- If the data are arranged for it, the user can have the data treated as "variable star data." In this case the comparison star will be "removed" from the variable (to get relative brightness). This is done by dividing the variable star's reduced intensity by the interpolated comparison star's reduced intensity. If *MAGNITUDE has been used, the process will be the difference of the reduced magnitudes. The object codes must be listed after the *CODES FOR OBJECTS control card in this order: variable star, sky variable, comparison star, sky comparison, another star, another sky, etc

*X TIME OFFSET -- The following parameter card can have up to a 15-digit number (read by F(15,14)) This number is added to the Julian date computed for each deflection Its units must therefore be days

DEXTOR

Program Outline

DEXTOR is a program written in PL1 which applies differential extinction coefficients to a dataset like that produced by PHRED

If the instrumental system is nearly the same as the standard UBV system, a simple linear set of equations can accurately describe the effects of a real atmosphere The equations normally used are

(1a) $v^o = v - k \cdot X$,

(1b) $(b-v)^o = ((b-v) - k_1 \cdot X)/(1 + k_1' \cdot X)$, and

(1c) $(u-b)^o = ((u-b) - k_2 \cdot X)/(1 + k_2' \cdot X)$,

where the superscript "o" indicates the outside-the-atmosphere color or magnitude of the star, X is the airmass, v, b, and u are the magnitudes of the star as viewed through the visual, blue, and ultraviolet filters, respectively, and k, k_1, k_1', k_2, and k_2' are the extinction coefficients. For a detailed development of the above equations see Hardie (1962).

The above equations apply to the measurement of one star, but the data can better be reduced differentially, rather than as individual magnitudes of the variable and comparison stars In order to do this, it is necessary to develop a set of equations which describe the differential extinction computations. Start by defining a difference operator D( ) which is equal to the variable minus the comparison in magnitudes. The above equations can then be defined for the variable star and for the comparison star. It can be shown that equations (1) above become,

$$\text{(2a)} \qquad D(v)^{0} = D(v) - k \cdot D(X),$$

$$\text{(2b)} \qquad D(b-v)^{0} = \frac{D(b-v) - k_1 \cdot D(X) - k_1 \cdot D(X \cdot (b-v))}{(1+k_1' \cdot X_v)\ (1+k_1 \cdot X_c)}, \text{ and}$$

$$\text{(2c)} \qquad D(u-b)^{0} = \frac{D(u-b) - k_2 \cdot D(X) - k_2 \cdot D(X \cdot (u-b))}{(1+k_2' \cdot X_v)\ (1+k_2' \cdot X_c)},$$

where the symbols have the same meanings as for equations (1), with the additions of X_v equals the airmass of the variable star, and X_c equals the airmass of the comparison star.

The equations (2) above are the ones which are used by DEXTOR in computing the instrumental differential magnitudes of the variable star. The extinction coefficients must be computed separately and supplied to the DEXTOR program via control cards.

In the computations performed by DEXTOR, a simplifying assumption has been made about the values of $D(X \cdot (b-v))$ and $D(X \cdot (u-b))$. It is assumed that the differences can be replaced by the approximations,

$$\text{(3a)} \qquad D(X \cdot (b-v)) = \frac{X_v + X_c}{2} D(b-v), \text{ and}$$

$$\text{(3b)} \qquad D(X \cdot (u-b)) = \frac{X_v + X_c}{2} D(u-b)$$

The error introduced by this approximation is small if $D(X)$ is small. For $D(X) = 0.01$ the error in $D(b-v)^{0}$ is only $0^{m}.0004$ for typical extinction coefficients. No error was introduced in the reduction of the RS CVn data for $D(u-b)^{0}$, because a value of zero was adopted for k_2.

Extinction Coefficients

An average value for each of the extinction coefficients was determined by the method of weighted least squares. The data used were those from the comparison and check stars. The evaluation of the coefficients was based on equations similar to equation (1a). The evaluation of these primary extinction coefficients was performed in the PHREO computer program for each night of data. The results of PHREO's computations were then weighted according to the precision of PHREO's least squares determination, and the final extinction coefficients were obtained by an additional application of the method of least squares. The values adopted for application by DEXTOR to all the data (1975 and 1976) were

$k = 0.308$,

$k_1 = 0.174$,

$k_1' = -0.03$,

$k_2 = 0.667$, and

$k_2' = 0.0$.

The values for k_1' and k_2' were adopted based on the closeness of the computed values to the expected values given by Hardie (1962).

The details of the computations are not critical to the quality of the results. The effects of differential extinction are small. In fact, the average value of the correction on a typical night was 0.001 magnitudes in the $D(v)^*$ value.

Data Reduction

PHREO Run

After the data were punched onto computer cards, the cards were collected for processing by PHREO. It was necessary to first punch all of the control cards for PHRED and verify that all the supplemental data transferred to the program via the control section were correct and in proper sequence.

When the above conditions were satisfied, the PHRED portion of the reduction was complete. The computer listings are not included here because they are bulky and do not easily conform to the required format. Copies are, however, available to interested investigators.

Correction of Errors

Since there were a large number of data, it was impossible to verify all numbers in the tabulations, reduction and printout. However, it was important to investigate all significant human errors so that they would not propagate through the remaining reduction.

The first step to reduce human errors was taken during the keypunching. The tabulated data were punched and then verified by the keypunch staff. Second, a program was written to scan the punched cards and to flag changes in the deflection value that were obviously too large or were changes in time sequence. This would locate many transpositions of digits in the tabulation process, or keypunch errors. The program was only partially successful. Third, the reduced data were converted by use of the equation

(4) $\mathrm{MJD} = 41825.042 + 4.797855E,$

to a common phase cycle and the light curve plotted. The linear ephemeris above is due to Catalano and Rodono (1974). Any datum which was obviously discrepant was carefully checked for errors in tabulation, keypunching, or data reduction. Fourth, to check the reduction process performed by PHRED, a sample set of calculations was performed manually with an HP-45 hand-held calculator. The sample calculations, in every respect, agreed with the values from the PHRED program to within the expected accuracy

The majority of effort was devoted to the third method, described above, for detecting errors More than 60 individual data were carefully checked in detail (requiring 10 full days of the writer's undivided attention) The majority of the errors detected occurred at the time the data were tabulated for keypunching. The corrections could easily be made and the data adjusted. In a few cases it was possible to identify the source of the error (miss-identification of star, clouds, telescope drift, etc), but the information necessary to correct these errors was not available In these few cases it was necessary to remove the offending data from the collection in order to avoid contamination of the results by these known errors. In only one case was a datum removed without an explanation that was completely satisfactory to this writer. The first star deflections (v,b,and u) were all significantly too high and the first variable star deflections (v,b and u) were significantly low on the night of 1, 2 April 1976. For the remainder of the night the data were very good, therefore these first measurements were removed from consideration

Check Star Data

The ratio of the check star (BD+35°2422) intensity to the comparison star intensity should not be time dependent if the stars are both of constant brightness. This allows the observer to have a 'check' on the assumption that the brightness of the comparison star is constant, and therefore that the variable-to-comparison ratio is a true measure of the variation in the variable star's brightness only

Occasionally during the course of the observing program, measurements of the check star brightness were obtained. In Fig. 6 e

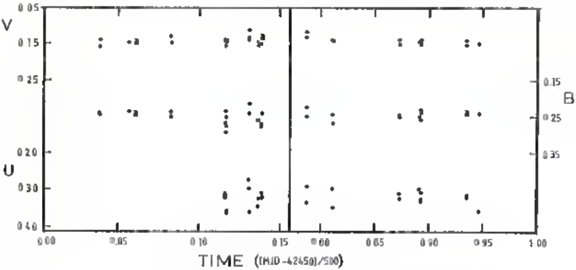

Fig. 6.–A plot of the differential magnitudes of the check star BD+35^0 2422. The left panel is for the time of the 1975 observations, while the right panel corresponds to the 1976 observational program. In most cases more than one differential measure was made on each night. All of the individual points are plotted here. The average values for the differential magnitude and color of BD+35^0 2422 are $v^0 = 0^m144 \pm 0^m005$, $(b-v)^0 = 0^m106 \pm 0^m018$, and $(u-b)^0 = 0^m073 \pm 0^m029$

TABLE 5

DIFFERENTIAL MAGNITUDES AND COLORS OF CHECK STAR

HELIO MJD	D(v)^{0}	D(b-v)^{D}	D(u-b)^{D}
42469.33188	0.159		
42469.40479	0.141	0.1033	
42479.31981	0.150	0.0869	
42480.34465	0.151	0.0904	
42480.42243	0.144	0.1019	
42491.32879	0.129	0.1084	
42491.41073	0.148	0.1048	
42508.06754	0.158	0.1111	0.0439
42508.23596	0.145	0.0933	0.0857
42508.24524	0.143	0.1536	0.0221
42508.41500	0.144	0.1066	0.1082
42508.42114	0.148	0.1297	0.0865
42515.38021	0.145	0.1058	0.0518
42515.38403	0.137	0.1050	0.0328
42515.41264	0.117	0.0995	0.1458
42518.12801	0.148	0.1143	0.0848
42518.31901	0.157	0.1046	0.0644
42519.10308	0.154	0.1259	0.0311
42519.16606	0.141	0.1317	0.0521
42519.39703	0.130	0.1117	0.0801
42843.30877	0.121	0.1308	0.0426
42843.38933	0.136	0.0912	0.1122
42855.22596	0.143	0.1942	0.0518
42855.43218	0.145	0.1254	0.0814
42886.22183	0.141	0.1059	0.0854
42886.29107	0.156	0.0966	0.0754
42895.25505	0.146	0.1038	0.0459
42896.10202	0.153	0.0872	0.0866
42896.15872	0.142	0.0890	0.0982
42896.28953	0.141	0.0954	0.0719
42896.36839	0.147	0.1124	0.0712
42917.17889	0.142	0.1022	0.0715
42917.31388	0.157	0.0793	0.0890
42923.12298	0.149	0.0929	0.1160

plot of the instrumental differential magnitudes is presented as a function of Modified Julian Date. Notice that the plot is not continuous in time, this is because the observing was carried out only during the spring months of 1975 and 1976. The data plotted in Fig. 6 appear in tabular form in Table 5.

Variable Star Data

The data for RS CVn obtained with the instrumentation described in Chapter II, during the 1975 and 1976 observing seasons from March to May, and reduced by PHRED and DEXTOR, appear in tabular form as instrumental differential magnitudes in the appendix.

Transformation to Standard System

The goals of this research do not require transformation to the standard system. Differential measurements with the same comparison star and subsequent use of WINK in the analysis (see Chapters IV and V) relaxes the requirements for standardization in the data. For these reasons, only a small effort was made to obtain transformation coefficients.

The standard stars used were observed on two nights during the course of the observing program. The transformation equations that apply are given as follows

(5a) $B-V = A_1 + A_2(b-v)^{o}$

(5b) $U-B = A_3 + A_4(u-b)^{o}$

(5c) $V-v^{o} = A_5 + A_6(b-v)^{o}$

The values for the A's in equations (5) were computed by the method of least squares using the data obtained from the photometry of nine standard stars and the comparison star. The data for RS CVn has not been transformed with these coefficients because the accuracy is so very low. The transformation coefficients to the UBV system are as follows:

$A_1 = 0.89 \pm 0.01$

$A_2 = 1.06 \pm 0.01$

$A_3 = -2.02 \pm 0.32$

$A_4 = 1.06 \pm 0.16$ (the estimated errors are standard errors)

$A_5 = 7.97 \pm 0.03$

$A_6 = 0.0 \pm 0.1$

More accurate transformations can be found in Markworth's (1977) dissertation. His photometry used virtually identical instrumentation.

CHAPTER IV
DATA ANALYSIS PROCEDURE

Introduction

The analysis of the data was carried out on an AMDAHL 470 computer at the Northeast Regional Data Center located on the Gainesville campus of the University of Florida. The processing was accomplished with several programs written in FORTRAN IV. One program (WINK), which was written by D. B. Wood (1971, 1972), models an eclipsing binary system. The remaining programs were written by the author except for the least square subroutine (used in the Fourier program) which was written by H. L. Cohen. The details of the operation will be discussed after an outline of the WAVE procedure is discussed.

Outline of WAVE Procedure

A simplified outline of the procedure appears in Fig. 7. The details of these computations are eliminated so that the process is clearer. The procedure that this figure represents was used as an in-stream procedure and was called WAVE. This term will be used in the remainder of this dissertation to refer to this sequence of computer programs which was used to analyze the data. The WAVE procedure starts basically with the WINK program which both improves the eclipsing binary elements and produces a theoretical light curve. The input data set to WINK (which it attempts to solve) is called OROBS. This term refers to the Old Revised OBServations from a previous WAVE run or to observations

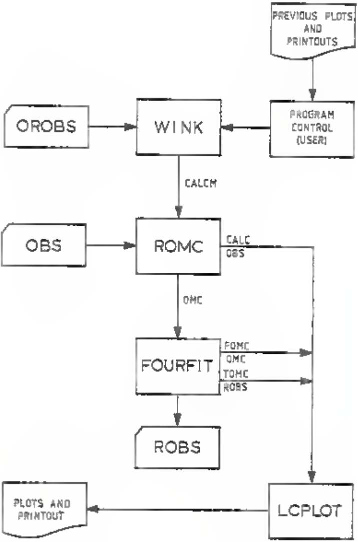
PREVIOUS PLOTS AND PRINTOUTS
OROBS
WINK
PROGRAM CONTROL (USER)
CALCM
OBS
ROMC
CALC
OBS
OMC
FOURFIT
FOMC
OMC
TOMC
ROBS
ROBS
PLOTS AND PRINTOUT
LCPLOT

Fig. 7.--Outline of basic WAVE procedure themselves when the procedure is initiated. In addition to the OROBS the user also supplies a set of control parameters to WINK. After five WINK iterations or after convergence (whichever comes first) the WINK program produces a dataset called CALCM. This is the theoretical light curve for the elements at the conclusion of the solution portion of WINK. The term (CALCM) refers to the fact that it is necessary to produce the calculated light curve in magnitudes in order to include the Quadrature Magnitude (QM) parameter in the values produced. This dataset and the observations (OBS) are used in the ROMC program which is next in the sequence. ROMC converts the magnitudes of the CALCM dataset to intensities and subtracts them from the OBS dataset. The result is the OMC dataset, which is a representation of the distortion wave. In addition, ROMC produces a CALC dataset which is the converted CALCM dataset. CALC is used later for plotting purposes. Next in the sequence is the program FOURFIT. It uses the OMC dataset to determine the coefficients of a truncated Fourier series, by the method of least squares, which represents the distortion wave. The Fourier representation is then subtracted from the OBS dataset. The result of the subtraction is a light curve of RS CVn as it would appear if it did not have the photometric complication. This dataset is called ROBS (Revised OBS). FOURFIT does additional computations which are used for plotting purposes. It computes a dataset from the truncated Fourier series at closely spaced phases. This dataset is called FOMC. Lastly, FOURFIT calculates the difference between the OMC dataset and the Fourier representation of it. This is called TOMC.

The last significant program in the WAVE procedure is called LCPLOT. This program plots the datasets produced in the previous steps

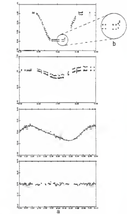

Fig. 8. A sample plot from LCPLOT program reduced EOE appears in (a) In (b) is an enlargement of primary eclipse.

of the procedure for evaluation by the user. A sample of the plots produced appears in Fig. 8.

The WINK Program

This program has been widely used to determine the elements of eclipsing binary systems. The program was written by D. B. Wood (1971, 1972) and has been updated by eight status reports (private communications). The model is that of triaxial ellipsoids. The parameters of the model which are pertinent to this investigation, their WINK codes and meanings are shown in Table 6.

TABLE 6

WINK PARAMETERS

WINK Code	Symbol	Meaning
1	i	orbital inclination
2	$e \sin \omega$	e is the orbital eccentricity and
3	$e \cos \omega$	ω is the longitude of periastron
4	T_c	time (or phase) of conjunction
5	u_A	linear limb darkening coefficient for star A
6	u_B	linear limb darkening coefficient for star B
9	w_A	reflection albedo of star A
10	w_B	reflection albedo of star B
11	QM	quadrature magnitude
13	T_A	effective temperature of star A
14	T_B	effective temperature of star B
15	a_{oA}	radius of a sphere with a volume equal to that of the triaxial ellipsoid of star A (equivalent radius of star A)
16	k_v	ratio of equivalent radii (a_{oB}/a_{oA})
17	β_A	gravity exponent for star A
18	β_B	gravity exponent for star B
19	q	mass ratio (star B to star A)
41	n_A	polytropic index of star A

TABLE 6 - Continued

WINK Code	Symbol	Meaning
42	n_B	polytropic index of star B
43	λ_e	effective wavelength of observations
45	log g_A	logarithm of surface gravity of star A
46	log g_B	logarithm of surface gravity of star B

For systems like RS CVn in which the stars are sensibly spherical the equivalent radii are useful parameters. On the other hand, they have very little physical meaning and the ellipsoidal axes are to be preferred. The reader is cautioned to remember that any set of parameters (whether it's a spherical radius, a set of radii for a triaxial ellipsoid, or 3 radii of a Roche lobe) is merely a way of conveying quantitatively information about a natural phenomena, which most likely does not actually conform (in detail) to any of the model parameters.

The WINK program as it was used here both improved the elements by the method of differential least sqaures and produced a synthetic light curve (the CALCM dataset referred to earlier). The integration was performed using the 4x4 Gaussian quadrature option, which has an accuracy of 0.6%. The model atmosphere used is that which was supplied by Wood in Status Report #7.

The first 19 parameters (only 16 of which are used here) may, by user selection, be improved by the differential least squares subroutine. These parameters, for the purpose of this research were divided into 4 groups by the author: the first-order parameters are i, k_v, a_{gA}, and T_B. The second-order parameters are w_A, w_B, u_A, and u_B. The third-order parameters are T_C and QM. The fourth-order parameters are e sin ω, e cos ω, T_A, q, β_A, and β_B. The other parameters of the WINK model must be assigned by the user and cannot be improved by the differential least squares routine.

In this dissertation the terms "free-parameter" and "adjustable-parameter" will refer to a parameter from the above set which has been designated by the user as a parameter to be improved by the differential least squares routine. Likewise, the term "fixed-parameter" refers to a parameter which has been assigned by the user a particular value and not allowed to be changed by the WINK routines.

No third light was allowed, and only the linear limb darkening law was used. Certain parameters were by necessity assumed at the outset and never altered. These parameters and their assumed values are given in Table 7.

TABLE 7

ASSUMED PARAMETER VALUES

Parameter	Assumed Value
$e \sin \omega$	0.0 i.e., a circular orbit
$e \cos \omega$	0.0
T_A	6700°K from Popper (1961)
q	1.045 from Popper (1961)
n_A	3.5
n_B	3.5
$\log g_A$	4.0 from Gray (1976)
$\log g_B$	3.5 from Gray (1976)

The program was modified to allow for up to 200 data to be read or written, and to produce an additional page of output, which is merely a summary of the least square iterations. In all other respects the program is complete through Status Report #8. The version of the WINK model used here was updated through Status Report #8.

The ROMC Program

This program is very simple. It reads the CALCM dataset produced by WINK and converts the magnitudes (m) to intensities (I) by the relation

$$I = 10^{-0.4m}.$$

This conversion is performed for each successive record in the CALCM dataset. At the same time a record from the OBS dataset is read. The phase of the two records are checked to assure that they are the same. If they are not the same, an error message is written and the program continues. After the subtraction of the CALC record intensity from the OBS record intensity the result is written to the OMC dataset along with the phase from the OBS record. These calculations are repeated until all the records have been processed. It should be noted that the CALC dataset is written for plotting by the LCPLOT program later in the procedure.

The FOURFIT Program

This program reads all the records from OMC dataset and by the method of least squares determines the coefficients of the following truncated Fourier series which best represents the data in OMC.

$$I(\theta) = A_0 + A_1 \cos \theta + A_2 \sin \theta + A_3 \cos 2\theta + A_4 \sin 2\theta.$$

Since the data in and around secondary eclipse are confused by the transit of the smaller star across the assumed non uniform surface of the larger star these points (from phase 0.43 to phase 0.57) are excluded from the least squares process.

After the coefficients of the truncated series have been determined they are used to evaluate the expression at each value of phase in the OBS dataset. The result of each evaluation is then subtracted from the OBS intensity at that phase. The results are what one would expect if RS CVn was not complicated by the non-uniform surface brightness of the larger star. This is not true, however, for the secondary eclipse because the photometric effects of the transit geometry cannot be so simply removed. These effects do contain important information about the surface brightness distribution on the larger star.

The other functions of FOURFIT are to produce two datasets for plotting by LCPLOT. The first dataset, called FOMC, is the evaluation of the truncated Fourier series at 240 phase points so that the plot of this dataset will appear to be a continuous line. The second dataset, called TOMC, is the difference between the intensity of a record in the OMC dataset and the evaluation of the Fourier series at the phase for that record. In other words, it is the difference between the "real" distortion wave and the Fourier fit to it. These points, when plotted, should be randomly displaced (by only a small amount) about a straight line of slope zero if the elements of the eclipsing system are nearly correct. Here again, the region of secondary eclipse is an exception.

The LCPLOT Program

This program is very complex and for the present purpose need not be discussed in detail. It plots the datasets the user wishes as a function of phase. It is a general purpose program and is not restricted to use in the WAVE procedure.

Detailed WAVE Procedure

The detailed JCL WAVE in-stream procedure appears in Fig. 9. It differs from the above only in the details of the procedure, but not in the results.

```
//WAVE PROC ROMC='ROMC',WINKOUT='&&CALCM',CALCM=,WINKIN='&&OROBS'
//GEN0 EXEC PGM=IEBGENER,COND=(4,LT)
//SYSPRINT DD DUMMY
//SYSIN DD DUMMY
//SYSUT1 DD DDNAME=REVO
//SYSUT2 DD DSN=&&OROBS,DISP=(NEW,PASS),SPACE-(TRK,(2,1),RLSE),
//   UNIT=SYSDA,DCB=(RECFM=FB,LRECL=80,BLKSIZE=6400,DSORG=PS)
//GEN1   EXEC PGM=IEBGENER,COND=(4,LT)
//SYSPRINT DD DUMMY
//SYSIN DD DUMMY
//SYSUT1 DD DDNAME=PARA
//SYSUT2 DD DSN=&&PARMS,SPACE=(TRK,(2,1),RLSE),DISP=(NEW,PASS),
//  DCB=(RECFM=FB,LRECL=80,BLKSIZE=6400,DSORG=PS),UNIT=SYSDA
//GEN2   EXEC PGM=IEBGENER,COND=(4,LT)
//SYSPRINT DD DUMMY
//SYSIN DD DUMMY
//SYSUT1 DD DDNAME=DATA
//SYSUT2 DD DSN=&&OBS,SPACE=(TRK,(2,1)RLSE),DISP=(NEW,PASS),
//  DCB=(RECFM=FB,LRECL=80,BLKSIZE=6400,DSORG=PS),UNIT=SYSDA
//GEN3   EXEC PGM=IEBGENER,COND=(4,LT)
//SYSPRINT DD DUMMY
//SYSIN DD DUMMY
//SYSUT1 DD  DDNAME=PRED
//SYSUT2 DD DSN=&&PRED,SPACE=(TRK,(2,1),RLSE),DISP=(NEW,PASS),
//  DCB=(RECFM=FB,LRECL=80,BLKSIZE=6400,DSORG=PS),UNIT=SYSDA
//GEN4   EXEC PGM=IEBGENER,COND=(4,LT)
//SYSPRINT DD DUMMY
//SYSIN DD DUMMY
//SYSUT1 DD DDNAME=STOP
//SYSUT2 DD DSN=&&STOP,SPACE=(TRK,(2,1),RLSE),DISP=(NEW,PASS),
//  DCB=(RECFM=FB,LRECL=80,BLKSIZE=6400,DSORG=PS),UNIT=SYSDA
//GEN5 EXEC PGM=IEBGENER,COND=(4,LT)
//SYSPRINT DD DUMMY
//SYSIN DD DUMMY
//SYSUT1 DD DSN=&&OBS DISP=(OLD,PASS)
         DD DSN=&&STOP DISP=(OLD,PASS)
//SYSUT2 DD DSN=&&NORM,SPACE=(TRK,(2,1),RLSE),DISP=(NEW,PASS),
//  UNIT=SYSDA,DCB=BLKSIZE=6400,LRECL=80,RECFM=FB,DSORG=PS)
//WINC   EXEC PGM=WINK,COND=(4,LT)
//FT05F001 DD DSN=&&PARMS,DISP=(OLD,PASS)
//          DD DSN=&WINKIN DISP=(OLD,PASS)
//          DD DSN=&&PRED,DISP-(OLD,PASS)
//          DD DSN=&&NORM,DISP=(OLD,PASS)
//FT06F001 DD SYSOUT=A
//FT07F001 DD DSN=&WINKOUT,SPACE=(TRK,(2,1),RLSE,DISP=(NEW,PASS),
//  DCB-(RECFM=FB,LRECL=80,BLKSIZE=6400,DSORG=PS),UNIT=SYSDA
//FT08F001 DD SYSOUT=A
//OMCA   EXEC PGM=&ROMC,COND=(4,LT)
//FT01F001 DD DSN=&&OBS,DISP=(OLD,PASS)
```

Fig. 9.-The WAVE procedure

```
//FT03F001 DD DSN=&&OMC,SPACE=TRK,(2,1),RLSE),OISP=(NEW,PASS),
//   OCB=(RECFM=FB,LRECL=80,BLKSIZE=6400,DSORG=PS),UNIT=SYSDA
//FT06F001 OD SYSDUT=A
//FT08FODI OO DSN=&WINKOUT,OISP=(OLO,PASS)
//FTD9F001 DD &CALCM DSN=&&CALC,DISP=(NEW,PASS),UNIT=SYSDA,SPACE=(TRK,
//  (2,I),RLSE),DCB=(RECFM=FB,LRECL=80,BLKSIZE=640D,DSDRG-PS)
//FOUR  EXEC PGM=FOURFIT,COND=(4,LT)
//FT01FD0I OO DSN=&&OBS,DISP=(OLO,PASS)
//FT03F001 DD DSN=&&OMC,DISP=(DLO,PASS)
//FT04FD0I DD DSN=&&ROBS,DISP-(NEW,PASS),SPACE=(TRK,(2,I),RLSE),
//   DCB=(RECFM=FB,LRECL=80,BLKSIZE=6400,DSORG=PS),UNIT=SYSDA
//FT06F00I OO SYSOUT=A
//FT18F00I OO DSN=&&TOMC,OISP=(NEW,PASS),UNIT=SYSDA,
//  SPACE=(TRK,(2,1),RLSE),DCB-(RECFM-FB,LRECL=80,BLKSIZE=6400,
//   DSORG=PS)
//PUN   EXEC PGM=IEBGENER,COND=(4,LT)
//SYSPRINT DD DUMMY
//SYSIN DD DUMMY
//SYSUT1 DO DSN=&&OMC,OISP=(OLD,PASS)
//SYSUT2 OO SYSOUT=B,DCB=BLKSIZE=80
//LCPT   EXEC PGM=LCPLDT,COND=(4,LT)
//SYSPDUT DD SYOUT=A
//SYSVECTR OD DSN-&&VECT,UNIT=SYSDA,DISP=(MOO,PASS),
//   DCB=BLKSIZE=2400,SPACE=(TRK,(75,1D),RLSE)
//FT06FD0I OD DUMMY
//FT07F001 DD SYSOUT=B
//FT05F001 DD DDNAME=PLOTS
//FTD8FOD1 DD DSN=&&OBS,DISP=(OLD,DELETE)
//FTD9F001 DD DSN=&&CALC,DISP=(OLD,DELETE)
//FT10F00I DD DSN=&&OMC,DISP (OLD,DELETE)
//FTI1F00I DD DSN=&&ROBS,DISP (OLO,PASS)
//FT12FD01 DD DSN=&&NDRM,DISP (OLD,DELETE)
//FT13F001 DD DSN=&&STOP,DISP (OLO,OELETE)
//FTI4FD01 OO DSN=&&PARMS,DISP (OLO,OELETE)
//FT15F00I DD DSN=&&PRED,DISP (OLD,OELETE)
//FTI6FD01 DD  &CALCM DSN &&CALCM,DISP (OLD,DELETE)
//FT17F001 DD DSN-&&OROBS,OISP (OLD,DELETE)
//FT18FD0I OD DSN=&&TOMC,OISP (OLO,DELETE)
//FT19FD0I OD DSN=&&FOMC,OISP (OLO,DELETE)
//PUNCH EXEC PGM=IEBGENER,COND=(4,LT)
//SYSPRINT DO DUMMY
//SYSIN DO DUMMY
//SYSUTI OD DSN=&&ROBS,OISP=(OLD,DELETE)
//SYSUT2 DO SYSOUT=B,DCB=BLKSIZE=80
//    PEND
```

Fig. 9 -Continued.

```
//CALL EXEC WAVE
//GEND REVO DD *

  the OROBS dataset
  phase and intensity read by (2F10 5)

/*
//GEN1 PARA DD *

  the WINK parameters and
  model atmosphere

/*
//GEN2 DATA DD *

  the OBS dataset
  phase and intensity read by (2F10 5)

/*
//GEN3 PREO DD *
-1 0
the  true-false" card (defines the free-parameters)
WINK
47 0 0
48 0 0
49 1 0
86 1 0
 0 -100 0
/*
//GEN4 STOP DD *
-1 0
STOP
/*
//LCPT PLOTS DD *

  the LCPLOT control cards for the
  generation of plots (see fig  8)

/*
//PLIT EXEC PLOT
```

Fig 10 -The input stream which uses the WAVE procedure Note that a partitioned load module library must be supplied with the necessary programs in it

The input stream which uses the WAVE procedure is given in Fig. 10. The missing datasets depend on the application of the procedure.

CHAPTER V
ANALYSIS AND SOLUTION

Introduction

The WAVE procedure was described in the preceding chapter. It was developed to assist in the solution of the light curves of RS CVn because previous techniques were inadequate. The WAVE procedure is not capable of arriving at a satisfactory solution without the critically important supervision of a knowledgeable human being. The human must be capable of analyzing intermediate results and determining the subsequent steps by which a better solution might be obtained. At this point, WAVE has been used in the analysis of the light curves of RS CVn, and it has not yet been determined whether the procedure can be applied to other eclipsing or non-eclipsing systems. It is the opinion of the author that WAVE will prove to be helpful in obtaining solutions, in either case, where unexplained photometric complications exist. Therefore, in order to assist with the implementation of WAVE in further research, a detailed account of the process by which the present solution of RS CVn was obtained will be presented.

The Data Analyzed

The light curves of RS CVn that have been analyzed with the use of the WAVE procedure are listed in Table 8. These do not represent all of the published data which are available, but they are a selection which meets the requirements of the research effort undertaken as the topic of this dissertation.

TABLE 8

SOURCE OF DATA

Publication	MJD of observations	λ_e	Name
Sitterly (1930)	22759.2 - 22898.2	5150Å	1921
Chisari and Lacona (1965)	38109.5 - 38227.0	5150Å	1963
Chisari and Lacona (1965)	38468.5 - 38572.0	5150Å	1964
Catalano and Rodono (1967)	38871.8 - 38944.0	5150Å	1965
Catalano and Rodono (1967)	39213.9 - 39316.0	5150Å	1966
This Dissertation	42465.0 - 42534.3	5500Å	1975v
This Dissertation	42469.0 - 42534.3	4450Å	1975b
This Dissertation	42506.0 - 42534.3	3770Å	1975u
This Dissertation	42843.3 - 42925.2	5500Å	1976v
This Dissertation	42843.3 - 42925.2	4450Å	1976b
This Dissertation	42843.3 - 42925.2	3770Å	1976u

In Table 8 the last column is a "name" which has been given to the data for easy reference in this present work. This "name" is also the year (and color in some cases) in which the data were obtained. In a few cases it will be convenient to group the 1963, 1964, 1965, and 1966 data into a set, and to refer to this set as the "Catania data." The astronomers who published these data were all observers at the Catania observatory.

All of the Catania data and the author's data of RS CVn were obtained using BD+35° 2420 as a comparison star. This greatly facilitates the comparison of the light curves from the different years, because the differential magnitudes are in the same light units. The difference in the effective wavelength used by the Catania observers and that used by the author has the effect of changing (only slightly) the effective light unit. Since the bandwidth of the filter used by the Catania observers was not available, it was impossible to make allowances for any differences in the two instrumental systems. Fortunately, to some extent this difference does not cause a problem with the analysis because the WINK model uses the effective wavelength as an input parameter. Thus, the majority of the WINK parameters that are subsequently determined are independent of the wavelength.

In Table 8 the specific dates for the observations are given because only portions of the published data were used for the 1921 and Catania light curves. The migration of the distortion wave would "wash-out" some of the detail in the light curve if the duration of the observing season was too long. For this reason the data which produced the light curves used in the WAVE procedure were limited to those points taken over a period of less than 140 days. The data taken by the author was deliberately limited to a short time span (95 days in 1975 and 96 days in 1976).

The modifications to WINK (see Chapter IV) extended the capacity of the model from 100 points to 200 points. This would have allowed light curves to be made with up to 200 normal points. However, such light curves would have been prohibitively expensive to run on the computing system available. Therefore, a compromise was made between the cost of computing (which increases approximately as the square of the number of normal points) and the desirability of a large number of normals which would give a good resolution of the details in the light curves. The compromised value was 150 normal points per light curve, or as close to this value as was realistic.

The calculation of the normal points was carried out on the digital computer. In computing the normal points the first step was to compute the phase for each individual differential magnitude from the linear ephemeris

$$\text{MJD (minimum light)} = 41825.042 + 4^{d}797855E$$

The period of this ephemeris was computed by Catalano and Rodono (1974). The initial epoch is from an observed minimum, published in the same paper, closest to the start of the author's observations in 1975. Only the decimal fraction was retained from the computation of the phase. The second step involved sorting, into phase order, all magnitude-vs-phase points. This process was done separately for each dataset as they are listed in Table 8. The final step in the normal point calculations was the most important. The average value of the phase, and the magnitude of the average value of the intensity for all points within many small phase intervals were computed. These calculations were defined by three parameters. The first two parameters together defined a section of the light curve. This was called the phase range. The third parameter defined a 'bin size' within the phase range. For example, suppose that a phase range of $0^{P}0$ to $1^{P}0$ is defined (i.e., the entire light curve), and a bin size of $0^{P}1$ is also defined. The first normal point will be computed from the individual points between phase 0.0 and 0.1. The second normal point will be computed from the individual points between $0^{P}1$ and $0^{P}2$. This process is continued until the last normal point is computed from the individual points between $0^{P}9$ and $1^{P}0$. In this example it is possible to have, at the most, 10 normal points. The actual number would depend on the distribution of individual points throughout the light curve.

In practice it is better to have more than one phase range and bin size for a light curve. There are two reasons for this. First, the distribution of individual points will, in all probability, be unequal.

Therefore, it would be advisable to choose the phase range and bin size to accommodate the real distribution of data in the light curve. Second, and more importantly, the slope of the light curve is much greater during eclipses than in the rest of the light curve. For this reason it is necessary to have a small bin size during an eclipse in order to accurately represent the individual points with the normal points. When the phase ranges and bin sizes are chosen, all of the above factors must be considered. The final set of normal points will inevitably be a compromise. The data which are ultimately used should be the ones which best represent the individual points. The normal points which were used in the WAVE procedure are here presented in Tables 12 through 22. Notice that each table gives the phase, differential magnitude (variable minus comparison), and number of individual points used for each normal point. In addition, the phase range and bin size used in the computations are given.

The Analysis

There were many computer runs using the WAVE procedure before a final solution was selected, 103 in fact. It would not be profitable to discuss each of these runs individually. The better approach is to group them according to steps in which the runs are related in some procedural way. This reduces the number to approximately a dozen steps, which serve to simplify the discussion which follows. In the future applications of the WAVE procedure it will be possible to reduce the number of runs and the number of steps considerably based on the experience which was gained in this effort for RS CVn. In this section, an

TABLE 9
SUMMARY OF RS CVN SOLUTION

Param.	1	2	3	4	5	6	7	8	9	10	11	12
i	87.98	88.17	87.35	87.38	84.16	87.19	88.34	86.41	86.40	88.46	85.34	85.34
	1.00	0.31		0.45	0.88	0.20	0.35	0.46		0.33	0.49	
u_A	[illegible]	[illegible]	[illegible]	[illegible]	[illegible]	[illegible]	[illegible]	[illegible]	[illegible]	[illegible]	[illegible]	[illegible]
	0.12	0.20			0.53	0.21						
u_B	[illegible]	[illegible]	[illegible]	[illegible]	[illegible]	0.91	1.00	1.00	1.00	[illegible]	1.00	1.00
	0.04				0.46	0.19						
w_A	[illegible]	[illegible]	[illegible]	[illegible]	[illegible]	[illegible]	[illegible]	[illegible]	[illegible]	[illegible]	[illegible]	[illegible]
				0.47	1.07	0.41						
w_B	0.00	[illegible]	[illegible]	[illegible]	[illegible]	[illegible]	[illegible]	[illegible]	[illegible]	[illegible]	[illegible]	[illegible]
				0.14	0.36	0.16						
T_A	[illegible]	[illegible]	[illegible]	[illegible]	[illegible]	[illegible]	[illegible]	[illegible]	[illegible]	[illegible]	[illegible]	[illegible]
	32											
T_B	[illegible]	[illegible]	[illegible]	[illegible]	[illegible]	[illegible]	[illegible]	[illegible]	[illegible]	[illegible]	[illegible]	[illegible]
		6		14	54	4	5	13	11	6	28	48†
a_{eA}	[illegible]	[illegible]	[illegible]	[illegible]	[illegible]	[illegible]	[illegible]	[illegible]	[illegible]	[illegible]	[illegible]	[illegible]
	0.002	0.001		0.002	0.005		0.001	0.002	0.002	0.001	0.002	
[illegible]	[illegible]	[illegible]	[illegible]	[illegible]	[illegible]	[illegible]	[illegible]	[illegible]	[illegible]	[illegible]	[illegible]	[illegible]
	0.029	0.013		0.028	0.105		0.013	0.051	0.026	0.012	0.006	0.011†
[illegible]	[illegible]	[illegible]	[illegible]	[illegible]	[illegible]	[illegible]	[illegible]	[illegible]	[illegible]	[illegible]	[illegible]	[illegible]
					5.23							
[illegible]	[illegible]	[illegible]	[illegible]	[illegible]	[illegible]	[illegible]	[illegible]	[illegible]	[illegible]	[illegible]	[illegible]	[illegible]
					[illegible]							
q	[illegible]	[illegible]	[illegible]	[illegible]	[illegible]	[illegible]	[illegible]	[illegible]	[illegible]	[illegible]	[illegible]	[illegible]
					0.39							
[illegible]	[illegible]	[illegible]	[illegible]	0.01	[illegible]	[illegible]	0.01	[illegible]	[illegible]	[illegible]	[illegible]	[illegible]
	0.002	0.012	0.012	0.002	0.013	0.003	0.002	0.008	0.009	-	0.009	0.003

† The quoted standard error is from the computation of the average. Elsewhere the quoted value of the standard error is the average value of the WINK standard errors.

outline of the process by which the light curves of RS CVn were solved will be presented.

A summary of the solution process is given in Table 9. The step names are listed as they are used in the discussion which follows. The values for the parameters in Table 9 are averages of the computer runs for each step. The standard error, below each value, is actually the average of the standard errors from the WINK program. The reader is cautioned that these are computed by assuming that all fixed-parameters are exactly known. Thus they represent an optimistic estimate of the precision with which the parameter was determined. If no standard error is listed, the number in the table was used as a fixed-parameter value for all of the WAVE runs of that step.

The values of Table 9 are only a guide as to the evolution of the solution process. In any given step it is possible that not all of the 11 light curves listed in Table 8 were run. Furthermore, in many steps the 1975v or 1965 light curves, or even others, may have been run several times. The 1921 light curve is of less precision than the others, but the averages were computed by giving it the same weight as the other light curves. The wavelength of the observations is different for some of the light curves, and this would also influence the validity of the averages for those parameters which are wavelength dependent. Therefore, the values of Table 9 are to be considered as only illustrative of the process by which a final solution was eventually determined.

At the outset of the solution process it was assumed that the solution was that of two bodies in circular orbits. Therefore, the eccentricity of the orbit and the value of third light were assumed to be zero.

Step One

The solution process was started by using the published elements (see Table 2) of Popper (1961) as the initial parameters. The 1975v light curve was used, and after only three runs a greatly improved distortion wave resulted. The procedure was then used only once with the 1976v light curves. These four runs showed that the WAVE procedure would give improved results compared with previous techniques. This step was in actuality a preliminary test of the WAVE procedure. The in-stream procedure which was used in this step was not as sophisticated as that which was developed later. The in-stream procedure described in Chapter IV was used in steps three and following.

These preliminary results showed that the K0 star corresponds, in the WINK model, to star S. The hotter star is the smaller and less massive star. It is designated by the 'A' subscript. It is especially important in the case of RS CVn to avoid the use of the terms "primary" and "secondary", because the terms are very ambiguous. For example, in the case of RS CVn the spectroscopic primary (i.e., the more massive K0 star) is the photometric secondary component (i.e., the fainter star).

Step Two

The same preliminary in-stream procedure was used in step two as in step one. The Catania data were used in an effort to obtain plots which would show the evolution of the distortion wave during the four years covered by these data. The plots were presented at an informal meeting of the RS CVn working group of IAU Commission 42 at Socorro, New Mexico in early April 1978.

Step Three

The WAVE procedure as described in Chapter IV was developed and first used in step three to improve the value of only the third-order parameters (T_c and QM). The results from steps one and two were preliminary, but of sufficient quality to begin a more rigorous process using them as the initial parameters. The third-order parameters are not actually elements of the model, but they must be determined in order to arrive at a satisfactory solution. The eleven runs of step three were the first to use the full in-stream WAVE procedure. Therefore, this step provided the needed values for the third-order parameters and the ROBS datasets necessary for subsequent improvement of the other parameters. Since T_c and QM are unique to each light curve no meaningful average can be computed for them. For this reason no third-order parameters are indicated in Table 9 for step three. However, it is of interest to compare the average RMS error for the 11 light curves of step three with the subsequent steps.

Steps Four and Five

These are very similar steps. They both represent runs which helped the author gain the necessary "feel" for the effects of various parameters and combinations of parameters on the solution and cost of running the procedure. Starting with step five the value of log g_B was changed from 4.00 to 3.50 to agree with the published values in Gray (1976).

The fourth-order parameters β_A and β_B were made free-parameters for two runs. The results indicated that these parameters could not be improved, and the theoretical von Zeiple values were adopted for both stars (0.25). Experimentation with the value of q (mass ratio) and the second-order parameters was also performed. The results indicated that the spectroscopic mass ratio was better determined than the photometric value of q, and the reflection albedoes were very poorly determined by the data. The limb darkening coefficients were better known.

Step Six

The first-, third-, and fourth-order parameters seemed to be reasonably well determined based on prior results. Therefore, it was decided that the second-order parameters should be improved before returning to the first-order parameters for their final adjustment.

This was the expected sequence of events. However, it was quickly found that the solution could not be improved by having only the second-order parameters as free-parameters. It was necessary to add QM, i, and T_B to the list of adjustable-parameters. Various combinations of these parameters with the second-order parameters were attempted in order to improve the solution.

At the conclusion of step six it was felt that the second-order parameters were as well determined as was possible with the available data, and they were never changed again. The values which were adopted were based on a selection of the better runs of all previous steps.

Step Seven

This step consisted of only three computer runs using the 1976v data. The purpose of these runs was to establish if it was necessary to improve all of the first-order parameters, or if a smaller subset would be sufficient. It was hoped that the inclination and temperature of star B were sufficiently well determined so that only k_V and e_{oA} would need to be improved. Unfortunately, it was found that all four parameters had to be changed from the average values which had been adopted in order for the WINK model to adequately represent the ROBS dataset

Step Eight

From the results of step seven it was obvious that the average values for the first-order parameters were not adequate to represent all of the light curves. So, the light curves for all the datasets in Table 8 were run with all four first-order parameters as adjustable-parameters. The intent was to find a trend in one or more of the parameters as a function of time and/or the position of the distortion wave.

No clear trends appeared except for an unexpected variation from light curve to light curve in the value of the inclination. It seemed totally impossible that the inclination of the system could have changed from about 82° in 1921 to about 89° in 1975. This inexplicable result led to the sequence of runs described in step nine.

Step Nine

The 1975v data were about the best of any used in this analysis, so this light curve was chosen to investigate the nature of the inclination of the system. It was hoped that by fixing the value of the inclination to an intermediate value ($86^{\circ}4$) between the extremes found in step eight, and then solving for various combinations of the other first-order parameters an adequate solution could be found. After six computer runs it was deemed impossible to find a solution with an inclination of $86^{\circ}4$ which was as acceptable as the one previously found with $i = 89^{\circ}$.

Step Ten

There seemed to be no reasonable explanation to the inclination problem. Therefore a complete review of previous results was made to see if some error had been made. Indeed an error had been committed between steps one and two. Originally in step one T_0 had been taken as a well known value because the color of this star could be observed independent of the other star during primary eclipse. The few runs of step one had resulted in a temperature of 6050°K for star A. This value was then used as a fixed-parameter value for all subsequent runs and T_B was adjusted. While this would not cause a large error in the determination of the relative brightnesses of the two stars it was noticeable in the determination of the solution. So, step 10 was a single run to test if taking 6700°K (Popper 1961) as the value of T_A could resolve the inclination problem.

As one might have expected, the temperatures of the stars had little affect on the value of the inclination. However, it did improve the RMS error of the WINK determination for the 1975v light curve.

At the conclusion of the run it was realized that the inclination problem was not really a problem at all. It was merely a manifestation of the non-uniform surface brightness of the KO star. Since the structure of this surface brightness distribution is a changing function of time, the transit of the smaller star will mimic different inclinations.

Step Eleven

The normal points in secondary eclipse were removed from all the light curves. Using the resulting datasets as input OBS decks a new set of runs were made with 1, T_C, QM, T_B, a_{gA}, and k_v as free-parameters. The new values for these first-order parameters were remarkably similar for each light curve. For example, the range in the value of the inclination was from $84^\circ.3$ for 1964 to $86^\circ.1$ for 1975u.

Step Twelve

The results from step 11 almost completed the solution. There was, however, one other use for the WAVE procedure which could add insight into the nature of RS CVn.

If the K0 star was pulsating it would follow that the temperature and radius of this star would be different for each light curve. On the other hand, if the surface of the K0 star is non-uniform, the radius would not change, only the temperature would vary.

With the above conditions in mind and the points of secondary eclipse still removed, another set of 11 runs was made with only T_B and k_v as free-parameters. The radius of star A (a_{0A}) was a fixed-parameter, so the changes in k_v would be solely due to the radius of star B (a_{0B}).

The value of a_{0B} was almost identical for all light curves, while the value of T_B was somewhat different. This would support a starspot model over a radial pulsating model.

Step Thirteen

The last step was to return the secondary eclipse points to the datasets, and run the WAVE procedure to produce a new set of ROBS datasets. The solution portion of WINK was not used because the solution from steps 11 and 12 was felt to be the best that could be achieved. This step was intended only to provide the final ROBS and OMC datasets. Table 9 does not have a listing for this step because there were no changes from step 12.

The Final Solution

It was noted in step 12 above that T_B was the only element which was significantly different in the 11 light curves which have been solved with the WAVE procedure. The value of T_B which has been determined for each light curve is an average over the non-uniform surface of the K0 star. In addition to different values of T_B, the various light

TABLE 10

FINAL VALUES OF WINK PARAMETERS

Parameter	Value	Max. s.e.
Orbital inclination (i)	85°34	±0°.32
$e \sin \omega$	assumed 0.0	
$e \cos \omega$	assumed 0.0	
limb darkening coef., star A (u_A)	0.72	±0.17
limb darkening coef., star B (u_B)	1.00	±0.08
reflection albedo of star A (w_A)	0.3	±1.6
reflection albedo of star B (w_B)	0.05	±0.35
temperature of star A (T_A)	assumed 6700°K	
temperature of star B (T_B)	~4800°K	±150°K
equivalent radius of star A (a_{oA})	0.1141	±0.0032
ratio of radii ($k_v = a_{oB}/a_{oA}$)	2.12	±0.09
gravity exponent of star A (β_A)	assumed 0.25	±5.3
gravity exponent of star B (β_B)	assumed 0.25	±0.7
mass ratio ($q = m_B/m_A$)	assumed 1.04	±1.6
polytropic index of star A (n_A)	assumed 3.5	
polytropic index of star B (n_B)	assumed 3.5	
log surface gravity of star A ($\log g_A$)	assumed 4.0	
log surface gravity of star B ($\log g_B$)	assumed 3.5	

Notes for Table 10

The maximum standard error (Max. s.e.) is defined in the text. This method has also yielded ±0.0005 for T_c and ±0.00162 for QM.

TABLE 11

FINAL VALUES OF EPOCH-DEPENDENT PARAMETERS

Para.	1921	1963	1964	1965	1966	1975v	1975b	1975u	1976v	1976b	1976u
QM	-1.91101 495	-0.32997 78	-0.34653 85	-0.31502 129	0.30686 185	-0.39800 79	-0.25328 73	-0.13865 189	-0.35128 102	-0.21373 112	-0.11115 177
T_c	0.00566 36	0.01652 6	0.01710 7	0.01525 8	0.01287 13	-0.00107 8	-0.00103 7	-0.00195 22	-0.00266 9	-0.00262 8	-0.00247 11
T_B	4762	4793	4818	4775	4897	4826	4814	4763	4779	4780	4700
l_B	0.35674	0.37080	0.38216	0.36263	0.41809	0.42213	0.30355	0.24350	0.40173	0.28740	0.20630
A_0	0.03810 445	-0.00645 72	-0.01604 81	0.00123 117	-0.02625 198	-0.01464 73	-0.01409 63	-0.02140 205	0.00015 90	-0.00399 100	-0.00841 156
A_1	-0.02001 639	0.07066 106	0.06167 125	0.01506 181	-0.05045 306	-0.05829 104	-0.04193 69	-0.04404 299	-0.07316 124	-0.05669 138	-0.04716 214
A_2	0.06761 562	-0.03405 102	-0.07108 119	-0.07324 162	-0.05246 266	-0.05614 109	-0.04011 93	-0.03570 398	-0.01500 132	-0.01002 147	-0.00182 229
A_3	0.00584 674	0.00832 100	0.01644 128	-0.00310 167	0.01055 268	0.02167 111	0.01651 96	0.00559 342	0.03208 133	0.02636 148	0.02324 229
A_4	0.01572 580	0.00624 96	0.01382 103	0.00528 148	0.00055 255	-0.00198 35	-0.00036 61	-0.00729 307	-0.03032 113	-0.02416 126	-0.01342 196
s.e.	0.03655	0.00670	0.00647	0.00576	0.01516	0.00634	0.00541	0.00584	0.00823	0.00916	0.01422
θ_{min}	0.8259	0.3690	0.3379	0.3079	0.1691	0.1819	0.1866	0.1485	0.1438	0.1454	0.1440
θ_{max}	0.2114	0.9721	0.9363	0.7584	0.5876	0.5567	0.5530	0.5436	0.4671	0.4657	0.4618

curves also have different Fourier coefficients to represent the distortion waves. Table 10 gives the elements of the system which are common to all light curves. Table 11 gives the values which are unique for each light curve as determined from steps 11,12 and 13.

The errors quoted in Table 10 are standard errors determined with the use of the WAVE procedure. The correlation among the system parameters makes it difficult to assess the precision of the determination of each value. The ideal method to obtain an estimate of this precision would be to use all the WINK model parameters as free-parameters and thus allow the least squares routine to determine the standard error. The only method currently available with the WAVE procedure technique is to use the maximum number of free parameters allowed (9) to estimate the standard errors. By repeating this two additional times, it is possible to include all of the parameters which can be adjusted. This was done using the 1975v light curve. The standard error given in Table 10 is the maximum value of the standard error from the three runs.

The Distortion Wave

The last step of the solution process produced a set of Fourier coefficients which represent the distortion wave. These coefficients are given in Table 11. The standard error of each coefficient is given below the parameter value. As a reminder, and for the convenience of the reader, the truncated Fourier series from which these coefficients have been determined is

(6) $I(\theta) = A_0 + A_1 \cos\theta + A_2 \sin\theta + A_3 \cos 2\theta + A_4 \sin 2\theta$

The A_0 term is a constant which resolves the normalization differences between the OBS light curve and the CALC light curve. Presumably, had it been possible to accurately normalize the observed light curve to unity outside eclipse, QM and A_0 would both be zero. Unfortunately, this was impossible to do, a priori, in the case of RS CVn because of the large asymmetric and dynamic distortion wave, as well as the large period changes in the system.

The other terms of the truncated Fourier series represent the shape of the distortion wave. It is possible to use this shape, the A_0 term, and the apparent normalized luminosity of star B (l_B, a quantity printed by WINK) to produce a light curve of the K0 star as it would appear if the brighter star were removed from the system. If the OMC dataset is used in place of the truncated Fourier series, the result will include the original observational error which has been partially smoothed from the data by use of the truncated Fourier series.

The computations which are outlined above were performed on each light curve. The equation that represents this process is

$$(7) \quad L_B(\theta) = OMC(\theta) + l_B \, 10^{-0.4(QM)},$$

where $L_B(\theta)$ is the intensity at phase θ of the isolated K0 star, OMC (θ) is the intensity of the distortion wave at phase θ, l_B is the normalized apparent luminosity of star B, and QM is the quadriture magnitude. The latter two quantities have been listed for each light curve in Table 11. The above equation produced light curves of the K0 star which are in units of the comparison star's brightness. These light curves are displayed in Figs. 11 through 21. The region of secondary eclipse, in these figures, is complicated by the transit phenomenon, and therefore this region does not represent the light changes due solely to the K0 star.

The values of distortion wave minimum and maximum (θ_{min} and θ_{max}) are listed in Table 11. They have been computed by differentiating the

Fourier series of equation (6) with coefficients from Table 11, setting the result equal to zero, and evaluating the solution by Newton's method.

Period Changes

If the period of a binary system changes with time it is an indication that the angular momentum of the system has changed or that the distance to the system has changed. There are many ways in which the system's angular momentum can be altered. The one which comes to mind most frequently is the transfer of mass from one star to the other through the inner Lagrangian point. This method of mass transfer has been of great interest during the last two decades as a means of explaining the evolution of binary stars. It is mentioned here, not as a possible explanation for period changes in RS CVn, but as a reminder that it is only one of several ways to change the angular momentum of a binary system, and only currently enjoys a large degree of attention.

This is not intended to minimize the importance to astronomical knowledge of any particular period change mechanism, but rather to help explain the current state of affairs. Batten (1973) has a good review of period change mechanisms, briefly they are as follows: apsidal motion, the presence of a third body, and real changes in orbital period which maybe due to mass transfer, mass loss, or mass gain. The later three mechanisms are in actuality changes in the angular momentum of the system. The mass exchange due to evolution is simply a special case. Of course, there is always the possibility of another unknown mechanism.

RS CVn and RS CVn binaries may prove to be extremely important laboratories for research into changes in angular momentum of binary systems, because it is reasonably certain that the period changes are not due to a light-time effect (orbital motion about a third body) or to mass transfer. Neither is it likely that mass loss nor apsidal motion are the causes of the quasi-periodic period changes. The research in the coming decades may return to one of these causes of period change, but at the present all seem impossible. Therefore it is important that the period be measured as accurately as possible. In the case of star systems like RS CVn which have very asymmetric primary eclipses it is difficult to accurately determine the time of minimum. This is compounded by the long periods (and earth-based photometry). The WINK parameter T_c can be determined to an accuracy equivalent to less than 40 seconds in the case of RS CVn. Unfortunately, this is somewhat misleading because the absolute time is not known. The parameter T_c is that which best represents a light curve. The mean epoch for the data which comprise the light curve is difficult to determine because the computation is complicated by the random nature of the data acquisition and the unequal effect on T_c of each datum. Nevertheless, the T_c parameter can be a useful tool in determining the nature of period changes since it affords a higher degree of confidence than other methods. This will allow the investigation of angular momentum changes due to processes that are more insidious.

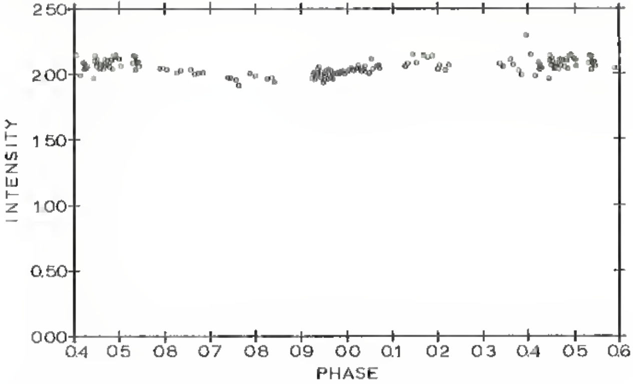

Fig 11.-Light curve of the K0 star in RS CVn based on Sitterly's (1930) data for 1921 Note that a different comparison star was used by him and therefore the intensity scale differs from the other light curves

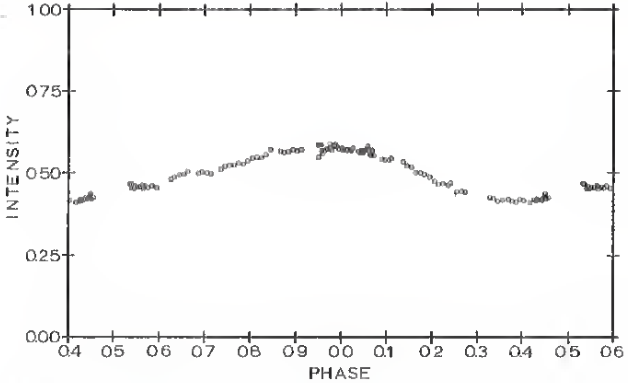

Fig. 12 -Light Curve of the K0 star in RS CVn based on Chisari and Lacona's (1966) data for 1963.

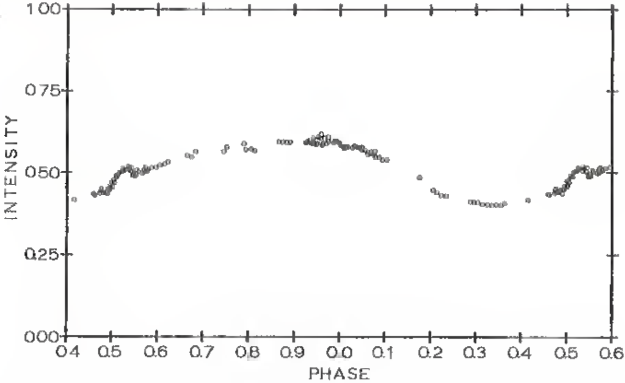

Fig. 13.—Light curve of the K0 star in RS CVn based on Chisari and Lacona's (1965) data for 1964.

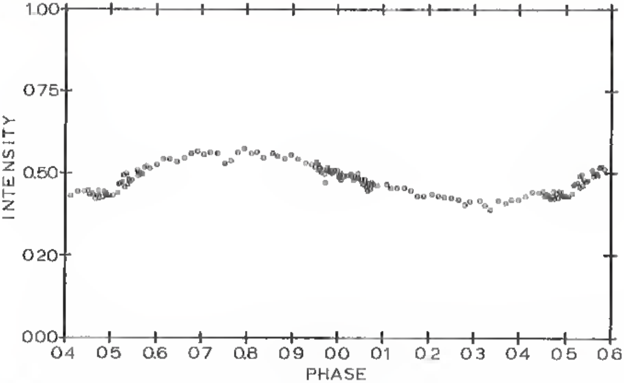

Fig 14 -Light curve of the K0 star in RS CVn based on Catalano and Rodono's (1967) data for 1965.

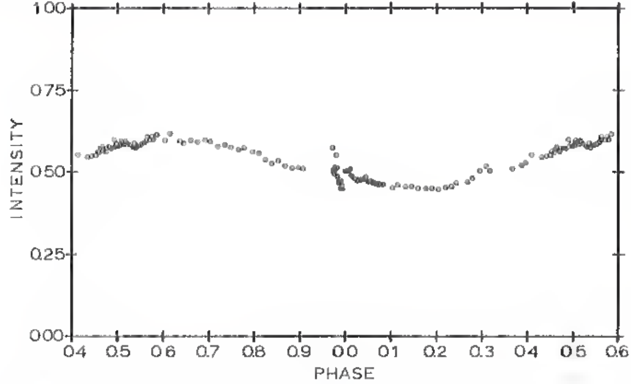

Fig. 15.—Light curve of the K0 star in RS CVn based on Catalano and Rodono's (1967) data for 1966

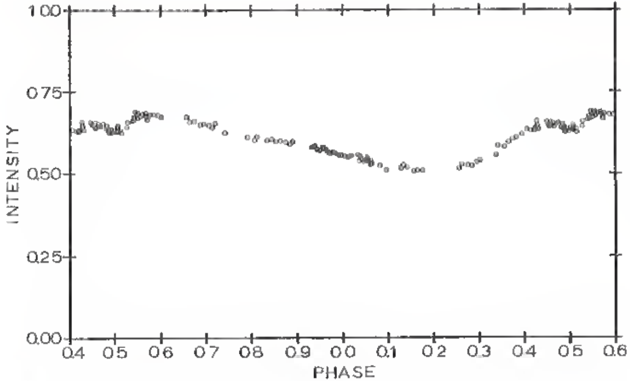

Fig 16 -Light curve of the KO star in RS CVn based on Ludington's 1975v data which appears in the Appendix

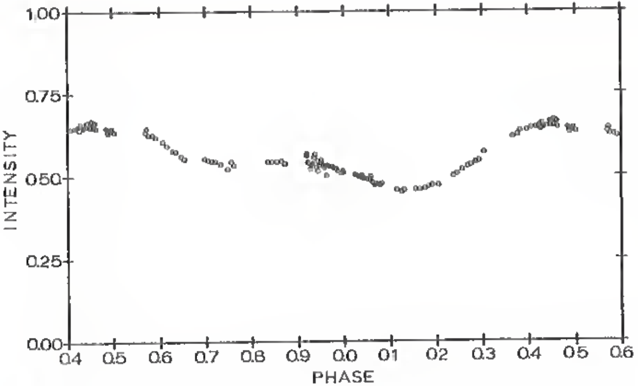

Fig. 17 -Light curve of the K0 star in RS CVn based on Ludington's 1976y data which appears in the Appendix

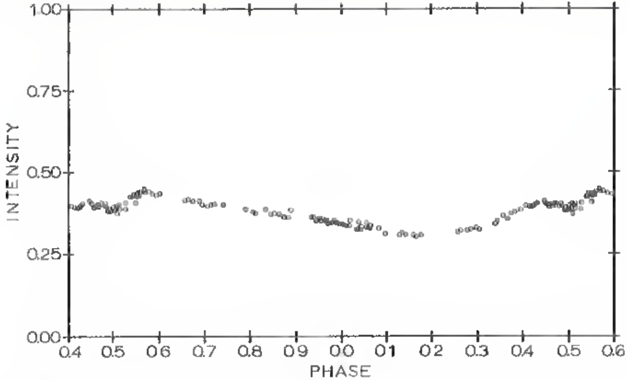

Fig 16.—Light curve of the K0 star in RS CVn based on Ludington's 1975b data which appears in the Appendix

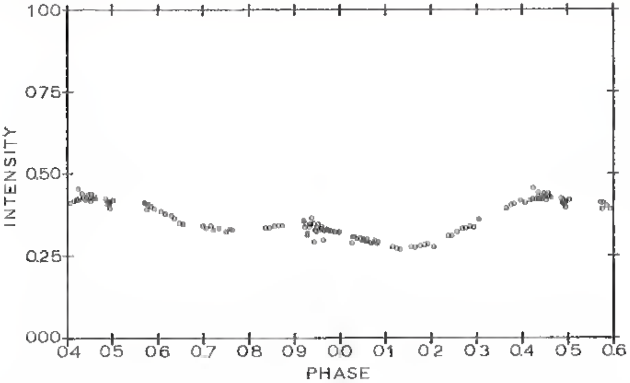

Fig 19 -Light curve of the K0 star in RS CVn based on Ludington's 1976b data which appears in the Appendix.

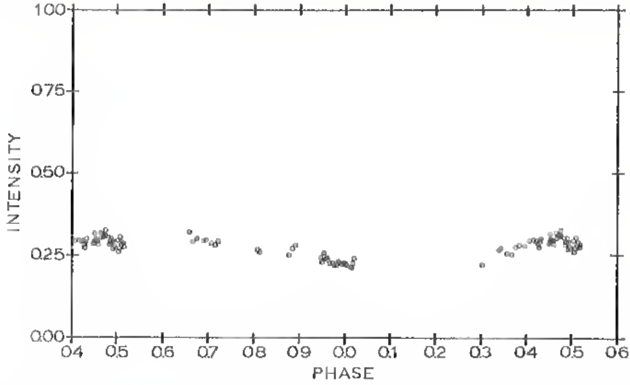

Fig. 20.-Light curve of the K0 star in RS CVn based on Ludington's 1975u data which appears in the Appendix

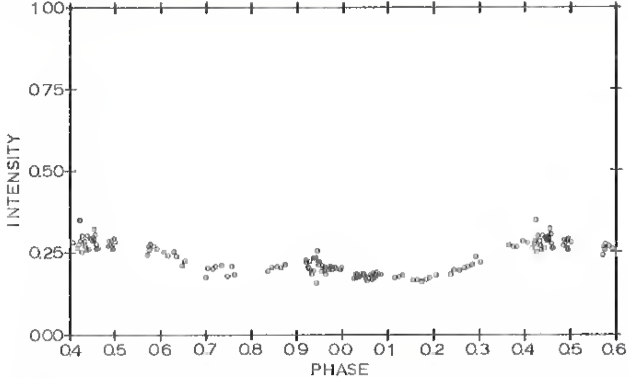

Fig. 21.-Light curve of the K0 star in RS CVn based on Ludington's 1976a data which appears in the Appendix.

TABLE 12

NORMAL POINTS FOR 1921 DATA

Bin Size 0.0020 Phase Range 0.0000 to 0.0800

Phase	Magn.	No.	Phase	Magn.	No.	Phase	Magn.	No.
0.0013	-0.530	2	0.0212	-0.600	1	0.0477	-1.560	1
0.0031	-0.560	1	0.0227	-0.600	2	0.0489	-1.606	2
0.0051	-0.600	1	0.0240	-0.710	1	0.0508	-1.657	3
0.0069	-0.610	2	0.0314	-0.890	1	0.0537	-1.830	1
0.0093	-0.530	2	0.0328	-1.022	2	0.0549	-1.770	2
0.0109	-0.630	2	0.0348	-1.108	5	0.0568	-1.800	3
0.0127	-0.570	2	0.0368	-1.213	5	0.0666	-1.870	2
0.0144	-0.520	1	0.0389	-1.330	2	0.0689	-1.876	2
0.0191	-0.563	2	0.0410	-1.337	3	0.0705	-1.850	2

Bin Size 0.0100 Phase Range 0.0800 to 0.4200

Phase	Magn	No.	Phase	Magn.	No.	Phase	Magn.	No.
0.1283	-1.877	5	0.1988	-1.870	1	0.3644	-1.892	5
0.1337	-1.899	7	0.2031	-1.900	5	0.3764	-1.841	8
0.1449	-1.976	2	0.2160	-1.861	15	0.3845	-1.810	9
0.1529	-1.907	5	0.2218	-1.902	5	0.3929	-2.100	1
0.1678	-1.965	4	0.3350	-1.907	6	0.4046	-1.960	1
0.1762	-1.950	1	0.3431	-1.883	6	0.4137	-1.790	5
0.1878	-1.970	2	0.3587	-1.935	2			

Bin Size 0.0020 Phase Range 0.4200 to 0.5800

Phase	Magn	No.	Phase	Magn.	No.	Phase	Magn	No.
0.4210	-1.900	1	0.4628	-1.864	3	0.4909	-1.868	3
0.4232	-1.844	4	0.4650	-1.817	6	0.4990	-1.817	3
0.4249	-1.876	2	0.4669	-1.889	4	0.5011	-1.806	2
0.4270	-1.851	2	0.4689	-1.837	3	0.5033	-1.746	2
0.4289	-1.860	1	0.4713	-1.827	3	0.5310	-1.820	1
0.4435	-1.760	1	0.4728	-1.871	2	0.5331	-1.888	2
0.4451	-1.950	1	0.4746	-1.865	2	0.5349	-1.890	1
0.4464	-1.910	1	0.4776	-1.830	1	0.5367	-1.780	2
0.4488	-1.870	1	0.4793	-1.790	1	0.5394	-1.850	1
0.4513	-1.920	1	0.4812	-1.851	2	0.5410	-1.856	2
0.4527	-1.859	3	0.4829	-1.833	3	0.5430	-1.870	1
0.4545	-1.842	3	0.4848	-1.755	2	0.5445	-1.837	2
0.4561	-1.850	1	0.4868	-1.856	2			
0.4610	-1.870	1	0.4889	-1.850	2			

TABLE 12 - Continued

Bin Size	0.0100			Phase Range		0.5800 to 0.9200		
Phase	Magn.	No.	Phase	Magn.	No.	Phase	Magn.	No.
0.5894	-1.860	2	0.6662	-1.821	9	0.7618	-1.730	1
0.5952	-1.852	11	0.6742	-1.831	13	0.7859	-1.834	7
0.6036	-1.845	7	0.5849	-1.834	7	0.7980	-1.817	5
0.6253	-1.823	7	0.7397	-1.800	1	0.8247	-1.782	6
0.6354	-1.847	7	0.7440	-1.795	5	0.8342	-1.790	8
0.6567	-1.856	7	0.7563	-1.782	6	0.8407	-1.754	3

Bin Size	0.0020			Phase Range		0.9200 to 1.0000		
Phase	Magn	No	Phase	Magn	No	Phase	Magn	No
0.9231	-1.761	2	0.9488	-1.803	4	0.9747	-1.113	4
0.9249	-1.800	1	0.9519	-1.730	1	0.9773	-0.970	2
0.9270	-1.814	3	0.9531	-1.800	1	0.9791	-0.916	2
0.9298	-1.750	1	0.9549	-1.760	2	0.9806	-0.840	1
0.9312	-1.770	2	0.9572	-1.660	2	0.9829	-0.691	2
0.9333	-1.800	1	0.9590	-1.673	4	0.9850	-0.620	2
0.9347	-1.840	2	0.9606	-1.678	3	0.9871	-0.585	2
0.9371	-1.815	2	0.9625	-1.610	2	0.9691	-0.547	3
0.9351	-1.860	3	0.9652	-1.445	2	0.9914	-0.536	2
0.9407	-1.823	3	0.9671	-1.370	2	0.9940	-0.450	1
0.9429	-1.770	6	0.9690	-1.361	4	0.9970	-0.560	1
0.9448	-1.789	5	0.9710	-1.294	3	0.9987	-0.510	1
0.9467	-1.724	6	0.9729	-1.221	5			

TABLE 13

NORMAL POINTS FOR 1963 DATA

Bin Size 0.0020 Phase Range 0.0000 to 0.0800

Phase	Magn.	No.	Phase	Magn.	No.	Phase	Magn.	No.
0.0010	0.622	11	0.0227	0.648	3	0.0530	0.057	4
0.0030	0.637	11	0.0251	0.632	3	0.0549	-0.013	7
0.0051	0.631	11	0.0267	0.635	2	0.0572	-0.088	6
0.0070	0.638	7	0.0373	0.613	4	0.0613	-0.173	2
0.0090	0.652	4	0.0391	0.575	2	0.0628	-0.201	3
0.0112	0.635	3	0.0410	0.502	7	0.0650	-0.241	4
0.0129	0.635	3	0.0430	0.449	5	0.0670	-0.295	3
0.0150	0.645	4	0.0450	0.362	5	0.0688	-0.317	3
0.0171	0.639	5	0.0468	0.292	6	0.0706	-0.324	2
0.0190	0.654	3	0.0490	0.216	7			
0.0208	0.643	6	0.0510	0.133	7			

Bin Size 0.0100 Phase Range 0.0800 to 0.4200

Phase	Magn.	No.	Phase	Magn.	No.	Phase	Magn.	No.
0.0894	-0.343	3	0.1956	-0.306	11	0.3344	-0.235	23
0.0960	-0.341	23	0.2070	-0.293	10	0.3448	-0.224	22
0.1053	-0.345	22	0.2161	-0.285	14	0.3562	-0.225	11
0.1103	-0.350	1	0.2246	-0.289	15	0.3682	-0.224	7
0.1373	-0.343	8	0.2348	-0.285	16	0.3763	-0.216	9
0.1449	-0.332	17	0.2400	-0.292	1	0.3847	-0.213	17
0.1550	-0.331	18	0.2642	-0.263	13	0.3954	-0.218	15
0.1650	-0.316	15	0.2664	-0.266	15	0.4024	-0.213	7
0.1748	-0.316	28	0.2730	-0.264	10	0.4165	-0.203	11
0.1831	-0.311	17	0.3280	-0.240	12			

Bin Size 0.0020 Phase Range 0.4200 to 0.5800

Phase	Magn.	No.	Phase	Magn.	No.	Phase	Magn.	No.
0.4232	-0.210	2	0.4461	-0.207	4	0.5409	-0.156	4
0.4250	-0.212	3	0.4472	-0.217	2	0.5431	-0.165	5
0.4270	-0.205	4	0.4493	-0.226	3	0.5449	-0.171	5
0.4291	-0.212	2	0.4508	-0.212	2	0.5470	-0.189	3
0.4331	-0.205	3	0.4529	-0.203	4	0.5488	-0.193	3
0.4350	-0.215	3	0.4554	-0.204	2	0.5509	-0.201	4
0.4371	-0.213	4	0.4568	-0.210	2	0.5532	-0.198	3
0.4391	-0.203	3	0.5353	-0.153	3	0.5551	-0.210	7
0.4413	-0.201	3	0.5370	-0.160	5	0.5572	-0.216	6
0.4430	-0.212	3	0.5388	-0.162	4	0.5589	-0.221	6

TABLE 13 - Continued

Bin Size 0.0020 Phase Range 0.4200 to 0.5800

Phase	Magn	No	Phase	Magn	No	Phase	Magn	No
0.5611	-0.224	7	0.5670	-0.235	7	0.5731	-0.250	7
0.5629	-0.238	3	0.5690	-0.260	7	0.5795	-0.247	4
0.5650	-0.236	6	0.5711	-0.248	7			

Bin Size 0.0100 Phase Range 0.5800 to 0.9200

Phase	Magn	No	Phase	Magn	No	Phase	Magn	No
0.5844	-0.254	43	0.7144	-0.321	12	0.8250	-0.372	16
0.5944	-0.248	18	0.7355	-0.338	11	0.8345	-0.379	18
0.6271	-0.285	10	0.7464	-0.348	28	0.8452	-0.392	17
0.6344	-0.293	14	0.7548	-0.351	49	0.8689	-0.383	3
0.6451	-0.304	16	0.7652	-0.353	45	0.8748	-0.378	15
0.6543	-0.309	12	0.7760	-0.359	30	0.8845	-0.379	13
0.6645	-0.319	16	0.7851	-0.356	34	0.8943	-0.382	12
0.6871	-0.318	5	0.7941	-0.365	26	0.9046	-0.378	14
0.6948	-0.323	14	0.8053	-0.373	14	0.9142	-0.379	15
0.7056	-0.323	13	0.8147	-0.374	13			

Bin Size 0.0020 Phase Range 0.9200 to 1.0000

Phase	Magn	No	Phase	Magn	No	Phase	Magn	No
0.9493	-0.385	1	0.9669	-0.343	3	0.9872	0.141	4
0.9511	-0.348	1	0.9709	-0.285	2	0.9889	0.218	3
0.9531	-0.388	3	0.9729	-0.255	4	0.9909	0.303	5
0.9551	-0.384	4	0.9749	-0.223	3	0.9930	0.367	5
0.9572	-0.369	2	0.9768	-0.164	4	0.9950	0.439	4
0.9591	-0.369	3	0.9791	-0.093	4	0.9970	0.516	8
0.9609	-0.369	3	0.9811	-0.056	3	0.9989	0.589	7
0.9630	-0.364	4	0.9830	0.006	4			
0.9651	-0.356	3	0.9850	0.076	5			

TABLE 14

NORMAL POINTS FOR 1964 DATA

Bin Size: 0.0020 Phase Range: 0.0000 to 0.0800

Phase	Magn	No	Phase	Magn	No	Phase	Magn.	No
0.0008	0.621	3	0.0328	0.631	4	0.0593	-0.144	4
0.0029	0.628	3	0.0350	0.632	4	0.0611	-0.180	4
0.0049	0.636	4	0.0371	0.578	4	0.0631	-0.234	5
0.0070	0.633	3	0.0391	0.513	5	0.0651	-0.263	7
0.0093	0.654	3	0.0410	0.448	3	0.0669	-0.297	5
0.0113	0.640	2	0.0430	0.381	4	0.0690	-0.328	4
0.0130	0.642	3	0.0450	0.307	4	0.0710	-0.335	3
0.0152	0.639	3	0.0469	0.229	3	0.0731	-0.344	4
0.0170	0.640	3	0.0489	0.153	4	0.0753	-0.347	3
0.0187	0.642	2	0.0509	0.096	3	0.0770	-0.357	2
0.0273	0.649	3	0.0529	0.027	4	0.0790	-0.337	4
0.0291	0.640	4	0.0550	-0.037	3			
0.0308	0.645	4	0.0570	-0.090	4			

Bin Size: 0.0100 Phase Range: 0.0800 to 0.4200

Phase	Magn.	No	Phase	Magn	No	Phase	Magn	No
0.0847	-0.339	13	0.2248	-0.240	11	0.3248	-0.202	17
0.0949	-0.333	18	0.2340	-0.238	7	0.3344	-0.200	10
0.1028	-0.335	9	0.2880	-0.218	6	0.3453	-0.200	8
0.1770	-0.293	5	0.2947	-0.215	10	0.3552	-0.196	9
0.2080	-0.255	7	0.3030	-0.214	10	0.3634	-0.201	5
0.2142	-0.248	7	0.3150	-0.208	13	0.4157	-0.200	5

Bin Size: 0.0020 Phase Range: 0.4200 to 0.5800

Phase	Magn	No	Phase	Magn	No	Phase	Magn	No
0.4588	-0.213	3	0.4909	-0.154	3	0.5152	-0.161	6
0.4608	-0.209	3	0.4930	-0.144	4	0.5171	-0.158	5
0.4717	-0.200	2	0.4950	-0.147	3	0.5189	-0.157	5
0.4731	-0.209	3	0.4969	-0.129	3	0.5209	-0.163	6
0.4749	-0.210	2	0.4989	-0.130	3	0.5229	-0.170	6
0.4770	-0.192	4	0.5009	-0.146	3	0.5249	-0.181	7
0.4791	-0.182	3	0.5029	-0.143	4	0.5270	-0.173	6
0.4809	-0.175	3	0.5050	-0.132	3	0.5292	-0.185	5
0.4829	-0.172	3	0.5069	-0.157	3	0.5310	-0.188	5
0.4848	-0.175	3	0.5088	-0.153	4	0.5329	-0.190	3
0.4869	-0.162	4	0.5107	-0.147	3	0.5348	-0.204	3
0.4891	-0.143	3	0.5130	-0.158	6	0.5369	-0.198	4

TABLE 14 — Continued

Bin Size 0.0020 Phase Range 0.4200 to 0.5800

Phase	Magn	No	Phase	Magn	No	Phase	Magn	No
0.5393	-0.212	5	0.5513	-0.228	3	0.5685	-0.288	3
0.5409	-0.208	5	0.5534	-0.242	3	0.5710	-0.298	3
0.5431	-0.225	6	0.5551	-0.262	2	0.5732	-0.302	4
0.5458	-0.208	1	0.5572	-0.265	2	0.5751	-0.287	3
0.5475	-0.223	2	0.5655	-0.275	1	0.5771	-0.290	1
0.5493	-0.227	3	0.5685	-0.285	2	0.5791	-0.296	2

Bin Size 0.0100 Phase Range 0.5800 to 0.9200

Phase	Magn	No	Phase	Magn	No	Phase	Magn	No
0.5880	-0.303	7	0.6750	-0.358	8	0.8053	-0.391	7
0.5963	-0.308	7	0.6836	-0.376	6	0.8134	-0.385	7
0.6051	-0.317	7	0.7452	-0.384	7	0.8677	-0.403	4
0.6145	-0.322	5	0.7513	-0.397	2	0.8747	-0.402	7
0.6232	-0.331	5	0.7887	-0.410	1	0.8851	-0.359	8
0.6670	-0.360	5	0.7939	-0.390	7	0.8910	-0.359	2

Bin Size 0.0020 Phase Range 0.9200 to 1.0000

Phase	Magn	No	Phase	Magn	No.	Phase	Magn.	No.
0.9253	-0.391	3	0.9468	-0.389	3	0.9711	-0.262	3
0.9270	-0.389	3	0.9491	-0.381	2	0.9731	-0.227	2
0.9288	-0.389	3	0.9512	-0.383	2	0.9746	-0.210	2
0.9309	-0.353	3	0.9528	-0.402	3	0.9859	0.187	4
0.9330	-0.395	4	0.9572	-0.397	3	0.9889	0.251	4
0.9350	-0.395	3	0.9597	-0.410	1	0.9908	0.320	4
0.9369	-0.390	3	0.9611	-0.374	4	0.9932	0.408	3
0.9395	-0.385	1	0.9631	-0.387	3	0.9950	0.472	4
0.9409	-0.392	3	0.9649	-0.371	3	0.9970	0.539	4
0.9425	-0.400	2	0.9665	-0.354	2	0.9989	0.592	3
0.9451	-0.383	3	0.9699	-0.282	1			

TABLE 15

NORMAL POINTS FOR 1966 DATA

Bin Size 0.0020 Phase Range 0.0000 to 0.0800

Phase	Magn	No.	Phase	Magn	No.	Phase	Magn	No.
0.0011	0.865	1	0.0312	0.839	4	0.0571	-0.051	4
0.0029	0.842	2	0.0331	0.844	3	0.0590	-0.098	3
0.0052	0.828	2	0.0348	0.823	6	0.0607	-0.112	2
0.0071	0.895	1	0.0369	0.714	5	0.0632	-0.169	7
0.0088	0.847	2	0.0389	0.655	5	0.0651	-0.191	6
0.0110	0.840	1	0.0409	0.568	7	0.0669	-0.206	6
0.0128	0.863	2	0.0427	0.489	2	0.0690	-0.251	4
0.0193	0.858	3	0.0450	0.357	6	0.0708	-0.267	4
0.0210	0.851	8	0.0472	0.301	5	0.0723	-0.247	1
0.0231	0.845	6	0.0492	0.228	4	0.0747	-0.271	2
0.0249	0.845	4	0.0508	0.161	4	0.0766	-0.260	1
0.0269	0.855	6	0.0530	0.075	5	0.0785	-0.266	2
0.0291	0.847	5	0.0560	0.033	4			

Bin Size 0.0148 Phase Range 0.0800 to 0.4500

Phase	Magn.	No.	Phase	Magn.	No.	Phase	Magn.	No
0.0876	-0.263	10	0.2224	-0.252	19	0.3545	-0.228	10
0.1075	-0.270	3	0.2341	-0.249	24	0.3697	-0.218	20
0.1171	-0.259	12	0.2501	-0.248	11	0.3831	-0.225	13
0.1314	-0.262	9	0.2651	-0.244	12	0.3986	-0.222	11
0.1469	-0.266	22	0.2794	-0.224	12	0.4124	-0.231	11
0.1605	-0.258	14	0.2901	-0.236	6	0.4278	-0.242	4
0.1758	-0.244	11	0.3120	-0.237	14	0.4430	-0.239	19
0.1902	-0.247	9	0.3241	-0.218	12			
0.2073	-0.256	10	0.3361	-0.201	2			

Bin Size 0.0032 Phase Range 0.4500 to 0.5800

Phase	Magn	No.	Phase	Magn.	No.	Phase	Magn.	No.
0.4517	-0.241	2	0.4810	-0.188	6	0.5166	-0.109	2
0.4548	-0.225	3	0.4840	-0.162	8	0.5196	-0.144	3
0.4592	-0.230	1	0.4879	-0.172	2	0.5231	-0.149	3
0.4615	-0.229	3	0.4905	-0.163	2	0.5267	-0.157	3
0.4649	-0.219	2	0.4935	-0.137	3	0.5302	-0.189	2
0.4678	-0.205	3	0.4971	-0.122	3	0.5331	-0.155	3
0.4714	-0.204	2	0.5008	-0.116	3	0.5361	-0.212	2
0.4748	-0.216	5	0.5042	-0.107	2	0.5380	-0.176	1
0.4778	-0.181	7	0.5071	-0.103	3	0.5429	-0.215	2

TABLE 15 - Continued

Bin Size 0.0032 Phase Range 0.4500 to 0.5800

Phase	Magn.	No.	Phase	Magn.	No.	Phase	Magn.	No.
0.5458	-0.220	3	0.5619	-0.282	5	0.5718	-0.296	5
0.5482	-0.231	1	0.5649	-0.295	4	0.5747	-0.320	2
0.5592	-0.296	3	0.5691	-0.298	4	0.5785	-0.324	2

Bin Size 0.0148 Phase Range 0.5800 to 0.9500

Phase	Magn.	No.	Phase	Magn.	No.	Phase	Magn.	No.
0.5870	-0.318	12	0.7210	-0.391	14	0.8567	-0.382	15
0.6034	-0.334	18	0.7358	-0.385	29	0.8679	-0.372	21
0.6157	-0.351	15	0.7510	-0.361	22	0.8834	-0.361	12
0.6320	-0.356	11	0.7648	-0.370	19	0.8966	-0.369	14
0.6462	-0.361	16	0.7798	-0.393	26	0.9128	-0.354	12
0.6634	-0.356	6	0.7948	-0.403	20	0.9296	-0.339	12
0.6785	-0.382	6	0.8105	-0.389	25	0.9428	-0.332	23
0.6911	-0.391	11	0.8228	-0.392	25			
0.7060	-0.385	9	0.8362	-0.374	9			

Bin Size 0.0020 Phase Range 0.9500 to 1.0000

Phase	Magn.	No.	Phase	Magn.	No.	Phase	Magn.	No.
0.9504	-0.323	2	0.9689	-0.183	3	0.9869	0.411	2
0.9530	-0.337	4	0.9710	-0.130	4	0.9887	0.469	1
0.9553	-0.331	4	0.9732	-0.041	4	0.9915	0.577	2
0.9570	-0.311	4	0.9747	-0.048	2	0.9930	0.654	1
0.9588	-0.315	5	0.9768	0.002	2	0.9948	0.711	2
0.9607	-0.315	4	0.9793	0.093	2	0.9971	0.780	2
0.9628	-0.277	3	0.9813	0.176	1	0.9994	0.806	2
0.9650	-0.256	4	0.9832	0.241	2			
0.9672	-0.225	3	0.9850	0.304	1			

TABLE 16

NORMAL POINTS FOR 1966 DATA

Bin Size 0.0020 Phase Range 0.0000 to 0.0800

Phase	Magn.	No.	Phase	Magn.	No.	Phase	Magn.	No.
0.0012	0.889	1	0.0289	0.973	5	0.0574	-0.011	2
0.0030	0.883	2	0.0308	0.964	5	0.0589	-0.041	3
0.0050	0.891	1	0.0329	0.891	5	0.0611	-0.082	4
0.0068	0.884	2	0.0349	0.815	6	0.0630	-0.117	2
0.0091	0.879	2	0.0369	0.729	4	0.0646	-0.142	3
0.0110	0.872	1	0.0391	0.624	4	0.0673	-0.163	2
0.0132	0.929	3	0.0412	0.538	2	0.0691	-0.165	1
0.0150	0.949	3	0.0429	0.451	3	0.0710	-0.170	2
0.0173	0.966	6	0.0451	0.359	3	0.0729	-0.164	1
0.0195	0.959	3	0.0471	0.289	3	0.0747	-0.167	2
0.0211	0.954	3	0.0489	0.227	3	0.0771	-0.170	2
0.0230	0.980	6	0.0510	0.170	3	0.0790	-0.170	1
0.0251	0.965	4	0.0530	0.097	1			
0.0269	0.960	5	0.0549	0.042	2			

Bin Size 0.0146 Phase Range 0.0800 to 0.4500

Phase	Magn.	No.	Phase	Magn.	No.	Phase	Magn.	No.
0.0833	-0.169	6	0.2057	-0.180	29	0.3178	-0.246	2
0.1047	-0.161	6	0.2209	-0.186	27	0.3690	-0.243	7
0.1168	-0.173	21	0.2342	-0.192	19	0.3887	-0.250	3
0.1329	-0.172	18	0.2451	-0.207	3	0.3978	-0.256	22
0.1484	-0.176	27	0.2686	-0.211	11	0.4107	-0.277	11
0.1605	-0.171	16	0.2792	-0.222	21	0.4322	-0.267	11
0.1779	-0.173	19	0.2961	-0.248	9	0.4426	-0.268	22
0.1908	-0.180	37	0.3095	-0.262	12			

Bin Size 0.0032 Phase Range 0.4500 to 0.5800

Phase	Magn	No	Phase	Magn	No	Phase	Magn	No
0.4516	-0.269	6	0.4808	-0.240	4	0.5101	-0.181	3
0.4551	-0.281	5	0.4843	-0.223	6	0.5136	-0.172	4
0.4591	-0.276	2	0.4873	-0.213	3	0.5164	-0.185	5
0.4616	-0.287	2	0.4908	-0.227	3	0.5203	-0.181	5
0.4645	-0.287	4	0.4938	-0.193	4	0.5234	-0.181	4
0.4677	-0.267	2	0.4970	-0.192	5	0.5269	-0.183	4
0.4712	-0.257	4	0.5001	-0.175	3	0.5296	-0.188	2
0.4746	-0.258	6	0.5038	-0.173	3	0.5329	-0.193	3
0.4780	-0.249	6	0.5069	-0.189	2	0.5360	-0.221	2

TABLE 16 - Continued

Bin Size: 0.0032 Phase Range: 0.4500 to 0.5800

Phase	Magn	No	Phase	Magn	No	Phase	Magn	No
0.5390	-0.216	3	0.5527	-0.279	2	0.5644	-0.325	1
0.5425	-0.237	3	0.5556	-0.289	6	0.5716	-0.320	3
0.5460	-0.252	3	0.5589	-0.301	5	0.5755	-0.333	2
0.5495	-0.265	3	0.5618	-0.308	4	0.5785	-0.322	3

Bin Size: 0.0148 Phase Range: 0.5800 to 0.9500

Phase	Magn.	No.	Phase	Magn.	No.	Phase	Magn.	No.
0.5855	-0.339	8	0.7039	-0.341	11	0.8231	-0.282	16
0.6043	-0.324	4	0.7210	-0.328	16	0.8390	-0.267	10
0.6143	-0.349	8	0.7360	-0.334	20	0.8539	-0.272	19
0.6382	-0.330	1	0.7492	-0.327	19	0.8694	-0.250	10
0.6462	-0.324	12	0.7666	-0.320	18	0.8832	-0.241	10
0.6600	-0.338	12	0.7776	-0.325	16	0.8984	-0.240	9
0.6772	-0.334	10	0.7972	-0.311	5	0.9072	-0.234	2
0.6911	-0.345	14	0.8096	-0.304	13			

Bin Size: 0.0010 Phase Range: 0.9500 to 1.0000

Phase	Magn	No	Phase	Magn	No	Phase	Magn.	No.
0.9710	-0.091	1	0.9804	0.227	1	0.9907	0.814	1
0.9723	0.036	1	0.9817	0.351	2	0.9918	0.876	1
0.9734	0.080	2	0.9829	0.447	2	0.9931	0.958	1
0.9746	0.113	2	0.9843	0.518	1	0.9943	1.037	1
0.9758	0.164	2	0.9856	0.597	1	0.9986	0.888	1
0.9770	0.173	2	0.9868	0.649	1	0.9999	0.889	1
0.9782	0.230	2	0.9881	0.725	1			
0.9793	0.256	2	0.9893	0.832	1			

TABLE 17

NORMAL POINTS FOR 1975V DATA

Bin Size	0.0020			Phase Range		0.0000 to 0.0800		
Phase	Magn.	No.	Phase	Magn.	No.	Phase	Magn.	No.
0.0004	0.778	1	0.0369	0.051	2	0.0570	-0.296	3
0.0035	0.781	1	0.0388	-0.013	2	0.0593	-0.288	2
0.0118	0.783	1	0.0410	-0.088	3	0.0615	-0.292	1
0.0149	0.780	1	0.0434	-0.140	2	0.0631	-0.277	1
0.0173	0.748	1	0.0451	-0.172	2	0.0644	-0.282	1
0.0187	0.707	2	0.0463	-0.188	1			
0.0351	0.081	2	0.0550	-0.299	1			

Bin Size	0.0100			Phase Range		0.0800 to 0.4200		
Phase	Magn.	No.	Phase	Magn.	No.	Phase	Magn.	No.
0.0834	-0.279	2	0.2569	-0.300	2	0.3560	-0.354	4
0.0975	-0.267	4	0.2630	-0.311	2	0.3655	-0.367	2
0.1282	-0.281	2	0.2773	-0.308	2	0.3750	-0.373	8
0.1343	-0.293	3	0.2861	-0.305	2	0.3832	-0.376	4
0.1415	-0.289	2	0.2988	-0.317	1	0.3947	-0.384	6
0.1587	-0.279	1	0.3025	-0.321	5	0.4057	-0.396	6
0.1639	-0.282	3	0.3383	-0.333	2	0.4150	-0.391	7
0.1759	-0.286	4	0.3423	-0.360	4			

Bin Size	0.0020			Phase Range		0.4200 to 0.5800		
Phase	Magn.	No.	Phase	Magn.	No.	Phase	Magn.	No.
0.4201	-0.391	1	0.4667	-0.344	1	0.5032	-0.256	1
0.4226	-0.389	2	0.4686	-0.338	2	0.5049	-0.259	2
0.4252	-0.394	2	0.4711	-0.330	2	0.5067	-0.273	1
0.4275	-0.417	1	0.4730	-0.325	1	0.5093	-0.260	1
0.4286	-0.402	1	0.4741	-0.324	1	0.5110	-0.266	2
0.4308	-0.392	2	0.4811	-0.285	2	0.5133	-0.270	2
0.4473	-0.409	1	0.4831	-0.287	1	0.5150	-0.265	1
0.4489	-0.403	2	0.4850	-0.269	2	0.5270	-0.327	1
0.4506	-0.400	1	0.4869	-0.270	1	0.5285	-0.350	1
0.4525	-0.390	2	0.4892	-0.252	2	0.5392	-0.391	2
0.4547	-0.382	2	0.4912	-0.257	1	0.5417	-0.407	1
0.4571	-0.389	1	0.4929	-0.259	2	0.5427	-0.402	1
0.4581	-0.374	1	0.4946	-0.250	1	0.5448	-0.429	2
0.4635	-0.366	1	0.4966	-0.245	2	0.5496	-0.428	1
0.4652	-0.349	2	0.5013	-0.259	2	0.5610	-0.423	1

TABLE 17 - Continued

Bin Size: 0.0020 Phase Range: 0.4200 to 0.6800

Phase	Magn.	No.	Phase	Magn.	No.	Phase	Magn.	No.
0.5530	-0.438	1	0.5596	-0.436	1	0.5721	-0.424	1
0.5552	-0.438	1	0.5677	-0.441	1	0.5741	-0.435	1
0.5674	-0.429	1	0.5699	-0.436	1	0.5763	-0.436	1

Bin Size: 0.0100 Phase Range: 0.5800 to 0.9200

Phase	Magn.	No.	Phase	Magn.	No.	Phase	Magn.	No.
0.5864	-0.439	3	0.7070	-0.434	5	0.8470	-0.380	8
0.5952	-0.439	5	0.7148	-0.427	7	0.8551	-0.372	5
0.6018	-0.438	1	0.7211	-0.439	2	0.8647	-0.371	5
0.6586	-0.448	2	0.7425	-0.413	1	0.8766	-0.365	8
0.6648	-0.437	6	0.7925	-0.398	3	0.8849	-0.357	10
0.6747	-0.439	8	0.8084	-0.387	2	0.8907	-0.363	2
0.6893	-0.433	2	0.8125	-0.395	5			
0.6952	-0.435	6	0.8367	-0.381	3			

Bin Size: 0.0020 Phase Range: 0.9200 to 1.0000

Phase	Magn.	No.	Phase	Magn.	No.	Phase	Magn.	No.
0.9341	-0.336	1	0.9594	-0.051	2	0.9787	0.665	1
0.9363	-0.336	1	0.9619	0.019	2	0.9801	0.711	1
0.9387	-0.339	1	0.9650	0.132	2	0.9848	0.749	1
0.9445	-0.319	1	0.9667	0.195	2	0.9862	0.752	1
0.9464	-0.309	2	0.9688	0.277	3	0.9884	0.757	1
0.9492	-0.267	2	0.9710	0.377	1	0.9916	0.763	1
0.9510	-0.244	1	0.9724	0.436	1	0.9943	0.763	1
0.9532	-0.208	1	0.9749	0.530	2	0.9968	0.763	1
0.9563	-0.138	1	0.9772	0.508	1			

TABLE 18

NORMAL POINTS FOR 1976V DATA

Bin Size	0.0020			Phase Range		0.0000 to 0.0800		
Phase	Magn	No	Phase	Magn	No	Phase	Magn	No
0.0251	0.480	1	0.0448	-0.149	2	0.0654	-0.234	3
0.0275	0.381	3	0.0464	-0.174	1	0.0672	-0.232	3
0.0289	0.326	3	0.0488	-0.211	2	0.0687	-0.236	1
0.0311	0.244	2	0.0507	-0.229	2	0.0708	-0.235	4
0.0325	0.186	1	0.0526	-0.246	2	0.0733	-0.241	1
0.0350	0.104	3	0.0546	-0.245	2	0.0749	-0.236	3
0.0380	0.002	1	0.0572	-0.257	1	0.0772	-0.236	3
0.0399	-0.036	1	0.0586	-0.247	2	0.0791	-0.231	3
0.0411	-0.071	2	0.0610	-0.240	4			
0.0424	-0.107	1	0.0631	-0.240	4			

Bin Size	0.0100			Phase Range		0.0800 to 0.4200		
Phase	Magn	No	Phase	Magn	No	Phase	Magn	No
0.0823	-0.239	3	0.1912	-0.258	2	0.2918	-0.340	2
0.1157	-0.225	8	0.2083	-0.261	3	0.3024	-0.363	4
0.1253	-0.223	10	0.2371	-0.294	7	0.3654	-0.400	5
0.1307	-0.228	2	0.2461	-0.302	11	0.3752	-0.404	10
0.1564	-0.237	4	0.2565	-0.315	10	0.3813	-0.413	1
0.1648	-0.238	8	0.2671	-0.324	7	0.3966	-0.413	6
0.1747	-0.245	5	0.2750	-0.329	7	0.4059	-0.415	5
0.1854	-0.255	9	0.2848	-0.336	5	0.4161	-0.416	12

Bin Size	0.0020			Phase Range		0.4200 to 0.5800		
Phase	Magn	No	Phase	Magn	No	Phase	Magn	No
0.4207	-0.420	4	0.4471	-0.426	2	0.4889	-0.281	1
0.4229	-0.423	4	0.4491	-0.406	2	0.4910	-0.288	2
0.4242	-0.421	1	0.4510	-0.405	3	0.4936	-0.286	2
0.4266	-0.409	1	0.4528	-0.420	1	0.4948	-0.284	1
0.4292	-0.425	2	0.4543	-0.419	1	0.4960	-0.290	1
0.4336	-0.413	1	0.4566	-0.392	1	0.5013	-0.279	1
0.4349	-0.413	1	0.4583	-0.398	1	0.6708	-0.402	1
0.4369	-0.417	2	0.4606	-0.396	1	0.5730	-0.412	2
0.4391	-0.417	1	0.4623	-0.373	1	0.5751	-0.396	1
0.4431	-0.426	3	0.4852	-0.301	1	0.5766	-0.395	2
0.4450	-0.429	2	0.4874	-0.297	2			

TABLE 18 - Continued

Bin Size	0.0100			Phase Range		0.5800 to 0.9200		
Phase	Magn.	No.	Phase	Magn.	No.	Phase	Magn.	No.
0.5847	-0.396	8	0.6989	-0.346	1	0.8366	-0.325	9
0.5918	-0.391	4	0.7049	-0.343	7	0.8444	-0.328	4
0.6078	-0.382	2	0.7153	-0.340	8	0.8547	-0.326	5
0.6159	-0.371	8	0.7217	-0.340	2	0.8648	-0.325	4
0.6295	-0.358	1	0.7334	-0.331	6	0.8730	-0.316	2
0.6357	-0.357	2	0.7494	-0.317	2	0.9195	-0.334	1
0.6475	-0.345	3	0.7563	-0.339	4			
0.6549	-0.338	4	0.7611	-0.328	1			

Bin Size	0.0020			Phase Range		0.9200 to 1.0000		
Phase	Magn.	No.	Phase	Magn.	No.	Phase	Magn.	No.
0.9203	-0.329	1	0.9471	-0.243	1	0.9710	0.478	3
0.9225	-0.309	2	0.9487	-0.227	3	0.9731	0.566	3
0.9253	-0.302	2	0.9510	-0.196	3	0.9753	0.660	3
0.9275	-0.285	1	0.9530	-0.138	2	0.9771	0.724	2
0.9283	-0.283	1	0.9552	-0.089	3	0.9788	0.777	2
0.9318	-0.298	1	0.9572	-0.017	2	0.9827	0.816	2
0.9326	-0.301	1	0.9587	0.014	3	0.9851	0.829	2
0.9349	-0.321	2	0.9606	0.073	3	0.9865	0.835	1
0.9373	-0.331	2	0.9628	0.204	4	0.9957	0.845	1
0.9413	-0.286	1	0.9646	0.217	1	0.9972	0.841	2
0.9431	-0.266	1	0.9670	0.316	2	0.9985	0.850	1
0.9447	-0.288	1	0.9694	0.409	2			

TABLE 19

NORMAL POINTS FOR 1975R DATA

Bin Size 0.0020 Phase Range 0.0000 to 0.0800

Phase	Magn	No	Phase	Magn	No	Phase	Magn	No
0.0004	1.304	1	0.0369	0.247	2	0.0570	-0.169	3
0.0035	1.310	1	0.0388	0.146	2	0.0593	-0.169	2
0.0118	1.327	1	0.0410	0.101	3	0.0615	-0.170	1
0.0149	1.325	1	0.0434	0.032	2	0.0631	-0.167	1
0.0173	1.272	1	0.0451	-0.012	2	0.0644	-0.175	1
0.0187	1.149	2	0.0463	-0.050	1			
0.0351	0.327	2	0.0550	-0.181	1			

Bin Size 0.0100 Phase Range 0.0800 to 0.4200

Phase	Magn	No	Phase	Magn	No	Phase	Magn	No
0.0834	-0.169	2	0.2569	-0.182	2	0.3560	-0.223	4
0.0975	-0.155	4	0.2630	-0.187	2	0.3655	-0.211	2
0.1282	-0.158	2	0.2773	-0.186	2	0.3750	-0.226	8
0.1343	-0.163	3	0.2861	-0.169	2	0.3832	-0.230	4
0.1415	-0.160	2	0.2968	-0.193	1	0.3947	-0.234	6
0.1587	-0.161	1	0.3025	-0.185	5	0.4057	-0.245	6
0.1639	-0.159	3	0.3383	-0.202	2	0.4150	-0.239	7
0.1759	-0.165	4	0.3423	-0.208	4			

Bin Size 0.0020 Phase Range 0.4200 to 0.5800

Phase	Magn	No	Phase	Magn	No	Phase	Magn	No
0.4201	-0.236	1	0.4667	-0.199	1	0.5032	-0.129	1
0.4226	-0.237	2	0.4686	-0.203	2	0.5049	-0.135	2
0.4252	-0.240	2	0.4711	-0.194	2	0.5067	-0.151	1
0.4275	-0.243	1	0.4730	-0.193	1	0.5093	-0.121	1
0.4286	-0.247	1	0.4741	-0.168	1	0.5110	-0.151	2
0.4306	-0.248	2	0.4811	-0.162	2	0.5133	-0.160	2
0.4473	-0.252	1	0.4831	-0.165	1	0.5150	-0.147	1
0.4489	-0.246	2	0.4850	-0.152	2	0.5270	-0.178	1
0.4506	-0.238	1	0.4869	-0.147	1	0.5285	-0.203	1
0.4525	-0.242	2	0.4892	-0.132	2	0.5392	-0.249	2
0.4547	-0.235	2	0.4912	-0.131	1	0.5417	-0.253	1
0.4571	-0.229	1	0.4929	-0.131	2	0.5427	-0.256	1
0.4581	-0.217	1	0.4946	-0.139	1	0.5448	-0.267	2
0.4635	-0.213	1	0.4966	-0.128	2	0.5496	-0.246	1
0.4652	-0.208	2	0.5013	-0.145	2	0.5510	-0.273	1

TABLE 19 - Continued

Bin Size 0.0020 Phase Range 0.4200 to 0.5800

Phase	Magn.	No	Phase	Magn	No	Phase	Magn	No
0.5530	-0.269	1	0.5595	-0.282	1	0.5721	-0.284	1
0.5552	-0.279	1	0.5677	-0.293	1	0.5741	-0.285	1
0.5574	-0.272	1	0.5699	-0.288	1	0.5763	-0.287	1

Bin Size 0.0100 Phase Range 0.5800 to 0.9200

Phase	Magn.	No	Phase	Magn	No	Phase	Magn	No
0.5864	-0.282	3	0.7070	-0.265	5	0.8470	-0.232	8
0.5952	-0.279	5	0.7148	-0.268	7	0.8551	-0.233	5
0.6018	-0.285	1	0.7211	-0.271	2	0.8647	-0.229	5
0.6685	-0.274	2	0.7425	-0.272	1	0.8766	-0.217	8
0.6548	-0.277	6	0.7925	-0.254	3	0.8849	-0.215	10
0.6747	-0.275	8	0.8084	-0.245	2	0.8907	-0.235	2
0.6893	-0.276	2	0.8125	-0.239	5			
0.6962	-0.267	6	0.8357	-0.249	3			

Bin Size 0.0020 Phase Range 0.9200 to 1.0000

Phase	Magn	No.	Phase	Magn	No	Phase	Magn	No
0.9341	-0.205	1	0.9594	0.149	2	0.9787	1.150	1
0.9363	-0.204	1	0.9619	0.235	2	0.9801	1.211	1
0.9387	-0.203	1	0.9650	0.379	2	0.9848	1.262	1
0.9445	-0.180	1	0.9667	0.458	2	0.9862	1.276	1
0.9464	-0.163	2	0.9688	0.572	3	0.9884	1.283	1
0.9492	-0.127	2	0.9710	0.713	1	0.9916	1.280	1
0.9510	-0.097	1	0.9724	0.789	1	0.9943	1.287	1
0.9532	-0.037	1	0.9749	0.943	2	0.9968	1.287	1
0.9563	0.050	1	0.9772	1.066	1			

TABLE 20

NORMAL POINTS FOR 1976B DATA

Bin Size	0.0020			Phase Range		0.0000 to 0.0800		
Phase	Magn.	No.	Phase	Magn.	No.	Phase	Magn.	No.
0.0251	0.865	1	0.0448	-0.015	2	0.0654	-0.115	3
0.0275	0.674	3	0.0464	-0.037	1	0.0672	-0.117	3
0.0289	0.594	3	0.0488	-0.085	2	0.0687	-0.116	1
0.0311	0.474	2	0.0507	-0.107	2	0.0708	-0.119	4
0.0325	0.409	1	0.0526	-0.121	2	0.0733	-0.121	1
0.0350	0.301	3	0.0546	-0.122	2	0.0749	-0.128	3
0.0380	0.187	1	0.0572	-0.131	1	0.0772	-0.117	3
0.0399	0.122	1	0.0586	-0.122	2	0.0791	-0.118	3
0.0411	0.080	2	0.0610	-0.126	4			
0.0424	0.051	1	0.0631	-0.122	4			

Bin Size	0.0100			Phase Range		0.0800 to 0.4200		
Phase	Magn.	No.	Phase	Magn.	No.	Phase	Magn.	No.
0.0823	-0.124	3	0.1912	-0.137	2	0.2918	-0.195	2
0.1157	-0.113	8	0.2053	-0.128	3	0.3024	-0.217	4
0.1253	-0.109	10	0.2371	-0.167	7	0.3654	-0.243	6
0.1307	-0.109	2	0.2451	-0.168	11	0.3752	-0.252	10
0.1564	-0.120	4	0.2555	-0.181	10	0.3813	-0.255	1
0.1646	-0.121	8	0.2671	-0.191	7	0.3966	-0.263	6
0.1747	-0.128	9	0.2750	-0.193	7	0.4059	-0.256	5
0.1854	-0.133	9	0.2848	-0.198	9	0.4161	-0.258	12

Bin Size	0.0020			Phase Range		0.4200 to 0.5800		
Phase	Magn.	No.	Phase	Magn.	No.	Phase	Magn.	No.
0.4207	-0.262	4	0.4471	-0.272	2	0.4869	-0.162	1
0.4229	-0.266	4	0.4491	-0.259	2	0.4910	-0.173	2
0.4242	-0.296	1	0.4510	-0.248	3	0.4936	-0.164	2
0.4266	-0.261	1	0.4528	-0.261	1	0.4948	-0.146	1
0.4292	-0.261	2	0.4543	-0.266	1	0.4960	-0.170	1
0.4336	-0.281	1	0.4568	-0.247	1	0.5013	-0.174	1
0.4349	-0.258	1	0.4583	-0.247	1	0.5708	-0.251	1
0.4369	-0.261	2	0.4606	-0.244	1	0.5730	-0.249	2
0.4391	-0.257	1	0.4623	-0.236	1	0.5751	-0.230	1
0.4431	-0.258	3	0.4852	-0.184	1	0.5766	-0.251	2
0.4450	-0.271	2	0.4874	-0.172	2			

TABLE 20 - Continued

Bin Size	0.0100			Phase Range		0.5800 to 0.9200		
Phase	Magn	No	Phase	Magn	No	Phase	Magn	No
0.5847	-0.243	8	0.6985	-0.199	1	0.8356	-0.187	9
0.5918	-0.236	4	0.7049	-0.192	7	0.8444	-0.186	4
0.6078	-0.230	2	0.7153	-0.201	8	0.8547	-0.189	5
0.6155	-0.224	8	0.7217	-0.188	2	0.8648	-0.189	4
0.6295	-0.221	1	0.7334	-0.193	6	0.8730	-0.187	2
0.6357	-0.213	2	0.7494	-0.183	2	0.9195	-0.198	1
0.6475	-0.199	3	0.7563	-0.191	4			
0.6549	-0.198	4	0.7611	-0.189	1			

Bin Size	0.0020			Phase Range		0.9200 to 1.0000		
Phase	Magn	No.	Phase	Magn	No.	Phase	Magn.	No.
0.9203	-0.193	1	0.9471	-0.095	1	0.9710	0.838	3
0.9225	-0.173	2	0.9487	-0.084	3	0.9731	0.958	3
0.9253	-0.183	2	0.9610	-0.045	3	0.9753	1.098	3
0.9275	-0.150	1	0.9530	0.033	2	0.9771	1.210	2
0.9283	-0.144	1	0.9552	0.089	3	0.9788	1.277	2
0.9318	-0.173	1	0.9572	0.161	2	0.9827	1.330	2
0.9326	-0.181	1	0.9587	0.199	3	0.9851	1.349	2
0.9349	-0.182	2	0.9606	0.284	3	0.9865	1.366	1
0.9373	-0.201	2	0.9628	0.449	4	0.9957	1.385	1
0.9413	-0.183	1	0.9646	0.486	1	0.9972	1.367	2
0.9431	-0.108	1	0.9670	0.609	2	0.9985	1.358	1
0.9447	-0.131	1	0.9694	0.735	2			

TABLE 21

NORMAL POINTS FOR 1975U DATA

Bin Size 0.0020 Phase Range 0.0000 to 0.0800

Phase	Magn.	No.	Phase	Magn	No	Phase	Magn.	No
0.0004	1.797	1	0.0118	1.857	1	0.0173	1.710	1
0.0035	1.824	1	0.0149	1.866	1	0.0187	1.542	2

Bin Size 0.0100 Phase Range 0.0800 to 0.4200

Phase	Magn.	No.	Phase	Magn	No.	Phase	Magn.	No.
0.3030	-0.071	4	0.3655	-0.096	2	0.4057	-0.134	5
0.3383	-0.116	2	0.3750	-0.117	8	0.4150	-0.134	7
0.3423	-0.120	4	0.3832	-0.123	4			
0.3560	-0.102	4	0.3947	-0.118	6			

Bin Size 0.0020 Phase Range 0.4200 to 0.5800

Phase	Magn.	No.	Phase	Magn.	No	Phase	Magn	No.
0.4201	-0.129	1	0.4635	-0.130	1	0.4912	-0.026	1
0.4226	-0.130	2	0.4662	-0.110	2	0.4929	-0.027	2
0.4252	-0.119	2	0.4667	-0.114	1	0.4946	-0.036	1
0.4275	-0.108	1	0.4686	-0.103	2	0.4966	-0.029	2
0.4286	-0.128	1	0.4711	-0.101	2	0.5013	-0.055	2
0.4308	-0.136	2	0.4730	-0.102	1	0.5032	-0.015	1
0.4473	-0.118	1	0.4741	-0.116	1	0.5049	-0.028	2
0.4489	-0.122	2	0.4811	-0.078	2	0.5067	-0.068	1
0.4506	-0.146	1	0.4831	-0.050	1	0.5093	-0.044	1
0.4525	-0.128	2	0.4850	-0.056	2	0.5110	-0.054	2
0.4547	-0.118	2	0.4869	-0.067	1	0.5133	-0.052	2
0.4571	-0.116	1	0.4892	-0.055	2	0.5150	-0.042	1
0.4581	-0.101	1	0.4912	-0.026	1			

Bin Size 0.0100 Phase Range 0.5800 to 0.9200

Phase	Magn.	No	Phase	Magn.	No.	Phase	Magn	No
0.6585	-0.172	2	0.7070	-0.144	5	0.8771	-0.095	6
0.6648	-0.143	6	0.7146	-0.141	7	0.8849	-0.113	6
0.6747	-0.154	8	0.7211	-0.152	2	0.8907	-0.124	2
0.6893	-0.150	2	0.8084	-0.122	2			
0.6962	-0.154	6	0.8125	-0.115	5			

TABLE 21 - Continued

Bin Size 0.0020				Phase Range		0.9200 to 1.0000		
Phase	Magn.	No.	Phase	Magn.	No.	Phase	Magn.	No.
0.9462	-0.045	1	0.9670	0.722	1	0.9801	1.707	1
0.9497	0.027	1	0.9690	0.851	2	0.9848	1.753	1
0.9532	0.076	1	0.9710	0.983	1	0.9862	1.748	1
0.9563	0.191	1	0.9724	1.101	1	0.9884	1.788	1
0.9591	0.290	1	0.9749	1.298	2	0.9916	1.812	1
0.9619	0.422	1	0.9772	1.473	1	0.9943	1.793	1
0.9658	0.646	1	0.9787	1.584	1	0.9968	1.775	1

TABLE 22

NORMAL POINTS FOR 1976U DATA

Bin Size: 0.0020 Phase Range: 0.0000 to 0.0800

Phase	Magn.	No.	Phase	Magn.	No.	Phase	Magn.	No.
0.0251	1.133	1	0.0448	0.091	2	0.0654	-0.019	3
0.0275	0.932	3	0.0464	0.057	1	0.0672	-0.044	3
0.0289	0.821	3	0.0488	0.019	2	0.0687	-0.026	1
0.0311	0.661	2	0.0507	0.004	2	0.0708	-0.037	4
0.0325	0.581	1	0.0526	-0.008	2	0.0733	-0.035	1
0.0350	0.466	3	0.0546	-0.020	2	0.0749	-0.046	3
0.0380	0.324	1	0.0572	-0.026	1	0.0772	-0.044	3
0.0399	0.249	1	0.0586	-0.030	2	0.0791	-0.042	3
0.0411	0.207	2	0.0610	-0.037	4			
0.0424	0.161	1	0.0631	-0.027	4			

Bin Size: 0.0100 Phase Range: 0.0800 to 0.4200

Phase	Magn.	No.	Phase	Magn.	No.	Phase	Magn.	No.
0.0823	-0.042	3	0.1912	-0.047	2	0.2918	-0.119	2
0.1157	-0.035	8	0.2063	-0.058	3	0.3024	-0.102	4
0.1253	-0.042	10	0.2371	-0.062	7	0.3664	-0.144	5
0.1307	-0.047	2	0.2461	-0.077	11	0.3752	-0.138	10
0.1564	-0.034	4	0.2555	-0.074	10	0.3813	-0.137	1
0.1648	-0.037	8	0.2671	-0.084	7	0.3966	-0.153	6
0.1747	-0.031	9	0.2750	-0.087	7	0.4059	-0.147	5
0.1854	-0.041	9	0.2848	-0.094	9	0.4161	-0.128	12

Bin Size: 0.0020 Phase Range: 0.4200 to 0.5800

Phase	Magn.	No.	Phase	Magn.	No.	Phase	Magn.	No.
0.4207	-0.139	4	0.4471	-0.154	2	0.4889	-0.080	1
0.4229	-0.150	4	0.4491	-0.145	2	0.4910	-0.089	2
0.4242	-0.215	1	0.4510	-0.156	3	0.4936	-0.063	2
0.4266	-0.113	1	0.4528	-0.145	1	0.4948	-0.060	1
0.4292	-0.164	2	0.4543	-0.175	1	0.4960	-0.054	1
0.4336	-0.147	1	0.4568	-0.155	1	0.5013	-0.084	1
0.4349	-0.133	1	0.4583	-0.124	1	0.5708	-0.103	1
0.4369	-0.120	2	0.4606	-0.105	1	0.5730	-0.131	2
0.4391	-0.164	1	0.4623	-0.103	1	0.5751	-0.121	1
0.4431	-0.122	3	0.4852	-0.075	1	0.5766	-0.139	2
0.4450	-0.157	2	0.4874	-0.091	2			

TABLE 22 – Continued

Bin Size 0.0100 Phase Range 0.5800 to 0.9200

Phase	Magn	No.	Phase	Magn	No.	Phase	Magn	No.
0.5847	-0.133	6	0.6985	-0.049	1	0.8356	-0.085	9
0.5918	-0.127	4	0.7049	-0.082	7	0.8444	-0.076	4
0.6078	-0.119	2	0.7153	-0.081	8	0.8547	-0.076	5
0.6159	-0.109	8	0.7217	-0.069	2	0.8646	-0.071	4
0.6295	-0.126	1	0.7334	-0.092	6	0.8730	-0.081	2
0.6357	-0.110	2	0.7494	-0.057	2	0.9195	-0.089	1
0.6475	-0.080	3	0.7563	-0.089	4			
0.6649	-0.096	4	0.7611	-0.081	1			

Bin Size 0.0020 Phase Range 0.9200 to 1.0000

Phase	Magn	No.	Phase	Magn	No.	Phase	Magn	No.
0.9203	-0.090	1	0.9471	-0.002	1	0.9710	1.139	3
0.9225	-0.082	2	0.9487	0.016	3	0.9731	1.316	3
0.9263	-0.065	2	0.9510	0.073	3	0.9753	1.480	3
0.9275	-0.084	1	0.9530	0.172	2	0.9771	1.671	2
0.9283	-0.060	1	0.9552	0.218	3	0.9788	1.762	2
0.9318	-0.054	1	0.9572	0.308	2	0.9827	1.850	2
0.9326	-0.041	1	0.9587	0.366	3	0.9851	1.873	2
0.9349	-0.051	2	0.9606	0.462	3	0.9866	1.888	1
0.9373	-0.094	2	0.9628	0.616	4	0.9957	1.902	1
0.9413	-0.093	1	0.9646	0.675	1	0.9972	1.884	2
0.9431	0.007	1	0.9670	0.832	2	0.9985	1.870	1
0.9447	-0.087	1	0.9694	1.030	2			

CHAPTER VI
DISCUSSION

Introduction

The topic of this, the last chapter, will be the implications of the data presented in the foregoing five chapters. First, the properties of the distortion wave will be considered. The dates of maximum and minimum light will be computed. The resulting quantities will be referred to as MJD_{max} and MJD_{min}, respectively. From these values it will be possible to compare the peak-to-peak amplitude for each of the 11 light curves under investigation. The values for the phase at minimum and the amplitude of the distortion wave can then be compared with those in Hall (1972, 1975a). By taking advantage of the complication in the distortion wave around secondary eclipse due to the non-uniform intensity of the surface on the K0 (star B) component an estimate of the temperature of the starspot will be made. The discussion of the distortion wave will conclude with some comments about the nature of the phenomenon.

The problems associated with the non-uniform period changes will be considered. The existence of short-term period variations, first pointed out by Hall (1972, 1975a), are not confirmed by the more accurate and realistic WAVE procedure model. The much longer period variations remain unexplained, at least in classical terms.

The Distortion Wave

The value of the phase at maximum and minimum light of the distortion wave are listed in Table 11. It would be more convenient if these values were not dependent on the ephemeris which was used to compute the phases for the construction of the light curves. As a first step in this direction, new estimates for the times of minimum (MJD_0) were computed for each light curve. These values for MJD_0 are listed in Table 23. They were computed by using the value of T_c (from Table 11) to correct the time predicted by the linear ephemeris (equation 4). The published values of the times of minimum (Catalano and Rodonò 1974) for the Catania data were used as a guide in establishing the number of orbital cycles. For the light curves of 1975 and 1976 a value, $\overline{MJD}$, was computed by averaging the observed dates of primary minimum, weighted by the square root of the number of points on each date. This value was then used to compute a cycle number, and thus a value of MJD_0 for each of these six light curves, by incorporating the appropriate values of T_c from Table 11.

The next step in computing estimates for the dates of maximum and minimum light of the distortion wave (MJD_{max} and MJD_{min}) involved the calculation of the number of days after MJD_0 that these events occurred. From Table 11 the values of θ_{min} and θ_{max} can be obtained. By multiplying these values by the period ($4\overset{d}{.}797855$) used in the linear ephemeris, the appropriate delay (in days) was obtained. This would have been somewhat inaccurate because θ_{min} and θ_{max} from Table 11 are dependent on the linear ephemeris. To reduce this effect, the appropriate value of T_c was added to the phase before it was multiplied by the period. The resulting phase values are listed in Table 23 as θ'_{min} and θ'_{max}. The values of MJD_{min} and MJD_{max} are also listed in Table 23. The values that were computed by this method are more reliable than previously published values.

TABLE 23

TIMES OF MINIMA AND CHARACTERISTICS OF THE DISTORTION WAVE

Light Curve	MJD_o	θ'_{min}	MJD_{min}	θ'_{max}	MJD_{max}	Wave Amp. Δv
1921	*	0.832	*	0.211	*	-0.15
1963	38145.176	0.408	38147.134	0.991	38149.931	-0.15
1964	38557.785	0.355	38559.488	0.953	38562.357	-0.22
1965	38888.828	0.323	38890.376	0.774	38892.542	-0.16
1966	39215.071	0.182	39215.944	0.600	39217.950	-0.17
†1975v	42491.939	0.181	42492.807	0.556	42494.607	-0.20
1975b	42491.939	0.186	42492.831	0.557	42494.611	-0.14
1975u	42491.935	0.147	42492.640	0.642	42494.535	-0.14
†1976v	42870.962	0.141 0.767	42871.639 42874.642	0.464	42873.188	-0.22
1976b	42870.962	0.143 0.762	42871.648 42874.618	0.453	42873.183	-0.17
1976u	42870.963	0.142 0.763	42871.644 42874.624	0.459	42873.165	-0.14

Notes for Table 23

* These values were not computed because the accuracy of the original data did not warrant the calculation.

† The period from the times of minima of these two light curves is 4.797758 ± 0.000010 days.

The amplitude of the distortion wave has also been calculated using the results from the WAVE procedure. Using the Fourier coefficients in Table 11 and the values of distortion wave minimum and maximum from Table 11, the amplitude in magnitudes was computed. The results are listed in Table 23 as Δv (this is the peak-to-peak amplitude). The values are in excellent agreement with those in Table 1 of Hall's (1972) paper. Unfortunately, the agreement with Hall's paper ends there.

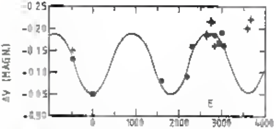

Fig. 22 -The visual band amplitude of the distortion wave plotted as a function of the orbital cycle (E) from Hall (1972).

Hall predicted that the variation in amplitude of the distortion wave was the result of a 23½-year 'sunspot cycle' operating in the subgiant of the system. Fig. 22 shows a plot of distortion wave amplitude in the visual band. The filled circles are from Hall's (1972) paper, while the crosses are from Table 23. The abscissa is plotted using Hall's emphemeris. The solid line is the functional dependence predicted by the 1800 orbital cycle (23½-year) "sunspot cycle." Note that the new observations are in direct conflict with the predictions, but the new estimates of the amplitude from the Catania data agree very well with Hall's graphical estimates.

This is circumstantial evidence that the phenomenon in RS CVn is not the same, in all respects, as that known as sunspots. Both effects are probably surface phenomena resulting in a non-uniform surface brightness, but they are quite different in other ways.

Another consequence of Hall's 'sunspot" model was a periodic variation in the migration rate of the distortion wave. The data for 1975 and 1976 are again in conflict with the extrapolation of this relationship. Hall plotted the phase of distortion wave minimum as a function of orbital cycles. The difference between the observed

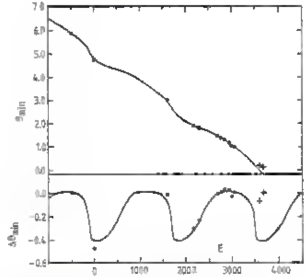

Fig. 23.--The phase of distortion wave minimum versus orbital cycle. Filled circles are from Hall (1972), while crosses are from the 1975 and 1976 data presented here. In the lower part are plotted the residuals from Hall's uniform migration rate equation for the distortion wave.

value of θ_{min} and a uniform rate was also plotted. In Fig. 23, Hall's plots have been extended.

The period of the variation in the distortion wave amplitude (1800 orbital periods) and the discontinuities in migration rate at E = 0 and E = 1800 led Hall to believe that the photometric phenomenon was similar to the sunspot cycle in our sun. The amplitude variation was considered akin to the variation in sunspot number, while the non-uniform migration rate of the distortion wave was considered to be the result of "sunspot" migration from high latitudes towards the equatorial region. In the sun the latter characteristic is represented by the familiar butterfly diagram. Hall discusses this in somewhat more detail. Since the analogy with the sunspot has not withstood observational testing, a more detailed discussion will not be given. The distortion wave in RS CVn is not the result of a phenomenon similar in all respects to sunspots, at least the similarity is not as great as it was originally portrayed.

The distortion wave is almost certainly caused by temperature variations on the surface of the cooler star of the system. If the size of the cooler region is larger than the disk of the smaller star as the transit is viewed from earth, then an estimate for the temperature in the cooler region can be made. In addition, the amplitude of the distortion wave also gives an estimate of the temperature variations. The latter approach will be considered first.

The average temperature of star B (T_B) and the normalized apparent luminosity (l_B) can be used to estimate the value of α in the following relation:

$$l_B \cdot 10^{-0.4QM} = \alpha r_B^2 T_B^4. \qquad (8)$$

The value for T_B, r_B, l_B and QM are taken from Tables 10 and 11, and give an average value of 1.8×10^{-14} for α (in units of the comparison star's energy output per unit orbital radii squared per degree Kelvin to the fourth power). The maximum temperature on the K0 star can be estimated by assuming that the hemisphere facing the earth at the maximum of the distortion wave is not spotted. This value is approximately 5000^0K, with a range from 4900^0K (1963) to 5100^0K (1975v). Similarly, the temperature of the cooler region can be estimated to be about 4400^0K.

Another way to estimate the maximum temperature of star B is to assume that the hemisphere facing the earth during secondary eclipse in

1975 and 1976 was the brighter unspotted hemisphere. The smaller star will then block more light than the WINK model predicted for star B with an average temperature of T_B. This method gives a temperature of approximately 5100°K. This is the same as the previous method and would therefore give the same temperature for the cooler region as before.

The temperature of the spotted region can be estimated by making similar assumptions as were made above. In actuality the estimates are only upper limits on the temperature of the cooler region. The upper limit on the temperature for a spot covering one hemisphere is (from the brightness of star B at distortion wave minimum, as was computed above) 4400°K. The probing effects of the smaller star during transit can be put to advantage only for the 1963 light curve. In this case the upper limit for a spot larger than the apparent disk of star A is 4400°K. The similarity in value from the two estimates would indicate that the size of the active region is almost the size of one hemisphere of star B. In addition, it indicates that the spotted area is probably symmetrical with the equator of star B, unless it is so asymmetric as to be entirely on one side of the equator of star B.

Before leaving the subject of spots it is important that the reader differentiate between the spots of RS CVn and those of the sun. The phenomenon observed on the sun may be quite different from that in RS CVn. The term "spot" has been used because it is convenient and it conveys the idea of a region of lower temperature surrounded by a hotter photosphere. The shape of this region is not circular, necessarily. This is demonstrated by the shape of the distortion wave in the 1963 light curve. The shape of the spot on the KO star would

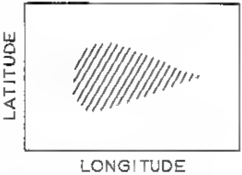

Fig. 24 -The shape of the spot is indicated by the shaded area

be something like that shown in Fig. 24. This shape is indicated because the light curve for 1963 is more of a "saw tooth" than a sine wave. Since the distortion wave is never flat at maximum in any of the light curves studied so far it is necessary that the spotted region extend at least 180 degrees in longitude on the star.

It is also apparent from the double minimum in 1976 (see Fig. 17 in Chapter V) that the concentration of spots is not limited to the region which migrates (approximately) uniformly. The significance of this is not clear, but certainly any model devised to explain the photometric distortion wave must be capable of reproducing the rapid changes in the detailed shape of the distortion wave. This is best visualized by comparing the changes in shape from 1975 to 1976 (see Figs. 16 and 17), or the changes from 1963 and 1964 (Figs. 12 and 13).

The radial pulsation of star B cannot be responsible for the photometric distortion wave. If the pulsation of star B is assumed, then it would cause a change in system brightness and a subsequent change in the radius of star B. In order for a change in only the radius to cause the observed amplitude of the distortion wave, the radius would have to change by approximately 20%. The data studied here represents only about a quarter of a migration cycle, thus a change of about 5% should present itself if radial pulsation is the cause of the distortion wave. The variation in a_{oB} in the computer runs of step 11 in Chapter V show a 2% variation, at the most. Additional, and higher quality data could improve the confidence with which radial pulsation is rejected as a cause for the distortion wave. However, the results here are reasonably convincing that radial pulsation, from observational data, is not responsible for this anomalous photometric behavior.

Obscuration of the light from the K0 star by intervening material as an explanation for the distortion wave has been rejected by Oliver (1974, 1975). Other possible explanations include non-radial pulsation, unusual convection patterns, magnetic effects (as in sunspots), and "something else." Time will perhaps eventually show what is the correct explanation.

Orbital Period Variations

The short-term period variations in RS CVn have been attributed to mass ejection by Hall (1972, 1975a). Hall claimed that mass was being ejected from the brighter hemisphere of star B. When this hemisphere was facing in the direction of orbital motion it would tend to reduce the period. In Fig. 25 are plotted the times of minima as corrected by Hall (1975a) for the effects of the distortion wave, and the times of minima as they appear in Table 23. Hall's estimates are the filled circles, while those from Table 23 appear as crosses.

The data in Fig. 25 are from Catalano and Rodono (1974), and were published as times of minima. Hall corrected these values by

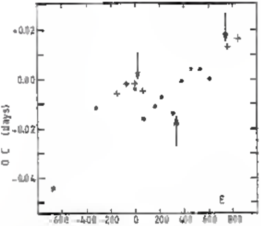

Fig 25 -The O-C curve of RS CVn based on photoelectric times of minima Filled circles are points corrected for the distortion wave effects by Hall (1975a). Crosses are points as computed in this dissertation Arrows indicate when the period is predicted to decrease and increase according to Hall (1972, 1975a)

estimating the effect of the distortion wave on the actual times of conjunction The WAVE procedure has accomplished the same thing (albeit with more effort) with greater accuracy Unfortunately, it was only possible to do this with the published data for 1963, 1964, 1965, and 1966, and of course, the 1975 and 1976 data obtained by the present writer The arrows indicate when Hall predicts an increase (or decrease) in orbital period due to the mass ejection from the brighter hemisphere. Note that with the change of the single point for 1966 the variation becomes less obvious In addition, the predicted decrease apparently did not occur in 1975 or 1976 It would appear that Hall's model for the short-term period variations is on "thin ice "

It is difficult to imagine that the short-term variations which appear to remain are observational error. This is, however, a possibility. If they are indeed real, then an adequate explanation would probably follow along similar lines to those of Hall, but with less reliance on the sunspot analogy. On the other hand, it would be expected that both stars are losing mass via a stellar wind, since they are very similar in age and mass. If this is the case, then variations in the difference in the loss rates might cause the short-term period changes. The data presented here do not show that any short-term variations exist. If they do not, the mechanism for the much longer term variations also vanishes. Here again, a stellar wind may be operating in one or both stars to cause the (almost) periodic O-C variations. If this cannot account for the variations, then it may be necessary to return to the consideration of a very under-luminous third body, such as a white dwarf, neutron star, or black hole. The latter two possibilities are highly unlikely.

Conclusion

Additional light curves of RS CVn have been obtained as a result of this research. They are the first complete light curves in more than one color to be published. The light curve for 1976 has shown a previously unknown characteristic of the system, namely, that the distortion wave can consist of more than one minimum. The 1976 distortion wave also shows an amplitude as large or larger than any previously published.

The computer program WINK and associated programs which comprised the WAVE procedure have provided a set of elements which are better than any previously obtained. The technique has also provided a mathematical characterization of the distortion wave which can be treated by less complicated models than are currently being used (Eaton 1977). This simplification is due to the less complicated case of studying the phenomenon of the distortion wave with the "complication" of the eclipses removed, or nearly removed.

The additional light curves and improved solution method have added more weight for the rejection of radial pulsation as the source of the distortion wave. Popper (1961) had far too little information with which to investigate the question. Catalano and Rodono (1968) perhaps had sufficient data, but they lacked a better and more efficient method of solution. Hall (1972) was in a similar predicament. Now, however, a measurement of the radius of star B to sufficient accuracy is possible. The analysis of the data has shown that the needed variation in r_B is not seen. Confirmation of this with additional data is desirable in order to confirm that radial pulsation is not responsible for the distortion wave.

The constancy of the comparison star BD+35° 2420 has been confirmed (see Fig. 5).

The analogy between the nonuniform surface brightness on the K0 star of RS CVn and classical sunspots has been shown to be over-rated. The amplitude of the distortion wave does not appear to follow a quasi-periodic variation as closely as does the number of sunspots on the sun. Furthermore, the nearly-periodic variation in the migration rate of the distortion wave did not continue into 1975 and 1976 as was predicted. The migration rate was nearly constant from 1963 through 1976, showing a slight decrease in rate rather than the predicted increase. Finally, the short-term period variations which were considered an integral part of the sunspot analogy were not seen in the data used in this investigation. In fact, a new ephemeris can be computed for the Catania and 1975-76 data studied here. The resulting ephemeris,

(9) $$\mathrm{HJD}_{\odot} = 42870.962 + 4^{d}.797752E,$$

indicates that the orbital period from 1963 to 1976 was nearly constant. The maximum deviation from the observed times of minima in Table 23 is 6 minutes (0.004 days) for the 1966 light curve.

The shape, temperature, and life-time of the spots have been estimated. The shape of the distortion wave is frequently a "saw tooth" which implies a triangular or tapered shape (see Fig. 24). The upper limit for the temperature of the spotted region has been set at 4400°K. The development time for a large-scale spot must be approximately one year. The smaller minimum in the distortion wave was clearly visible in 1976, but there was only a hint of its existance in 1975. In addition, an estimate of the surface temperature on the unspotted photosphere was made; it was 5100°K.

Additional research is needed before a complete model for RS CVn can be developed. High time-resolution photometry and spectroscopy in the optical region is desirable and would be especially useful during eclipses. Secondary eclipse could yield more information about the nature of the spots, i.e. uniform versus blotchy spots and a more detailed map of the distribution of the spot. Primary eclipse could provide information on the atmosphere of the K0 star from observations during the four contact points.

Of course, observations in other spectral regions would provide needed information. In addition, more information from the X-ray and radio regions would be helpful in determining if the distortion wave phenomenon is associated with the emission at these wavelengths.

You have not heard the last from RS CVn binaries.

APPENDIX

APPENDIX

DIFFERENTIAL MAGNITUDES AND COLORS OF RS CVN

HELIO MJD	D(v)[a]	D(b-v)[a]	D(u-b)[a]
42469.18048	-0.298	0.0829	
42469.19367	-0.301	0.1532	
42469.20756	-0.316	0.1243	
42469.22527	-0.306	0.1235	
42469.27666	-0.313	0.1229	
42469.29298	-0.304	0.1212	
42469.31659	-0.303	0.1230	
42469.33812	-0.308	0.1088	
42469.37840	-0.317	0.1244	
42469.39576	-0.309	0.1270	
42477.23415	-0.336	0.1310	
42477.24457	-0.336	0.1320	
42477.25603	-0.339	0.1360	
42477.28380	-0.319	0.1390	
42477.29422	-0.303	0.1442	
42477.30464	-0.272	0.1345	
42477.31540	-0.244	0.1470	
42477.35707	-0.042	0.1941	
42477.36714	0.025	0.2014	
42477.37825	0.099	0.2270	
42477.38867	0.177	0.2530	
42477.39874	0.255	0.2796	
42478.15986	-0.279	0.1186	
42478.17132	-0.282	0.1265	
42478.18276	-0.300	0.1316	
42478.19111	-0.291	0.1290	
42478.20952	-0.287	0.1293	
42478.22236	-0.291	0.1381	
42478.23591	-0.288	0.1207	
42478.31160	-0.279	0.1183	
42478.32375	-0.280	0.1232	
42478.33660	-0.277	0.1236	
42478.34945	-0.289	0.1216	
42478.37619	-0.288	0.1162	
42478.38799	-0.285	0.1226	
42478.40014	-0.284	0.1218	
42478.41264	-0.287	0.1238	
42480.07865	-0.327	0.1493	
42480.08594	-0.350	0.1473	
42480.13351	-0.382	0.1347	
42480.14115	-0.400	0.1499	
42480.14973	-0.407	0.1536	
42480.15399	-0.402	0.1461	
42480.16198	-0.425	0.1683	
42480.16615	-0.433	0.1548	
42480.18733	-0.428	0.1922	
42480.19393	-0.423	0.1492	
42480.20365	-0.438	0.1699	
42480.21406	-0.438	0.1591	
42480.22448	-0.429	0.1570	
42480.23455	-0.436	0.1540	
42480.27379	-0.441	0.1481	
42480.28455	-0.436	0.1486	
42480.29457	-0.424	0.1401	
42480.30469	-0.435	0.1496	

APPENDIX – Continued

HELIO MJD	D(v)[a]	D(b-v)[a]	D(u-b)[a]
42480.31545	-0.438	0.1508	
42480.35434	-0.438	0.1590	
42480.36407	-0.436	0.1544	
42480.37344	-0.442	0.1564	
42480.38143	-0.435	0.1538	
42480.39671	-0.440	0.1607	
42480.40678	-0.440	0.1683	
42480.41719	-0.442	0.1567	
42480.42761	-0.436	0.1560	
42480.43768	-0.438	0.1538	
42486.14052	-0.402	0.1466	
42486.14990	-0.385	0.1305	
42486.16136	-0.408	0.1568	
42486.34747	-0.387	0.1308	
42486.35719	-0.378	0.1243	
42486.36830	-0.377	0.1421	
42486.39678	-0.371	0.1492	
42486.40962	-0.369	0.1383	
42491.20340	-0.394	0.1490	
42491.20583	-0.387	0.1628	
42491.21034	-0.396	0.1627	
42491.21451	-0.364	0.1486	
42491.21833	-0.380	0.1425	
42491.22215	-0.380	0.1349	
42491.22631	-0.371	0.1301	
42491.23499	-0.370	0.1364	
42491.24472	-0.376	0.1375	
42491.26485	-0.372	0.1424	
42491.27145	-0.372	0.1578	
42491.27492	-0.375	0.1394	
42491.28569	-0.367	0.1417	
42491.29437	-0.372	0.1477	
42491.30409	-0.378	0.1423	
42491.31347	-0.367	0.1423	
42491.32319	-0.365	0.1476	
42491.36728	-0.364	0.1465	
42491.37701	-0.359	0.1462	
42491.39124	-0.348	0.1277	
42491.39437	-0.345	0.1303	
42491.40305	-0.360	0.1453	
42492.10930	0.100	0.2334	
42492.11520	0.062	0.2593	
42492.11902	0.056	0.2172	
42492.12264	0.046	0.1758	
42492.12770	-0.009	0.1740	
42492.13222	-0.016	0.1431	
42492.13639	-0.055	0.1763	
42492.14090	-0.091	0.1649	
42492.14472	-0.117	0.2046	
42492.14992	-0.135	0.1777	
42492.15409	-0.145	0.1665	
42492.15791	-0.169	0.1716	
42492.16242	-0.175	0.1483	
42492.16624	-0.188	0.1380	
42492.20756	-0.299	0.1183	

APPENDIX - Continued

HELIO MJD	$D(v)^a$	$D(b-v)^b$	$D(u-b)^c$
42492.21277	-0.291	0.1307	
42492.21798	-0.294	0.1251	
42492.22180	-0.304	0.1253	
42492.22597	-0.283	0.1106	
42492.23048	-0.289	0.1241	
42492.23881	-0.292	0.1213	
42492.24645	-0.277	0.1101	
42492.25305	-0.282	0.1070	
42492.34229	-0.280	0.1172	
42492.34541	-0.279	0.1043	
42492.40548	-0.273	0.1058	
42492.40895	-0.263	0.1051	
42492.43381	-0.267	0.1023	
42492.41798	-0.263	0.1317	
42505.10198	-0.413	0.1407	
42506.07831	-0.315	0.1487	0.1215
42506.09598	-0.262	0.1548	0.1442
42506.11299	-0.208	0.1710	0.1132
42506.12757	-0.138	0.1879	0.1410
42506.14112	-0.061	0.2058	0.1445
42506.15486	0.013	0.2307	0.1787
42506.17341	0.165	0.2684	0.2131
42506.17931	0.214	0.2723	0.2358
42506.18520	0.266	0.2858	0.2569
42506.19161	0.312	0.3203	0.2622
42506.19813	0.377	0.3355	0.2708
42506.20507	0.436	0.3532	0.3120
42506.21389	0.507	0.4036	0.3385
42506.21988	0.554	0.4235	0.3714
42506.22778	0.608	0.4584	0.4066
42506.23542	0.665	0.4846	0.4343
42506.24181	0.711	0.4952	0.4965
42506.26473	0.749	0.5138	0.4909
42506.27097	0.752	0.5233	0.4725
42506.28174	0.757	0.5262	0.5047
42506.29702	0.763	0.5164	0.5327
42506.30986	0.763	0.5242	0.5060
42506.32202	0.763	0.5235	0.4879
42506.33938	0.778	0.5260	0.4929
42506.35431	0.781	0.5268	0.5138
42506.39389	0.783	0.5435	0.5309
42506.40982	0.780	0.5457	0.5396
42506.42062	0.748	0.5236	0.4377
42506.42444	0.705	0.4860	0.3801
42506.42965	0.709	0.3996	0.4042
42508.08344	-0.369	0.1683	0.1121
42508.09872	-0.366	0.1451	0.1179
42508.11316	-0.367	0.1546	0.1257
42508.11802	-0.361	0.1396	0.0911
42508.12837	-0.368	0.1479	0.1110
42508.13344	-0.369	0.1469	0.0977
42508.14080	-0.373	0.1495	0.1113
42508.14573	-0.370	0.1436	0.0977
42508.15413	-0.392	0.1497	0.1167
42508.15934	-0.386	0.1479	0.1195

APPENDIX – Continued

HELIO. MJD	D(v)[a]	D(b–v)[a]	D(u–b)[a]
42508.16780	-0.377	0.1466	0.1137
42508.17247	-0.376	0.1397	0.0969
42508.17983	-0.372	0.1488	0.1226
42508.18469	-0.379	0.1502	0.0950
42508.21295	-0.385	0.1508	0.1153
42508.21837	-0.379	0.1480	0.1001
42508.22609	-0.386	0.1571	0.1215
42508.23163	-0.387	0.1545	0.1055
42508.24670	-0.385	0.1481	0.1257
42508.25198	-0.383	0.1424	0.1271
42508.25899	-0.398	0.1600	0.1443
42508.27739	-0.400	0.1501	0.1020
42508.28434	-0.383	0.1402	0.0859
42508.29719	-0.403	0.1583	0.1188
42508.30184	-0.396	0.1477	0.1056
42508.31066	-0.388	0.1486	0.1026
42508.31536	-0.397	0.1586	0.1159
42508.32274	-0.387	0.1492	0.1106
42508.32760	-0.384	0.1469	0.0922
42508.33586	-0.398	0.1613	0.1037
42508.34052	-0.392	0.1491	0.0992
42508.34830	-0.393	0.1507	0.1125
42508.35288	-0.391	0.1544	0.1069
42508.36246	-0.387	0.1569	0.1098
42508.36760	-0.391	0.1472	0.1037
42508.37496	-0.395	0.1556	0.1231
42508.38003	-0.393	0.1537	0.1185
42508.38850	-0.417	0.1735	0.1351
42508.39364	-0.402	0.1554	0.1191
42508.40149	-0.398	0.1519	0.1096
42508.40684	-0.386	0.1352	0.1149
42515.32958	-0.362	0.1475	0.1197
42515.33340	-0.363	0.1488	0.1250
42515.34090	-0.375	0.1536	0.1302
42515.34610	-0.365	0.1434	0.1193
42515.35256	-0.363	0.1479	0.1255
42515.35694	-0.360	0.1430	0.1167
42515.36353	-0.370	0.1553	0.1120
42515.36791	-0.362	0.1528	0.0969
42515.37464	-0.355	0.1452	0.1084
42515.37902	-0.361	0.1509	0.0802
42515.39826	-0.357	0.1356	0.1260
42515.40159	-0.351	0.1225	0.0858
42515.40636	-0.359	0.1291	0.1123
42515.41062	-0.368	0.1282	0.1099
42518.07935	-0.409	0.1574	0.1340
42518.08373	-0.401	0.1595	0.1217
42518.09039	-0.405	0.1534	0.1269
42518.09505	-0.400	0.1624	0.0895
42518.10192	-0.395	0.1471	0.1195
42518.10636	-0.385	0.1498	0.1070
42518.11289	-0.387	0.1518	0.1278
42518.11678	-0.377	0.1428	0.1052
42518.12616	-0.389	0.1599	0.1132
42518.13095	-0.374	0.1574	0.1156

APPENDIX - Continued

HELIO. MJD	D(v)^{o}	D(b-v)^{m}	D(u-b)^{o}
42518.15678	-0.366	0.1530	0.0833
42519.16157	-0.342	0.1385	0.0903
42518.16817	-0.356	0.1441	0.1048
42519.17254	-0.344	0.1463	0.0840
42518.17935	-0.345	0.1388	0.1158
42518.18379	-0.332	0.1318	0.0842
42518.19101	-0.334	0.1386	0.0972
42518.19560	-0.326	0.1335	0.0897
42518.20268	-0.325	0.1323	0.0908
42519.20782	-0.324	0.1354	0.0729
42518.23907	-0.289	0.1274	0.0837
42518.24393	-0.281	0.1192	0.0949
42518.25122	-0.287	0.1215	0.1155
42518.25580	-0.275	0.1230	0.1053
42518.26421	-0.262	0.1101	0.0862
42518.26900	-0.270	0.1238	0.0795
42518.27789	-0.249	0.1228	0.0752
42518.28247	-0.255	0.1183	0.0788
42518.28983	-0.257	0.1252	0.1050
42518.29441	-0.262	0.1209	0.0964
42518.30115	-0.257	0.1353	0.1132
42518.30629	-0.250	0.1115	0.1026
42518.31316	-0.250	0.1184	0.1005
42518.31782	-0.240	0.1160	0.0961
42518.33559	-0.269	0.1137	0.1052
42518.34094	-0.249	0.1151	0.0737
42518.34740	-0.255	0.1264	0.1133
42519.35219	-0.257	0.1268	0.0948
42518.35893	-0.261	0.1209	0.1186
42518.36406	-0.273	0.1218	0.0830
42518.37649	-0.260	0.1385	0.0775
42518.38101	-0.261	0.1054	0.0801
42518.38823	-0.270	0.1245	0.1136
42518.39392	-0.265	0.1034	0.1099
42518.39823	-0.275	0.1176	0.1051
42518.40420	-0.265	0.1174	0.1058
42519.09015	-0.449	0.1723	0.1148
42515.09460	-0.448	0.1764	0.0887
42519.10723	-0.432	0.1517	0.1332
42519.11210	-0.428	0.1481	0.1267
42519.12050	-0.444	0.1682	0.1562
42519.12501	-0.433	0.1558	0.1484
42519.13376	-0.442	0.1669	0.1265
42519.13821	-0.442	0.1663	0.1239
42519.14779	-0.439	0.1708	0.1056
42519.15258	-0.435	0.1592	0.1167
42519.16057	-0.440	0.1613	0.1254
42519.16550	-0.443	0.1626	0.1234
42519.17397	-0.443	0.1733	0.1398
42519.17855	-0.434	0.1559	0.1318
42519.18813	-0.435	0.1647	0.1242
42519.19313	-0.440	0.1631	0.0998
42519.23751	-0.440	0.1620	0.1395
42519.24299	-0.427	0.1533	0.1113
42519.25098	-0.441	0.1757	0.1184

APPENDIX – Continued

HELID MJD	D(v)^a	D(b-v)^a	D(u-b)^a
42519.25723	-0.428	0.1603	0.0959
42519.26596	-0.438	0.1710	0.1195
42519.27112	-0.439	0.1616	0.1212
42519.28049	-0.436	0.1698	0.1272
42519.28619	-0.429	0.1678	0.0916
42519.31348	-0.431	0.1724	0.1282
42519.31834	-0.428	0.1634	0.1057
42519.32591	-0.439	0.1654	0.1314
42519.33091	-0.425	0.1541	0.1099
42519.33827	-0.447	0.1792	0.1314
42519.34355	-0.434	0.1603	0.1150
42519.35084	-0.427	0.1537	0.1255
42519.35563	-0.420	0.1473	0.1131
42519.36264	-0.440	0.1655	0.1468
42519.36834	-0.426	0.1628	0.1283
42519.37688	-0.430	0.1678	0.1505
42519.38146	-0.410	0.1509	0.1098
42519.39063	-0.450	0.1802	0.1305
42519.39549	-0.427	0.1554	0.1076
42522.17525	-0.325	0.1447	0.1188
42522.18115	-0.314	0.1401	0.0903
42522.18893	-0.336	0.1423	0.1254
42522.19400	-0.321	0.1288	0.1240
42527.14928	-0.334	0.1229	0.0992
42527.15435	-0.331	0.1398	0.0724
42527.16206	-0.344	0.1428	0.1208
42527.16565	-0.367	0.1472	0.1096
42527.17533	-0.371	0.1701	0.0732
42527.18026	-0.357	0.1473	0.0476
42527.22630	-0.373	0.1502	0.1031
42527.23157	-0.352	0.1241	0.1132
42527.24281	-0.343	0.1098	0.1306
42527.24768	-0.349	0.1392	0.1387
42534.20243	-0.371	0.1292	0.1435
42534.20771	-0.403	0.1543	0.1029
42534.21437	-0.401	0.1622	0.1064
42534.21868	-0.396	0.1494	0.1191
42534.22507	-0.397	0.1560	0.1078
42534.22972	-0.395	0.1541	0.1258
42534.23680	-0.389	0.1675	0.1628
42843.31458	-0.299	0.1283	0.1125
42843.31879	-0.294	0.1067	0.1267
42843.33083	-0.299	0.1287	0.1196
42843.33389	-0.279	0.1360	0.0906
42843.35681	-0.296	0.1672	0.0600
42843.36215	-0.282	0.1246	0.0698
42843.37815	-0.318	0.1728	0.0479
42843.38375	-0.316	0.1324	0.0939
42855.13603	-0.346	0.1480	0.1458
42855.14221	-0.354	0.1704	0.1179
42855.15061	-0.343	0.1617	0.0825
42855.15610	-0.342	0.1457	0.1119
42855.16555	-0.340	0.1320	0.1199
42855.17075	-0.347	0.1537	0.1106
42855.18145	-0.334	0.1310	0.1217

APPENDIX – Continued

HELIO MJD	$D(v)^a$	$D(b-v)^a$	$D(u-b)^a$
42855.18680	-0.338	0.1607	0.1047
42855.19443	-0.344	0.1424	0.1324
42855.19902	-0.345	0.1364	0.1337
42855.20603	-0.339	0.1467	0.0982
42855.21048	-0.344	0.1410	0.1153
42855.21825	-0.338	0.1351	0.1145
42855.22284	-0.341	0.1478	0.1146
42855.23207	-0.336	0.1260	0.1358
42855.23666	-0.336	0.1436	0.1133
42855.24360	-0.333	0.1457	0.1084
42855.24805	-0.346	0.1578	0.0895
42855.28707	-0.328	0.1327	0.1123
42855.29159	-0.327	0.1332	0.0851
42855.29302	-0.335	0.1522	0.1031
42855.30374	-0.336	0.1400	0.0973
42855.31214	-0.333	0.1345	0.1189
42855.31700	-0.327	0.1385	0.0874
42855.37631	-0.325	0.1384	0.1289
42855.38096	-0.309	0.1291	0.1243
42855.39964	-0.347	0.1444	0.1129
42855.40450	-0.339	0.1429	0.0992
42855.41763	-0.333	0.1579	0.1031
42855.42478	-0.336	0.1454	0.0933
42855.43457	-0.328	0.1395	0.1282
42861.12929	-0.249	0.1502	0.0983
42861.13519	-0.217	0.1378	0.1018
42861.14262	-0.198	0.1497	0.1247
42861.14790	-0.171	0.1577	0.1135
42861.16019	-0.108	0.1787	0.1426
42861.16485	-0.085	0.1864	0.1414
42861.17241	-0.037	0.1788	0.1545
42861.17721	-0.002	0.1952	0.1726
42861.18200	0.026	0.1891	0.1703
42861.18679	0.056	0.2059	0.1623
42861.19228	0.077	0.2161	0.1746
42861.19707	0.131	0.2357	0.1809
42861.20304	0.190	0.2267	0.1953
42861.20860	0.217	0.2695	0.1881
42861.21644	0.284	0.2803	0.2074
42861.22471	0.350	0.3049	0.2414
42861.22915	0.384	0.3165	0.2954
42861.23436	0.436	0.3365	0.2948
42861.23623	0.450	0.3378	0.2952
42861.24026	0.481	0.3651	0.3078
42861.24200	0.505	0.3772	0.3017
42861.24479	0.544	0.3882	0.3472
42861.24866	0.557	0.3907	0.3559
42861.25339	0.557	0.3982	0.3734
42861.25526	0.622	0.4130	0.3603
42861.26151	0.664	0.4519	0.3823
42861.26332	0.695	0.4506	0.4060
42861.26811	0.720	0.4848	0.4548
42861.26991	0.729	0.4876	0.4669
42861.27533	0.769	0.4904	0.4735
42861.27981	0.785	0.5088	0.4967

APPENDIX – Continued

HELIO MJD	D(v)^{a}	D(b−v)^{a}	D(u−b)^{a}
42861.24311	0.808	0.5172	0.5302
42861.24783	0.829	0.5113	0.5095
42861.30304	0.835	0.5137	0.5287
42861.31151	0.824	0.5263	0.5194
42861.31401	0.835	0.5311	0.5225
42861.35818	0.845	0.5400	0.5164
42861.36276	0.844	0.5190	0.5188
42861.36734	0.838	0.5326	0.5166
42861.37158	0.850	0.5074	0.5125
42863.17247	−0.402	0.1571	0.1262
42863.13303	−0.415	0.1681	0.1092
42863.14219	−0.403	0.1624	0.1089
42870.16315	−0.334	0.1425	0.1418
42870.16780	−0.330	0.1472	0.1058
42870.17197	−0.326	0.1409	0.1119
42870.18322	−0.336	0.1407	0.1420
42870.18760	−0.331	0.1418	0.1310
42870.19204	−0.326	0.1419	0.1236
42870.14648	−0.321	0.1332	0.1124
42870.20121	−0.325	0.1455	0.1032
42870.20579	−0.327	0.1435	0.1202
42870.21797	−0.329	0.1426	0.1140
42870.22211	−0.323	0.1342	0.0971
42870.22600	−0.328	0.1417	0.1110
42870.24447	−0.330	0.1466	0.1210
42870.25655	−0.327	0.1309	0.1232
42870.26686	−0.329	0.1359	0.1103
42870.27752	−0.332	0.1414	0.1244
42870.29405	−0.322	0.1438	0.1013
42870.29850	−0.323	0.1352	0.1001
42870.30488	−0.327	0.1326	0.1219
42870.31897	−0.322	0.1330	0.1140
42871.09480	0.480	0.3855	0.2869
42871.10327	0.411	0.2958	0.2665
42871.10751	0.366	0.2921	0.2448
42871.10751	0.366	0.2921	0.2448
42871.11084	0.344	0.2784	0.2277
42871.11084	0.344	0.2784	0.2277
42871.11709	0.292	0.2440	0.2244
42871.12126	0.263	0.2330	0.2049
42871.12557	0.225	0.2267	0.1711
42871.13050	0.186	0.2231	0.1725
42871.13772	0.135	0.2058	0.1816
42871.14244	0.105	0.1953	0.1611
42871.14668	0.074	0.1881	0.1562
42871.15675	0.002	0.1847	0.1372
42871.16563	−0.036	0.1580	0.1270
42871.16466	−0.058	0.1525	0.1254
42871.17383	−0.085	0.1502	0.1281
42871.17794	−0.107	0.1578	0.1100
42871.19716	−0.141	0.1306	0.1175
42871.19181	−0.157	0.1377	0.0932
42871.19688	−0.174	0.1365	0.0934
42871.20633	−0.208	0.1256	0.1078
42871.21091	−0.218	0.1267	0.0999

APPENDIX - Continued

HELIO. MJD	D(v)^a	D(b-v)^a	D(u-b)^a
42871.21494	-0.224	0.1239	0.1094
42871.22008	-0.235	0.1210	0.1130
42871.22473	-0.247	0.1270	0.1120
42871.22924	-0.248	0.1254	0.1148
42871.23376	-0.243	0.1204	0.1047
42871.23862	-0.247	0.1252	0.1008
42871.24904	-0.257	0.1258	0.1050
42871.25362	-0.246	0.1246	0.0905
42871.25758	-0.248	0.1250	0.0945
42871.26466	-0.248	0.1158	0.0928
42871.26897	-0.243	0.1156	0.0946
42871.27452	-0.244	0.1202	0.1003
42871.27549	-0.242	0.1179	0.0985
42871.28001	-0.237	0.1129	0.0852
42871.28494	-0.240	0.1219	0.1066
42871.28966	-0.238	0.1157	0.0938
42871.29410	-0.237	0.1142	0.0729
42871.31334	-0.244	0.1203	0.0758
42871.31716	-0.240	0.1097	0.0855
42871.32612	-0.241	0.1204	0.0855
42871.33473	-0.246	0.1014	0.0822
42871.34702	-0.240	0.1201	0.0735
42871.35278	-0.230	0.1133	0.0610
42871.35751	-0.236	0.1194	0.0758
42871.36473	-0.236	0.1147	0.0835
42871.36917	-0.239	0.1169	0.0808
42871.37376	-0.241	0.1122	0.0831
42873.10129	-0.433	0.1763	0.1541
42873.10824	-0.435	0.1579	0.1269
42873.11580	-0.432	0.1580	0.1219
42873.12289	-0.418	0.1480	0.1144
42873.13060	-0.401	0.1391	0.1320
42873.13844	-0.417	0.1437	0.0954
42873.14712	-0.420	0.1591	0.1157
42873.15421	-0.419	0.1532	0.0910
42873.16615	-0.392	0.1444	0.0926
42873.17337	-0.398	0.1509	0.1231
42873.18435	-0.396	0.1517	0.1393
42873.19254	-0.373	0.1373	0.1328
42873.30240	-0.301	0.1178	0.1083
42873.31059	-0.301	0.1289	0.0708
42873.31504	-0.293	0.1203	0.0919
42873.32031	-0.281	0.1184	0.0825
42873.32747	-0.292	0.1157	0.0731
42873.33240	-0.265	0.1148	0.0553
42873.34066	-0.286	0.1226	0.0994
42873.34427	-0.285	0.1210	0.1028
42873.34858	-0.284	0.1377	0.0864
42873.35427	-0.240	0.1207	0.0759
42873.37969	-0.279	0.1046	0.0905
42880.18382	-0.334	0.1359	0.1096
42880.18792	-0.329	0.1362	0.1026
42880.19632	-0.306	0.1382	0.0760
42880.20014	-0.311	0.1337	0.1068
42880.20973	-0.313	0.1314	0.1194

APPENDIX - Continued

HELIO MJD	D(v)^0	D(b-v)^0	D(u-b)^0
42880.21341	-0.291	0.1065	0.1178
42880.22243	-0.285	0.1354	0.0664
42880.22605	-0.283	0.1390	0.0842
42880.24271	-0.298	0.1254	0.1186
42880.24667	-0.301	0.1202	0.1403
42880.25618	-0.322	0.1375	0.1212
42880.25972	-0.320	0.1401	0.1405
42880.26757	-0.329	0.1255	0.1095
42880.27111	-0.333	0.1356	0.1043
42880.28875	-0.286	0.1025	0.0900
42880.29715	-0.286	0.1577	0.1156
42880.30475	-0.288	0.1568	0.0841
42880.31639	-0.243	0.1481	0.0929
42880.32472	-0.234	0.1403	0.1008
42880.33208	-0.220	0.1452	0.1148
42880.34021	-0.164	0.1712	0.1432
42880.34889	-0.111	0.1708	0.1330
42880.35778	-0.074	0.1681	0.1032
42880.36542	0.003	0.1783	0.1396
42880.37333	0.017	0.1708	0.1571
42880.38167	0.087	0.2102	0.1980
42880.39055	0.242	0.2441	0.1616
42880.39271	0.258	0.2740	0.1286
42886.10481	-0.236	0.1188	0.0745
42886.11210	-0.240	0.1243	0.0978
42886.12057	-0.241	0.1126	0.0920
42886.13468	-0.232	0.1132	0.0796
42886.14162	-0.233	0.1173	0.0785
42886.14481	-0.245	0.1230	0.0913
42886.15182	-0.232	0.1118	0.0963
42886.15585	-0.236	0.1126	0.0663
42886.16224	-0.241	0.1187	0.0853
42886.16613	-0.233	0.1122	0.0750
42886.17175	-0.242	0.1260	0.0898
42886.17578	-0.245	0.1157	0.0896
42886.18550	-0.240	0.1098	0.1040
42886.18939	-0.237	0.1138	0.1027
42886.19641	-0.237	0.1069	0.1058
42886.20036	-0.237	0.1129	0.0840
42886.20627	-0.252	0.1232	0.0952
42886.21015	-0.255	0.1235	0.1025
42886.21668	-0.241	0.1183	0.0893
42886.22092	-0.247	0.1191	0.0841
42886.22904	-0.255	0.1225	0.1052
42886.23328	-0.255	0.1254	0.0949
42886.24397	-0.254	0.1257	0.0869
42886.24779	-0.260	0.1254	0.0900
42886.25390	-0.261	0.1181	0.0834
42886.25765	-0.251	0.1260	0.0833
42886.26404	-0.249	0.1213	0.0795
42886.26772	-0.255	0.1206	0.1004
42886.27362	-0.257	0.1195	0.1100
42886.27737	-0.257	0.1203	0.0958
42886.28342	-0.257	0.1174	0.0889
42886.28703	-0.258	0.1246	0.0901

APPENDIX – Continued

HELIO MJD	D(v)[a]	D(b-v)[a]	D(u-b)[c]
42886.34612	-0.288	0.1308	0.0791
42886.35273	-0.240	0.1523	0.0691
42886.35932	-0.255	0.1171	0.0609
42887.10672	-0.412	0.1628	0.1008
42887.11477	-0.367	0.1624	0.1116
42887.12151	-0.404	0.1610	0.1037
42887.12783	-0.396	0.1450	0.1054
42887.13463	-0.401	0.1521	0.0792
42887.14873	-0.404	0.1418	0.1004
42887.15547	-0.405	0.1495	0.1048
42887.16186	-0.395	0.1320	0.0953
42887.16574	-0.411	0.1582	0.1173
42887.17026	-0.407	0.1471	0.1298
42887.17359	-0.390	0.1475	0.1063
42887.19109	-0.411	0.1537	0.1446
42887.19762	-0.413	0.1587	0.1180
42887.25456	-0.417	0.1505	0.1134
42887.26088	-0.417	0.1584	0.1152
42887.26741	-0.407	0.1445	0.1029
42887.27394	-0.410	0.1437	0.1014
42887.28046	-0.417	0.1511	0.1090
42887.28657	-0.412	0.1556	0.1135
42887.30275	-0.422	0.1561	0.1117
42887.30886	-0.428	0.1683	0.1145
42887.31518	-0.416	0.1546	0.1270
42887.32185	-0.387	0.1631	0.0946
42887.32652	-0.423	0.1534	0.0975
42887.34879	-0.412	0.1550	0.0844
42887.35546	-0.406	0.1576	0.1614
42887.36199	-0.423	0.1639	0.1523
42887.36546	-0.419	0.1607	0.1317
42887.36997	-0.425	0.1717	0.1104
42887.37351	-0.428	0.1726	0.1263
42887.37747	-0.422	0.1653	0.1586
42887.38324	-0.424	0.1638	0.1145
42887.38671	-0.429	0.1711	0.1514
42887.39275	-0.425	0.1722	0.1185
42887.39615	-0.431	0.1670	0.1381
42887.40060	-0.429	0.1450	0.0870
42887.40344	-0.421	0.1252	0.0811
42888.10654	-0.402	0.1507	0.1476
42888.11342	-0.415	0.1501	0.1227
42888.12071	-0.408	0.1644	0.1341
42888.12724	-0.396	0.1652	0.1096
42888.13244	-0.394	0.1490	0.1087
42888.13626	-0.397	0.1390	0.1167
42888.15286	-0.399	0.1491	0.0995
42888.16029	-0.396	0.1527	0.0998
42888.16654	-0.399	0.1569	0.1115
42888.17015	-0.394	0.1646	0.1076
42888.17411	-0.399	0.1567	0.1152
42888.17821	-0.383	0.1425	0.1270
42888.18966	-0.400	0.1543	0.1166
42888.19439	-0.399	0.1487	0.1071
42888.20015	-0.396	0.1512	0.1163

APPENDIX – Continued

HELIO MJD	O(v)°	O(b−v)°	O(u−b)°
42888.20404	−0.380	0.1511	0.1054
42888.20897	−0.395	0.1569	0.1106
42888.21633	−0.394	0.1598	0.1068
42888.28053	−0.384	0.1612	0.1080
42888.28783	−0.380	0.1430	0.1143
42888.30307	−0.375	0.1563	0.1062
42888.30972	−0.387	0.1535	0.1228
42888.31625	−0.374	0.1576	0.1174
42888.32278	−0.380	0.1555	0.1331
42888.32949	−0.376	0.1431	0.1091
42895.25188	−0.234	0.1034	0.0836
42895.26097	−0.233	0.1128	0.0817
42895.26756	−0.237	0.1212	0.0934
42895.27903	−0.225	0.1187	0.0895
42895.28492	−0.227	0.1176	0.0768
42895.28929	−0.231	0.1136	0.0669
42895.29321	−0.235	0.1187	0.0900
42895.30073	−0.229	0.1163	0.0931
42895.30443	−0.228	0.1200	0.0733
42895.32025	−0.233	0.1167	0.0794
42895.32455	−0.228	0.1045	0.0842
42895.32856	−0.234	0.1205	0.0720
42895.33687	−0.234	0.1164	0.0727
42895.34057	−0.228	0.1091	0.0898
42896.09400	−0.298	0.1263	0.1828
42896.10305	−0.294	0.1280	0.1001
42896.10946	−0.294	0.1313	0.0856
42896.11725	−0.294	0.1241	0.0922
42896.12442	−0.298	0.1226	0.0871
42896.12799	−0.295	0.1190	0.1054
42896.13448	−0.306	0.1300	0.1018
42896.13851	−0.307	0.1267	0.0960
42896.14530	−0.301	0.1271	0.1210
42896.16311	−0.307	0.1285	0.1203
42896.16902	−0.306	0.1353	0.1040
42896.17234	−0.313	0.1398	0.0868
42896.17616	−0.314	0.1298	0.0916
42896.18190	−0.310	0.1324	0.0913
42896.18737	−0.324	0.1377	0.1083
42896.19308	−0.317	0.1304	0.1038
42896.19672	−0.318	0.1360	0.1222
42896.20071	−0.312	0.1358	0.1087
42896.20699	−0.316	0.1295	0.1236
42896.21065	−0.318	0.1352	0.1289
42896.23005	−0.316	0.1321	0.1110
42896.23584	−0.326	0.1365	0.1230
42896.24045	−0.325	0.1406	0.1169
42896.24713	−0.325	0.1268	0.1045
42896.25042	−0.322	0.1303	0.1104
42896.25399	−0.323	0.1353	0.0922
42896.25815	−0.330	0.1308	0.0900
42896.26424	−0.331	0.1402	0.0979
42896.26833	−0.328	0.1465	0.1014
42896.27405	−0.328	0.1350	0.1214
42896.27765	−0.331	0.1453	0.1160

APPENDIX – Continued

HELIO MJD	D(v)^0	D(b-v)^0	D(u-b)^0
42896.29512	-0.326	0.1280	0.1138
42896.29865	-0.325	0.1260	0.1019
42896.30481	-0.330	0.1262	0.0954
42896.30874	-0.335	0.1321	0.1104
42896.31223	-0.334	0.1314	0.1004
42896.31913	-0.338	0.1453	0.0928
42896.32314	-0.336	0.1385	0.1109
42896.32708	-0.335	0.1244	0.1018
42896.33622	-0.338	0.1471	0.0995
42896.34394	-0.334	0.1297	0.1255
42896.34758	-0.338	0.1462	0.1104
42896.35164	-0.334	0.1448	0.0842
42896.36159	-0.351	0.1660	0.0719
42896.36527	-0.328	0.1233	0.0802
42901.20461	-0.367	0.1472	0.1397
42901.21110	-0.354	0.1502	0.1127
42901.21545	-0.373	0.1463	0.1052
42901.21893	-0.358	0.1399	0.1049
42916.13336	-0.411	0.1459	0.1261
42916.14186	-0.413	0.1508	0.1182
42916.15241	-0.406	0.1416	0.1236
42916.15907	-0.406	0.1474	0.1264
42916.16592	-0.416	0.1586	0.1439
42916.17155	-0.417	0.1554	0.1069
42916.17833	-0.410	0.1416	0.1177
42916.18483	-0.407	0.1482	0.1169
42916.20194	-0.409	0.1483	0.1481
42916.21087	-0.435	0.1702	0.0909
42916.21757	-0.414	0.1575	0.1034
42916.23540	-0.413	0.1316	0.1344
42916.24164	-0.413	0.1447	0.1349
42916.24814	-0.417	0.1526	0.1402
42916.25454	-0.417	0.1597	0.1416
42916.26195	-0.417	0.1595	0.0932
42916.27646	-0.419	0.1555	0.1101
42916.28391	-0.426	0.1718	0.1436
42916.29142	-0.423	0.1587	0.0995
42916.30851	-0.415	0.1585	0.0963
42916.31511	-0.386	0.1558	0.0858
42916.32238	-0.412	0.1722	0.0943
42917.11234	-0.356	0.1274	0.1122
42917.12237	-0.362	0.1378	0.1007
42917.12868	-0.360	0.1506	0.1148
42917.17549	-0.358	0.1366	0.0954
42917.20162	-0.356	0.1446	0.0894
42917.20900	-0.356	0.1444	0.1166
42917.25502	-0.357	0.1529	0.1117
42917.26143	-0.339	0.1516	0.1304
42917.26886	-0.339	0.1332	0.1170
42917.27527	-0.353	0.1432	0.0923
42917.28219	-0.339	0.1366	0.0928
42917.31007	-0.331	0.1444	0.1400
42917.32093	-0.330	0.1374	0.0847
42923.11231	-0.325	0.1434	0.1162
42923.11965	-0.325	0.1355	0.1202

APPENDIX – Continued

HELIO. MJD	D(v)[a]	D(b-v)[a]	D(u-b)[a]
42923.13857	-0.312	0.1458	0.0988
42923.14416	-0.321	0.1135	0.1125
42929.08054	-0.220	0.0865	0.1040
42929.08740	-0.225	0.1128	0.0731
42929.09774	-0.225	0.1118	0.0767
42929.10410	-0.228	0.1215	0.0731
42929.10825	-0.228	0.1260	0.0644
42929.11394	-0.224	0.1086	0.0633
42929.11793	-0.223	0.1119	0.0780
42929.12158	-0.230	0.1182	0.0538
42929.12494	-0.220	0.1127	0.0639
42929.12859	-0.221	0.1067	0.0654
42929.14194	-0.213	0.1142	0.0437
42929.14538	-0.219	0.0992	0.0435
42929.14861	-0.226	0.1118	0.0580
42929.15432	-0.220	0.1172	0.0753
42929.15784	-0.231	0.1266	0.0779
42929.16190	-0.224	0.1211	0.0775
42929.16527	-0.224	0.1067	0.0717
42929.16861	-0.228	0.1160	0.0743
42929.17393	-0.230	0.1189	0.0691
42929.17738	-0.225	0.1189	0.0550

LIST OF REFERENCES

Andersen, J., and Popper, D. M. 1975, *Astron. Astrophys.*, **39**, 131.

Arnold, C. N., and Hall, D. S. 1973, *IAU Inf. Bull. Var. Stars* No. 642.

Atkins, H. L., and Hall, D. S. 1972, *Pub. A.S.P.*, **84**, 638.

Batten, A. H. 1973, *Binary and Multiple Systems of Stars*, (Oxford: Pergamon).

Bidelman, W. P. 1954, *Ap. J. Suppl.*, **1**, 175.

Biermann, P., and Hall, D. S. 1976, in *IAU Symposium No. 73, Structure and Evolution of Close Binary Systems*, eds. P. Eggleton et al. (Dordrecht: Reidel).

Blanco, C., and Catalano, S. 1970, *Astron. Astrophys.*, **4**, 482.

Bopp, B. W. 1976, *IAU Inf. Bull. Var. Stars* No. 1175.

________ 1978, private communications*.

Bopp, B. W., Espenak, R., Hall, D. S., Landis, H. J., Lovell, L. P., and Reucroft, S. 1977, *A.J.*, **82**, 47.

Cash, W., Bowyer, S., Charles, P., Lampton, M., Garmire, G., and Riegler, G. 1978, *Ap. J. (Letters)*, in press.

Catalano, S., and Rodono, M. 1967, *Mem. Soc. Ast. Italiano*, **38**, 2.

________ 1968, in *IAU Colloquium No. 4, Non-Periodic Phenomena in Variable Stars*, ed. L. Detre (Budapest: Academic Press), p. 435.

________ 1974, *Pub. A.S.P.*, **86**, 390.

Ceraski, L. 1914, *A.N.*, **197**, 256.

Chambliss, C. R. 1976, *Pub. A.S.P.*, **88**, 762.

Charles, P. A. 1976, private communications*.

Chen, K-Y., and Rekenthaler, D. A. 1966, *Q.J. Florida Ac. Sci.*, **29**, No. 1.

Chisari, D., and Lacona, G. 1965, *Mem. Soc. Ast. Italiano*, **36**, 463.

Conti, P. S. 1967, *Ap. J.*, **149**, 629.

Eaton, J. A. 1977, IAU Inf. Bull. Var. Stars No. 1297.

Eggen, O. J. 1955, Pub. A.S.P., 67, 315.

Field, J. V. 1969, M.N.R.A.S., 144, 419.

Gadomski, J. 1926, Cir. Obs. Cracovie No. 22.

Gibson, D. M., and Hjellming, R. M. 1974, Pub. A.S.P., 86, 652.

Gibson, D. M., Hjellming, R. M., and Owen, F. N. 1975, Ap. J. (Letters), 200, L99.

Glebocki, G., and Stawikowski, A. 1977, Acta Ast., 27, 225.

Gratton, L. 1950, Ap. J., 111, 31.

Gray, D. F. 1976, The Observation and Analysis of Stellar Photospheres (New York: Wiley), p. 388.

Hall, D. S. 1967, A.J., 72, 301.

_______ 1972, Pub. A.S.P., 84, 323.

_______ 1975a, Acta Ast., 25, 215.

_______ 1975b, Acta Ast., 25, 225.

_______ 1976, in IAU Colloquim No. 29, Multiple Periodic Variable Stars, ed. W. S. Fitch (Dordrecht: Reidel), p. 287.

_______ 1977, Acta Ast., 27, 281.

_______ 1978, private communications*

Hall, D. S., Henry, G. W., Burke, E. W., and Mullins, J. L. 1977, IAU Inf. Bull. Var. Stars No. 1311.

Hall, D. S., Montle, R. E., and Atkins, H. L. 1975, Acta Ast., 25, 125.

Hall, D. S., Richardson, T. R., and Chambliss, C. R. 1967, A.J., 81, 1138.

Hardie, R. H. 1962, in Astronomical Techniques, ed. W. A. Hiltner (Chicago: University of Chicago Press), p. 178.

Hearnshaw, J. B., and Oliver, J. P. 1977, IAU Inf. Bull. Var. Stars No. 1342.

Herbst, W. 1973, Astron. Astrophys., 26, 137.

Hiltner, W. A. 1947, Ap. J., 106, 481.

Hoffmeister, C. 1915, A.N., 200, 177.

________ 1919, *A.N.*, **208**, 258.

Joy, A. H. 1930, *Ap. J.*, **72**, 41.

Keller, G., and Limber, D. N. 1951, *Ap. J.*, **113**, 637.

Kron, G. E. 1947, *Pub. A.S.P.*, **59**, 261.

Landis, H. J., Lovell, L. P., Hall, D. S., Henry, G. W., and Renner, T. R. 1978, *A.J.*, **83**, 176.

Liller, W. 1978, invited address to AAS in Madison, Wisc.

Ludington, E. W. 1978, *Bull. AAS*, **10**, 418.

Maggini, M. 1916, *Pubbl. Oss. Arcetri*, Fasc. 34.

Markworth, N. L. 1977, Ph.D. Dissertation, University of Florida at Gainesville.

Merrill, J. E. 1950, *Contr. Princeton Univ. Obs.*, No. 23.

Mergentaler, A. 1950, *Wroclaw Contr.* No. 4.

Milone, E. F. 1968, *A.J.*, **73**, 708.

________ 1976a, in *IAU Colloquium No. 29*, *Multiple Periodic Variable Stars*, ed. W. S. Fitch (Dordrecht: Reidel), p. 321.

________ 1976b, *Ap. J. Suppl.*, **31**, 93.

________ 1977, *A.J.*, **82**, 998.

Miner, E. D. 1966, *Ap. J.*, **144**, 1101.

Montle, R. E. 1973, M.A. Thesis, Vanderbilt University, Nashville, Tennessee.

Mullan, D. J. 1974, *Ap. J.*, **192**, 149.

________ 1976, *Ap. J.*, **204**, 818.

Naftilan, S. A. 1975, *Pub. A.S.P.*, **87**, 321.

Naftilan, S. A., and Drake, S. A. 1977, *Ap. J.*, **216**, 508.

Nelson, B., and Duckworth, E. 1968, *Pub. A.S.P.*, **80**, 562.

Oliver, J. P. 1971, *Bull. AAS*, **3**, 14.

________ 1973, in *IAU Symposium No. 51*, *Extended Atmospheres and Circumstellar Matter*, ed. A. H. Batten (Dordrecht: Reidel), p. 279.

________ 1974, Ph.D. Dissertation, University of California at Los Angeles.

________ 1975, *Pub. A.S.P.*, **87**, 695.

________ 1976, *Rev. Sci. Inst.*, **47**, 581.

Owen, F. N., Jones, T. W., and Gibson, D. M. 1976, *Ap. J. (Letters)*, **210**, L27.

Owen, F. N., and Spangler, S. R. 1977, *Ap. J. (Letters)*, **217**, L41.

Payne-Gaposchkin, C. 1939, *Proc. Am. Philosph. Soc.*, **81**, 189.

Pfeiffer, R. J. 1978, *Bull. AAS*, **10**, 418.

Pfeiffer, E. F., and Koch, R. H. 1973, *Bull. AAS*, **5**, 345.

________ 1977a, *Pub. A.S.P.*, **89**, 147.

________ 1977b, *IAU Inf. Bull. Var. Stars* No. 1260.

Plavec, M. 1967, *B.A.C.*, **18**, 334.

Plavec, M., and Smetanova, M. 1959, *B.A.C.*, **10**, 192.

Plavec, M., Smetanova, M., and Pekny, A. 1961, *B.A.C.*, **12**, 117.

Popper, D. M. 1961, *Ap. J.*, **133**, 148.

________ 1967, *Ann. Rev. Astr. Ap.*, **5**, 85.

________ 1970, in *IAU Colloquim No. 6*, *Mass Loss and Evolution in Close Binaries*, ed. K. Gyldenkerne and R. M. West (Copenhagen: Copenhagen University Observatory), p. 13.

________ 1974, *Bull. AAS*, **6**, 245.

Popper, D. M., and Ulrich, R. K. 1977, *Ap. J. (Letters)*, **212**, L131.

Rhombs, C. G., and Fix, J. D. 1977, *Ap. J.*, **216**, 503.

Rucinski, S. M. 1977, *Pub. A.S.P.*, **89**, 280.

Sadik, A. R. 1978, *IAU Inf. Bull. Var. Stars* No. 1381.

Schneller, H. 1928, *A.N.*, **233**, 361.

Sitterly, B. W. 1930, *Contr. Princeton Univ. Obs.*, No. 11.

Spangler, S. R. 1977, *A.J.*, **82**, 169.

Spangler, S. R., Owen, F. N., and Hulse, R. A. 1977, *A.J.*, **82**, 989

Struve, O. 1946, *Ann. d'Astrophys.*, **9**, 1

________ 1948, *Ap. J.*, **108**, 155

Townley, S. D. 1915, *Pop. Astr.*, **23**, 25

Ulrich, R. K., and Popper, D. M. 1974, *Bull. AAS*, **6**, 461.

Walker, M. F. 1978, *Pub. A.S.P.*, **89**, 874

Walter, F., Charles, P., and Bowyer, S. 1978a, in press.

________ 1978b, submitted to *Nature*

Weiler, E. J. 1975a, *Bull. AAS*, **7**, 287.

________ 1975b, *IAU Inf. Bull. Var. Stars* No. 1014

________ 1978a, *M.N.R.A.S.*, **182**, 77.

________ 1978b, private communications*

White, N. E., Sanford, P. W., and Weiler, E. J. 1978, submitted to *Nature*

Wielen, R. 1974, *IAU Highlights of Astronomy*, **3**, 395

Wood, D. B. 1971, *A.J.*, **76**, 701

________ 1972, *A Computer Program for Modeling Non-Spherical Eclipsing Binary Star Systems*, GSFC X-110-72-473 (Greenbelt, Maryland: Goddard Space Flight Center)

Wood, F. B. 1946, *Contr. Princeton Univ. Obs.*, No. 21, 10

Young, A., and Koniges, A. 1977, *Ap. J.*, **211**, 836.

Notes for list of references:

* Talk given at the IAU Comm. 42-sponsored RS CVn Workshop, Socorro, New Mexico, April 6-7, 1978

BIOGRAPHICAL SKETCH

On 17 December 1949, Elwyn Whit Ludington was born to Berchel A. and Leone Inez Ludington in Eugene, Oregon. He attended public school in Eugene and spent the summer months of his teenage years with his uncle and aunt (Robert and Esther Ludington) on their farm in Idaho. He married Nancy A. Sutterfield in August 1970. After receiving a B.S. degree in electrical engineering from Oregon State University in June 1972 he moved to Gainesville, Florida, to study astronomy in the graduate program of the University of Florida. In November 1972 his son Philip Jay Ludington was born. In June 1978 he married Karen Paige Rockwell, three years after a divorce from his first wife. Shortly after their marriage he and Karen moved to Austin, Texas, where he had a postdoctoral research associateship in the Department of Astronomy at the University of Texas at Austin. The degree of Doctor of Philosophy from the University of Florida is expected to be conferred in December 1979.

I certify that I have read this study and that in my opinion it conforms to acceptable standards of scholarly presentation and is fully adequate, in scope and quality, as a dissertation for the degree of Doctor of Philosophy.

John P. Oliver, Chairman
Associate Professor of Astronomy

I certify that I have read this study and that in my opinion it conforms to acceptable standards of scholarly presentation and is fully adequate, in scope and quality, as a dissertation for the degree of Doctor of Philosophy.

F B Wood

F. Bradshaw Wood
Professor of Astronomy

I certify that I have read this study and that in my opinion it conforms to acceptable standards of scholarly presentation and is fully adequate, in scope and quality, as a dissertation for the degree of Doctor of Philosophy

Kwan yu Chen

Kwan-Yu Chen
Professor of Astronomy and
Physical Sciences

I certify that I have read this study and that in my opinion it conforms to acceptable standards of scholarly presentation and is fully adequate, in scope and quality, as a dissertation for the degree of Doctor of Philosophy

Stanley S. Ballard

Stanley S. Ballard
Distinguished Service Professor of
Physics

I certify that I have read this study and that in my opinion it conforms to acceptable standards of scholarly presentation and is fully adequate, in scope and quality, as a dissertation for the degree of Doctor of Philosophy.

Howard L Cohen

Howard L. Cohen
Associate Professor of Physical
Sciences and Astronomy

This dissertation was submitted to the Graduate Faculty of the Department of Astronomy in the College of Liberal Arts and Sciences and to the Graduate Council, and was accepted as partial fulfillment of the requirements for the degree of Doctor of Philosophy.

December 1978

Dean, Graduate School